Detection of Coral Spawn Slicks at The Great Barrier Reef with Multispectral Imagery and Synthetic Aperture Radar

A thesis presented in partial fulfilment of the requirements for the degree of

Master of Science in

Earth Science
at Massey University, Manawatū, New Zealand.

Jonathan David Magson

2024

Abstract

Understanding the fate and dispersal of coral spawn slicks is crucial for conserving coral reef ecosystems, which are under extreme pressure from climate change and habitat loss. Corals reproduce through broadcast spawning, which involves the synchronous mass release of eggs and gamete, which may manifest as coral spawn slicks on the sea surface.

This study is the first attempt to integrate satellite-based multispectral and Synthetic Aperture Radar (SAR) data for detecting coral spawn slicks. In addition, other features that may be confused with coral spawn slicks, such as algal blooms (biogenic slicks) and natural sea surface slicks, are also investigated.

Numerous slick-like features were detected in PlanetScope imagery between 2016 and 2022 on the Great Barrier Reef. Their spectral properties were analysed with the help of ancillary information to determine coral spawn slick validity. Corresponding Sentinel-1A SAR data were then examined to see if these validated slicks were visible in this alternate data type. Coral spawn slicks were confidently detected on two occasions. The remaining slicks are likely macroalgae mats and cyanobacteria blooms, such as *Trichodesmium* and *Sargassum.*

The coral spawn slicks displayed pink hues and were small and localised compared to other biogenic slicks, which often spanned vast areas. The red / green band ratio (RGR) was effective for discriminating coral spawn slicks but was limited by the spatial resolution of PlanetScope.

Slicks of all types were often aligned within natural sea surface slicks (natural films), highlighting that coral spawn slicks may be undetectable in SAR images when this phenomenon occurs. The presence of look-alike features challenged the identification of coral spawn slicks in SAR, yet biogenic slicks could be matched on several occasions – though not consistently. There was evidence that cyanobacteria blooms appeared as areas of low backscatter, whereas macroalgae mats displayed positive backscatter compared to the surrounding ocean.

This study showcases how multispectral imagery and SAR technologies may complement each other, with multispectral imagery providing detailed information on spectral properties and SAR giving insights into the surface structure.

Acknowledgements

I want to thank Melody Whitehead, Jonathan Procter, and Stuart Mead for their guidance, feedback and support throughout this thesis. I also couldn't have done it without my wife, Luiza, who kept me in line with my studies when I wanted to go surfing or fishing instead.

Contents

LIST OF FIGURES

LIST OF TABLES

List of Abbreviations

AEST	Australian Eastern Standard Time
AI	Artificial Intelligence
AIMS	Australian Institute of Marine Science
API	Application programming interface
CSD	Indo-Pacific Coral Spawning Database
CDOM	Colored Dissolved Organic Matter
CSIRO	Commonwealth Scientific and Industrial Research Organisation
EOTR	Eyes on the Reef sighting network
ESA	European Space Agency
GBR	Great Barrier Reef
GBRMPA	Great Barrier Reef Marine Park Authority
GIS	Geographic Information Systems
LAF	Look-alike features
LiDAR	Light Detection and Ranging
MODIS	Moderate Resolution Image Spectrometer
MS	Multispectral
m/s	Meters per second
NASA	National Aeronautics and Space Administration
NDVI	Normalised Difference Vegetation Index
NIR	Near-infrared
nm	nanometres
RADAR	Radio Detection and Ranging
RGR	Red/green ratio
SAR	Synthetic Aperture Radar
SNAP	Sentinel Application Platform
SWIR	Shortwave Infrared
TIR	Thermal Infrared
UTC	Coordinated Universal Time

1 INTRODUCTION

Coral reef ecosystems globally are under severe threat from anthropogenic impacts, mainly driven by climate change (Hoegh-Guldberg et al., 2017). Rapid Increases in sea temperatures result in more frequent coral bleaching events, leading to widespread mortality of coral populations (Cheung et al., 2021). Other factors include pollution, overfishing, and habitat loss (Hoegh-Guldberg et al., 2017). Research into coral reproduction benefits the restoration and recovery efforts of coral communities (Jamodiong et al., 2018).

Most scleractinian corals (stony corals) reproduce through broadcast spawning, which involves the simultaneous release of gamete bundles into the water column between colonies (Harrison et al., 1984). This may manifest as a mass spawning event when spawning is synchronized within populations, sometimes involving hundreds of coral species from multiple genera (Harrison et al., 1984; Harrison & Wallace, 1990).

The coral spawn bundles, which contain eggs and sperm, are positively buoyant, and when sufficient quantities of bundles are released, coral spawn slicks may form on the sea surface (Figure 1). These slicks are dispersed away from the natal reef and can persist for several days before being broken up by physical processes or consumed by predators (Oliver & Willis, 1987). The size of coral spawn slicks varies depending on the scale of the mass spawning event and the sea conditions. They have been recorded at lengths over 5km long and are usually a few meters wide (Oliver & Willis, 1987). The colour of coral spawn slicks includes pink, red, orange, brown, and creamy white, depending on the species of the coral and the proportion of live embryos (Oliver & Willis, 1987; Yamano et al., 2020; Gan et al., 2021). The slicks can also be transported several kilometres daily by currents and wind (Oliver & Willis, 1987; Willis & Oliver, 1990; Yamano et al., 2020). Understanding the fate and dispersal of coral-spawn slicks is beneficial for conserving and monitoring coral reef ecosystems.

Figure 1. Left: Milky white Coral spawn slick off Townsville (AIMS). Right: Coral spawn slick near Heron Island in the Great Barrier Reef (CSIRO).

There is usually one major spawning event per year for a given location, where corals may spawn over a few consecutive nights (Simpson, 1991). However, there can also be sporadic, more localised coral spawning outside the major spawning events (Babcock et al., 1986; Hock et al., 2019). The major coral spawning events can be predicted with relative accuracy and depend on the lunar cycles and other environmental triggers such as wind conditions, water chemistry, and sea temperature (Jamodiong et al., 2018). Mass coral spawning occurs in the Great Barrier Reef (GBR) between October and

December, and the timings within this period can differ between locations (Willis et al., 1985; Hock et al., 2019). There are still significant research gaps in the timings of coral spawning events, especially regarding small-scale events and spawning timing differences (Hock et al., 2019).

While traditional field surveys effectively monitor coral spawning slicks over small scales, they can be time-consuming and costly. In contrast, satellite-based remote sensing offers a cost-effective solution for large-scale monitoring (Hedley et al., 2016). Advancements in remote sensing are making it increasingly more feasible to monitor coral spawning slicks over large scales and in remote places (Yamano et al., 2020), yet it is still an underutilised technology. Until now, the research of Jones et al. (2006), Cresswell et al. (2019), and Yamano et al. (2020) are the only known studies whose primary focus was monitoring coral spawn slicks using satellite remote sensing.

2 AIMS AND RESEARCH OBJECTIVES

This study evaluates the effectiveness of satellite-based multispectral imagery and Synthetic Aperture Radar (SAR) in detecting and monitoring coral spawn slicks in the Great Barrier Reef (GBR). The study period is the 2016 to 2022 GBR coral spawning season. While the primary focus is on coral spawn slicks, other phenomena that may be confused with coral spawn slicks in the GBR, such as biogenic and natural sea surface slicks, are also investigated to help find methods to differentiate between these features. By analysing the strengths, weaknesses, and limitations of these remote sensing technologies, this study aims to advance the understanding and capacity of large-scale coral spawn detection. Several research gaps are addressed; this is the first attempt to integrate the use of multispectral and SAR data for coral spawn detection. The effectiveness of spectral indexes previously used for discriminating coral spawn is applied in the GBR. Finally, this study examines whether slicks detected in multispectral imagery can consistently be detected in corresponding SAR data.

The thesis has the following objectives:

- Comprehensively review previous literature on the use of remote sensing for coral spawn slick detection
- Review the literature on phenomena that may be confused with coral spawn slicks, and identify methods that may differentiate between them
- Collect multispectral satellite imagery of potential coral spawn slicks
- Assess whether the identified slicks may be coral spawn slicks or other look-alike features by analysing their spectral characteristics with the help of ancillary data
- Investigate if the red/green ratio (RGR) spectral index is effective at discriminating coral spawn slicks in the GBR
- Assess whether the identified slicks can also be detected in corresponding SAR data

This research aims to determine if multispectral and SAR data can robustly detect coral spawn slicks and, if so, under which conditions. The integration of these two remote sensing technologies is also investigated to explore how they may complement each other. By enhancing the detection, differentiation and monitoring of coral spawn slicks, this study aims to contribute to a broader understanding and management of coral reef ecosystems.

3 LITERATURE REVIEW

This section provides an introduction to remote sensing, particularly multispectral and SAR sensors, and discusses how they can be used for coral spawn detection. Previous literature on remote sensing for detecting coral spawn slicks and other sea surface slicks that may be confused with coral spawn slicks is investigated.

3.1 Remote sensing

Remote sensing can broadly be defined as acquiring information on the physical characteristics of an object or an area at a distance using various sensing instruments. It enables the collection of information without in-situ measurements, allowing for data acquisition at large scales that would otherwise be impractical using traditional methods.

Remote sensing instruments can be categorised into passive and active sensors (Figure 2). Passive sensors measure the reflected electromagnetic radiation from a surface illuminated by an external source. This energy is usually emitted from the sun. Because passive sensors rely on the sun's radiation to illuminate the target, they typically cannot operate at night. Examples of passive sensors include cameras, multispectral spectrometers and radiometers. In contrast, active remote sensing instruments emit their own electromagnetic signal and measure the reflected energy. RADAR (radio detection and ranging) and LiDAR (light detection and ranging) are commonly used active sensors.

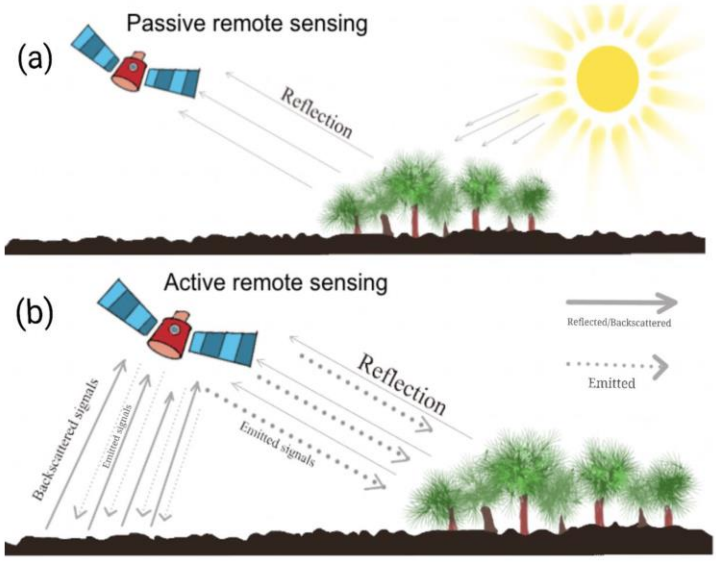

Figure 2. Illustration of passive (a) and active (b) remote sensing (Janga et al., 2023).

Currently, the use of satellite-based remote sensing for coral-spawn slick detection is relatively limited and can be separated into two categories: multispectral imagery and Synthetic Aperture Radar (SAR).

3.1.1 Multispectral imagery

Multispectral sensors are passive remote sensing instruments that capture data at multiple bands across the electromagnetic spectrum, often extending beyond the visible wavelengths (Figure 3). The human eye can only perceive a small portion of the electromagnetic spectrum, approximately 400 to 700 nanometres (nm). In contrast, multispectral data is often captured in near-infrared (NIR), shortwave infrared (SWIR), and thermal infrared (TIR) wavelengths (Holzman et al., 2021).

Different objects have unique spectral signatures, which are how they reflect electromagnetic energy across the spectrum (Thenkabail et al., 2000). The capacity of multispectral sensors to acquire information across multiple wavelengths enhances the ability to distinguish between these objects. Effective discrimination depends on the band configuration of the sensor, that is, whether bands are positioned in regions that effectively capture spectral differences (Jensen, 1996). Also important is the sensor's spatial, spectral, and radiometric resolutions.

The number of spectral bands in a multispectral sensor ranges from three to several dozen (hyperspectral). The spectral resolution of a sensor defines the width of these bands and is measured in nm (Alavipanah et al., 2008). Each band is tuned to a specific portion of the electromagnetic spectrum and may be narrow or wide (Jafarbiglu & Pourreza, 2022). The radiometric resolution refers to the sensor's ability to differentiate between slight differences in energy levels, i.e., how precisely the sensor can measure the radiation of a surface (Jafarbiglu & Pourreza, 2022). The bit-depth of the data measures the radiometric resolution (Jafarbiglu & Pourreza, 2022). The spatial resolution defines the smallest feature that the sensor can detect and is generally measured as the pixel size of the imagery.

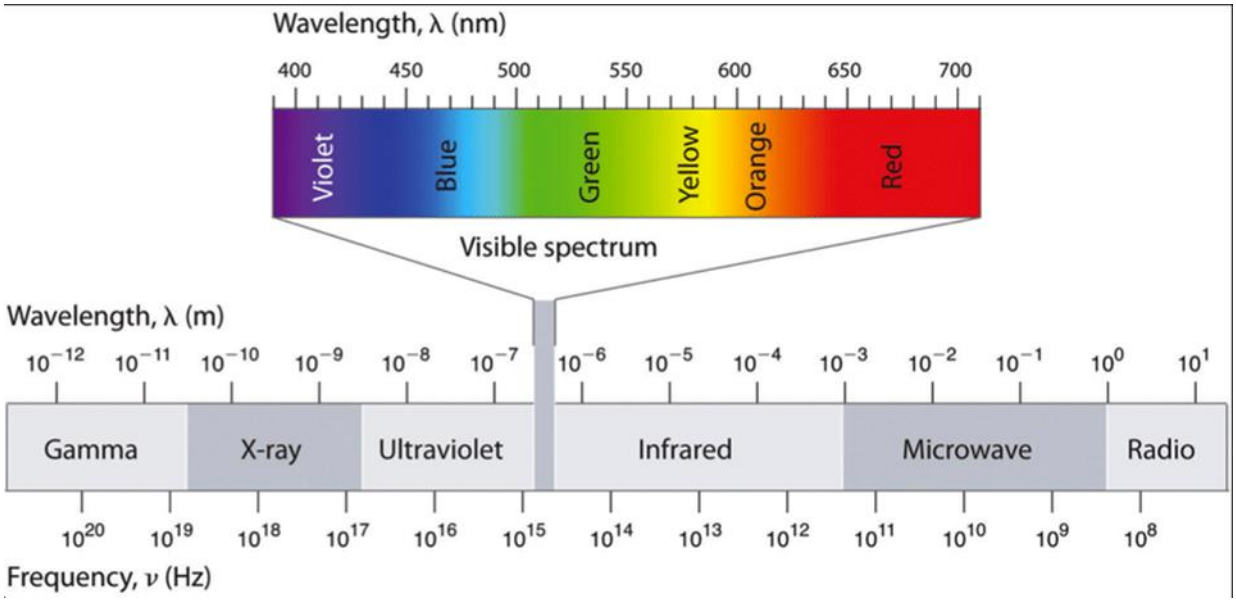

Figure 3. Diagram showing the electromagnetic spectrum (Ziemann, 2015).

A limitation of multispectral sensors is that they generally cannot operate at night when corals spawn (Harrison et al., 1984; Babcock et al., 1986; Baird & Guest, 2009). Additionally, cloud cover commonly obstructs their view, leading to images being partially or entirely covered by clouds.

3.1.1.1 Multispectral sattellites

The deployment of multispectral sensors on satellites has revolutionized Earth observation, enabling detailed and comprehensive monitoring of the planet's surface. Table 1 overviews commonly used multispectral satellites and highlights their spatial, radiometric, and temporal resolutions. In addition to the properties of multispectral sensors discussed earlier, the temporal resolution of a satellite is another factor in Earth Observation. Temporal resolution describes the time elapsed between subsequent image acquisition at the same location (Bair et al., 2023). There is often a trade-off between spatial and temporal resolution (Bair et al., 2023). High-resolution spatial provides fine detail but usually covers smaller areas and revisits less frequently (Bair et al., 2023). Sensors with low spatial

resolution generally have to cover much larger areas in a single image (Bair et al., 2023). However, in recent times, the emergence of satellite constellations, such as PlanetScope, has made it possible for high-resolution imagery to be captured daily in many parts of the world.

Table 1. Commonly used satellite multispectral sensors

Satellite	Mission life span	Bands	Spatial resolution (m)	Max revisit time (days)
Landsat 1-5 (MSS)	1972-1992	4	80	180
Landsat 4-5 (TM)	1982-present	7	30, 120	16
Landsat 7 (ETM+)	2013-present	8	15 (Pan), 30, 60	16
Landsat 8-9 (OLI)	2013-present	11	15 (Pan), 30	16
Sentinel-2	2015-present	13	10, 20, 60	5
MODIS	2000-present	36	250, 500, 1000	1-2
AVHRR	1980-present	5	1100-5000	1
IKONOS	1999-2015	5	4	1-2
Quickbird	2001-present	5	2.4	1-3
Rapid Eye	2008-2020	5	5	5
SPOT 1-3	1986-2004	4	10, 20	1-3
SPOT 4-5	1998-present	4	10, 20	1-3
SPOT 6-7	2012-present	4	1.5	1-3
Worldview-2	2014-present	8	0.46 (pan), 1.84	1
WorldView-3	2014-present	16	0.31 (pan), 1.24	<1
WorldView-4	2016-2019	5	0.31 (pan), 1.24	<1
GeoEye-1	2008-present	5	0.41 (pan) , 1.64	1-3
Dove Classic (PS2)	2014-2020	4	3	1
Dove-R (PS2.SD)	2014-present	4	3	1
SuperDove (PSB.SD)	2020-present	8	3	1
Pleiades	2011-present	5	0.5	<1

3.1.2 Synthetic Aperture Radar (SAR)

Synthetic Aperture Radars (SAR) are active remote sensing instruments that send pulses of microwave radiation to a target surface and then measure the strength and phase of back-scattered energy (Jesus & Kuplich, 2020). The backscattered energy provides information about the geometry of the surface, independent of weather conditions and sun illumination, making it an ideal technology for monitoring various marine phenomena (Angelliaume et al., 2018; Blondeau-Patissier et al., 2023).

The wavelengths emitted by SAR sensors are in the cm to metre range. Each SAR system operates in a specific band of the microwave region of the electromagnetic spectrum (Table 2). The wavelength directly affects how the SAR signal will interact with a surface; hence, it is essential to consider what wavelengths are suitable for a specific task. Longer wavelengths have a greater ability to penetrate through the atmosphere, vegetation, and even into the ground (Pourshamsi et al., 2021). In contrast, short wavelengths have a higher resolving power and are more likely to detect smaller objects rather than pass through them (Luo et al., 2014). SAR sensors with shorter wavelengths, like C-band and X-band systems, are often used for sea slick monitoring because they provide better contrast between the slick and the ambient sea surface (Skrunes et al., 2012; Zheng et al., 2017).

Table 2. List of SAR bands and corresponding wavelength/ frequencies.

Band	Wavelength (cm)	Frequency (GHz)
P	30-100	0.3-1.0
L	15-30	1.0-2.0
S	7.5-15	2.0-4.0
C	3.75-7.5	4.0-8.0
X	2.4-3.75	8.0-12.5
Ku	1.67-2.4	12.5-18.0
K	1.13-1.67	18.0-26.5
Ka	0.75-1.13	26.5-40.0

SAR Sensors can control the angle of polarization that they transmit and receive; they typically transmit and receive linear polarized signals at vertical or horizontal angles, denoted by the letters V and H. The signal can be transmitted and received in the same polarization, or the signal can be cross-polarized where a different polarization is received than the one transmitted (Figure 4). A fully polarimetric (or quad-pol) SAR sensor operates in all four linear polarization combinations. The backscattered signal of a surface differs depending on the polarization (Migliaccio et al., 2015). Hence, certain polarizations are preferred depending on the application. For example, VV is most suited for detecting sea surface slicks because the backscattered signals on the sea surface tend to be vertically polarized (Angelliaume et al., 2018). In contrast, cross-polarization bands (VH and HV) are often chosen for vegetation and crop research due to their sensitivity to volumetric targets such as crops and tree branches (Guan et al., 2023).

Polarimetry is an emerging field in SAR technology, which utilises the different polarization states of SAR sensors using various polarimetric parameters (Migliaccio et al., 2018). Analysing the different polarization states enriches the information acquired and increases the ability to differentiate between target features. Various polarimetric parameters have successfully improved oil spill detection, such as stokes parameters, entropy, and eigenvalues (Migliaccio et al., 2015, 2018; Li et al., 2021).

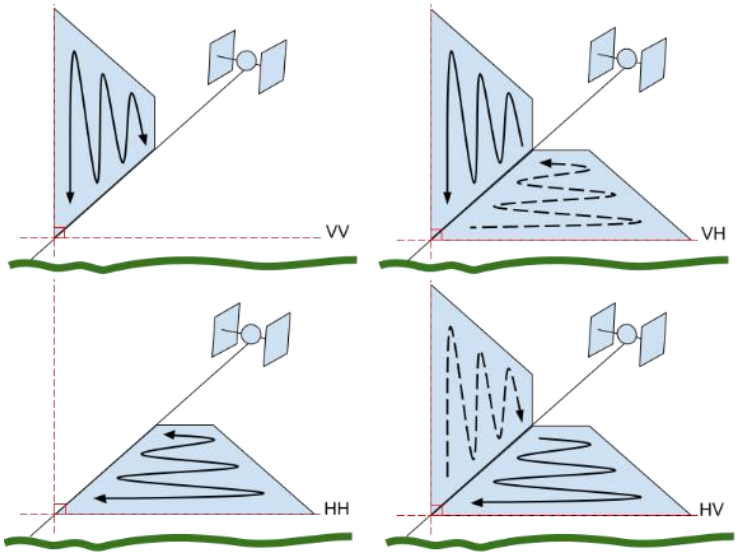

Figure 4. SAR polarization. SAR signals can be transmitted and received in vertical or horizontal polarization. The signal can be received in the opposite polarization than the one transmitted; this is called cross-polarization and is shown in the examples on the right. Credit: Alaska Satellite Facility.

Table 3 presents an overview of various satellite-mounted SAR sensors. The quantity of SAR satellites is increasing, with several new systems in recent years. Furthermore, the development of SAR constellations, such as ICEYA and Capella Space, provides comprehensive coverage of the globe, with revisit times down to a few hours.

Table 3. Commonly used satellite SAR sensors

Satellite	Mission life span	Band	Wavelength	Polarization	Resolution	Revisit time
Seasat	1978-1978	L	24.6cm	HH	Az: 25m Rg: 25m	-
JERS-1	1991-1998	L	24.6cm	HH	Az: 18m Rg: 18m	44 days
ERS-1	1991-2001	C	5.6cm	VV	Az: 6-30m Rg: 26m	35 days
ERS-2	1995-2011	C	5.6cm	VV	Az: 6-30m Rg: 26m	35 days
RADARSAT-1	1991-2013	C	5.6cm	HH	Standard: 25x28m Fine: 9x9m Wide: 35x28m ScanSAR: 50x50-100x100m	24 days
ENVISAT	2002-2012	C	5.6cm	HH, VV, VV/HH, HH/HV, VV/VH	Az: 28m Rg: 28m	35 days
ALOS-1	2006-2011	L	24.6cm	FBS: HH, VV FBD: HH/HV, HH/VH PLR: HH/HV /VH /VV ScanSAR: HH, VV	FBS: 10x10m FBD: 20x10m PLR: 30x10m ScanSAR: 100m	46 days
RADARSAT-2	2007-Present	C	5.6cm	Single: HH, VV, HV, VH Dual: HH/HV, VV/VH Quad: HH/HV/VH/VV	Spotlight: ~1.5m Stripmap: ~3x3-25x25m ScanSAR: 35x35-100x100m	24 days
COSMO-SkyMed	2007-Present	X	3.5cm	Single: HH, VV, HV, VH Dual: HH/HV, HH/VV, VV/VH	Spotlight: ≤1m Stripmap: 3-15m ScanSAR: 30-100m	~hours
TerraSAR-X	2007-Present	X	3.5cm	Single: HH, VV Dual: HH/VV, HH/HV, VV/VH Twin: HH/VV, HH/VH, VV/VH	Spotlight: 0.2x1.0-1.7x3.5m Stripmap: 3x3m ScanSAR: 18-40m	11 day
Sentinel-1	2014-Present	C	5.6cm	Single: HH, VV Dual: HH/HV, VV/VH	Stripmap: 5x5m IW: 5x20m EW: 20-40m	6 days
ALOS-2	2014-Present	L	24.6cm	Single: HH, VV, HV, VH Dual: HH/HV, VV/VH Quad: HH/HV/VH/VV	Spotlight: 1x3m Stripmap: 3-10m ScanSAR: 25-100m	14 days
SAOCOM	2018-Present	L	24.6cm	Single: HH, VV Dual: HH/HV, VV/VH	Stripmap: 10x10m TopSAR: 100x100m	8 days

				Quad: HH/HV/VH/VV		
Capella Space	2018-Present	X	3.1 cm	Single: HH, VV	0.5	~hours
ICEYE	2018-Present	X	3.1 cm	Single: HH, VV	0.5	~hours

3.1.2.2 The interaction of microwave energy with the sea surface

The sea surface can be modelled as small-scale capillary waves superimposed on gravity waves (Figure 5). SAR in marine monitoring often involves analysing the interaction of microwave energy with these waves (Zhang et al., 2014).

Bragg scattering and specular scattering are the two primary mechanisms by which SAR signals interact with the sea surface (Phillips, 1988; Jackson, 2004). Specular scattering occurs when the sea surface is smooth and at small incident angles—typically less than 20 to 30 degrees (Valenzuela, 1978). This mechanism reflects the signal directly to the sensor, like a mirror. On the other hand, Bragg scattering occurs at medium or large incident angles (greater than 30 degrees) or when the radar signal interacts with small-scale capillary waves on the sea surface (Valenzuela, 1978), causing a diffuse scattering pattern (Figure 5).

A material with a higher viscosity than the sea surface, such as oil or natural films, produces elastic resistance that can dampen capillary waves (Jenkins & Jacobs, 1997; Voskuhl & Rahlff, 2022). This may result in a departure from Bragg scattering from the radar signal, resulting in areas of reduced backscatter compared to the surrounding sea surface in SAR images (Zhang et al., 2014).

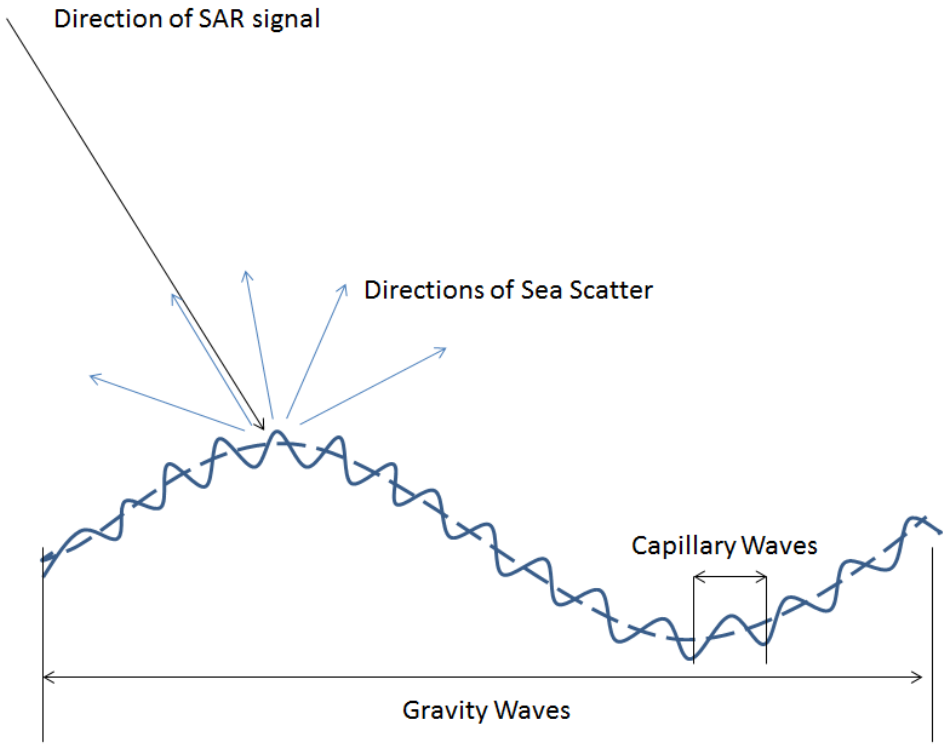

Figure 5. The interaction of a radar signal with gravity and capillary waves (Zhang et al., 2014).

SAR is, therefore, highly sensitive to the surface conditions of the ocean, providing valuable insights for marine monitoring. Different oceanographic, atmospheric, biological, and hydrocarbon phenomena may suppress wave action and appear as discrete dark regions in SAR imagery (Jones et

al., 2006). This makes it possible to detect sea surface slicks such as oil spills, biogenic films, and coral spawn slicks using SAR (Jones et al., 2006; Alpers et al., 2017; Wu et al., 2018). The most established of these applications is oil spill detection, where SAR has been extensively used for over three decades (Alpers et al., 2017). Figure 6 shows an example of an oil spill detected using Sentinel-1 SAR data. The dampening effect that the oil has on the sea surface makes it highly invisible in the SAR imagery, appearing as a discrete area of low backscatter (dark areas).

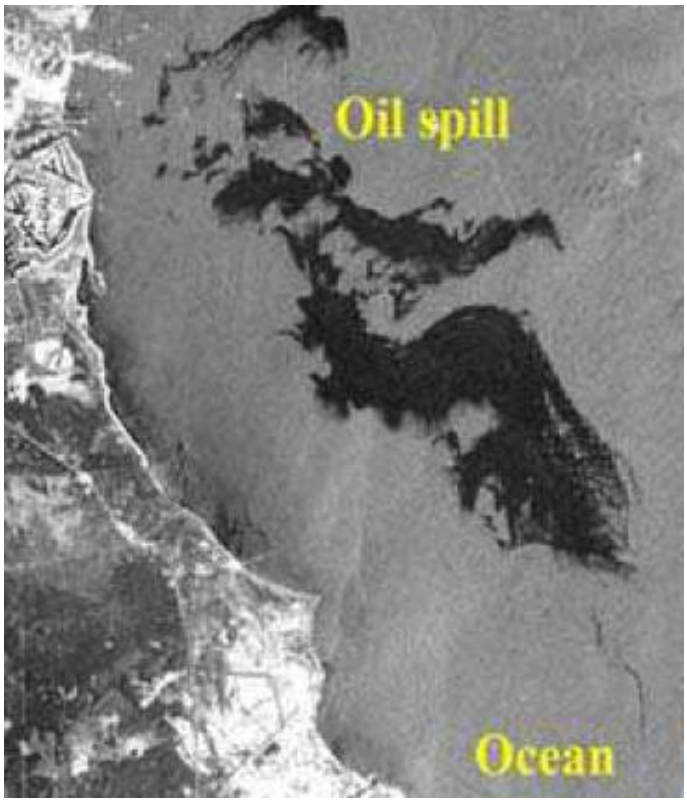

Figure 6. Sentinel-1 image of an oil spill over the Indian Ocean (Naz et al., 2021).

The detection of sea surface slicks using SAR depends on the wind conditions. At very low windspeeds, there is no contrast in backscatter between the slicks and the surrounding ocean, while at high windspeeds, the slicks are broken up from wave action (Brekke & Solberg, 2005; Garcia-Pineda et al., 2009). The optimal wind condition for SAR detection has been debated; it depends on the properties of the SAR sensor, and analysis techniques can improve detection when conditions are less favourable. (Alpers et al., 2017). Table 4 shows some of the optimal thresholds reported in the literature concerning oil spill detection.

Table 4. Optimal windspeed thresholds for oil slick detection in SAR images reported by the literature.

Windspeed threshold m/s	Source
3 to 7-10	Brekke and Solberg (2005)
3.5 to 7	Garcia-Pineda et al. (2009)
2 to 7	La et al. (2018)
3 to 9	Naz et al. (2021)

3.2 Early aerial surveys of coral-spawn slicks

The earliest use of remote sensing concerning coral-spawn slicks was aerial photography in conjunction with in-situ measurements to capture the extent and monitor the movement of coral-spawn slicks in the GBR (Oliver & Willis, 1987; Willis & Oliver, 1990). Oliver and Willis (1987) observed several coral-spawn slicks in the Central GBR region over consecutive days after a coral-mass spawning event. The slicks ranged from approximately 15 to 5000m long and up to 10m wide. The colour of the slicks was creamy white or pink. Sampling revealed that pink slicks contained high concentrations of live coral embryos, whereas the white slicks had a low proportion of live material. They recorded slicks drifting 6.5km in 8 hours in light wind conditions. When wind conditions were strong, they observed no slicks.

They found that *Trichodesmium* slicks were often located close to coral-spawn slicks. The coral-spawn slicks usually formed long streaks of irregular clumped material, with either a creamy white or pink colour, and commonly occurred close to reefs. On the other hand, *Trichodesmium* slicks tended to be reddish-brown and were more diffused in appearance, often forming parallel streaks. However, they also observed several faint white streaks that were harder to distinguish from coral-spawn slicks. Sampling showed these slicks were made up of pumice, foam, and traces of *Trichodesmium*.

Interpretation of the aerial survey data found that hydrodynamic forces played a vital role in the distribution of coral spawn slicks (Oliver & Willis, 1987; Willis & Oliver, 1990). Coral spawn slicks were found to be aggregated along topographical fronts, island wakes, and at boundary mixing at reef surfaces (Willis & Oliver, 1990). The slicks were transported along longshore currents adjacent to the reef in the early dispersal stages. They concluded that the dispersal of the slicks is initially more dependent on hydrological processes rather than wind direction. Only once the slicks have been transported away from reefs does wind direction become the dominant factor for dispersal.

3.3 Multispectral imagery for coral-spawn slick detection

The study by Yamano et al. (2020) marks the first and only known in-depth analysis of multispectral imagery for detecting coral spawn. This study discovered some critical insights into the spectral properties of coral spawn slicks during a spawning event at Ishigaki Island, Okinawa, Japan. Their research integrated a laboratory spectral analysis of coral reproductive materials with the analysis of coral spawn slicks identified in multispectral satellite imagery.

The laboratory spectral analyses revealed differences in colour and reflectance between coral spawn bundles of various species. *Acropora* and *Dipsastraea* bundles displayed pink hues, whereas *Montipora* bundles were brown. In terms of reflectance, all the bundles showed a relatively low reflectance in the visible regions and higher reflectance in the NIR regions (Figure 7). The bundles of *Acropora and Dipsastraea* species show a slightly increasing trend in reflectance in the visible region from approximately 500nm to 600nm. Between 600nm and 700nm, there is a sharp increase in reflectance, except for a notable flat shoulder between 620 and 640nm for *Acropora*. The reflectance of *Montipora* was different due to the presence of symbiotic algae, with an even sharper increase in reflection between 680 and 700nm.

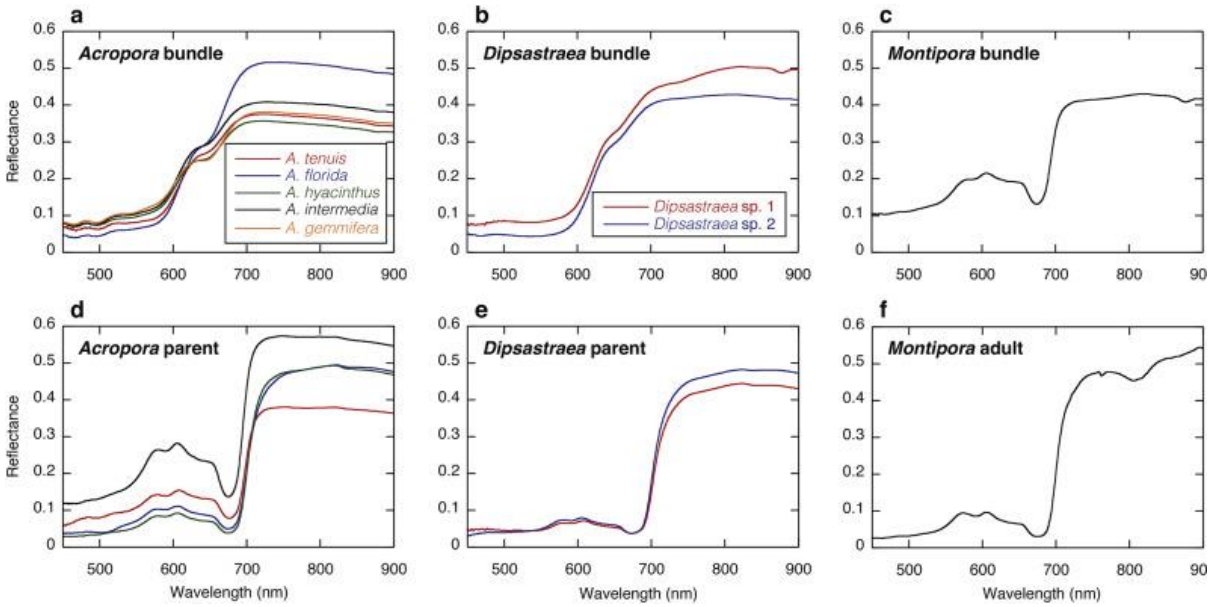

Figure 7. Reflectance spectra of coral-spawn bundles and parent colonies of Arcopora, Dispastraea, and Montipora coral-spawn bundles (Yamano et al., 2020).

Yamano et al. (2020) used the spectral analysis results to detect coral spawn slicks in PlanetScope and Sentinel-2 imagery. Coral spawn mainly lacks the absorption peak near ~680nm of chlorophyll-born organisms such as *Trichodesmium*, *Ulva* and *Sargassum* (Hu et al., 2015). Multispectral instruments with wavelengths that capture the absorption peak may be used to discriminate coral-spawn slicks from chlorophyll-born organisms. Therefore, Yamano et al. (2020) used the red/green ratio (RGR) to map coral spawn extents because coral spawn slicks should display higher RGR than *Trichodesmium*, *Ulva* and *Sargassum.* In PlanetScope imagery, coral-spawn slick had RGR values near 1.8, and *sargassum* had RGR values near 1.2. The red band of Sentinel-2 is situated more precisely over the absorption peak and may provide better discrimination of coral-spawn slicks from other biogenic slicks. In the Sentinel-2 imagery, the RGR value of coral-spawn slicks was about 2.7 compared to 0.83 for *sargassum.* A limitation of using the RGR index to map coral spawn slicks was that narrower parts displayed low RGR values, often below 1, making them appear smaller than they were.

The slicks Yamano et al. (2020) detected were ~10-20m wide and ~500m long in the imagery. The slicks had pink hues and displayed high red and NIR values compared to blue and green in both planet scope and sentinel-2 (Figure 8), corresponding with the spectral analysis reflectance results for coral bundles/embryos.

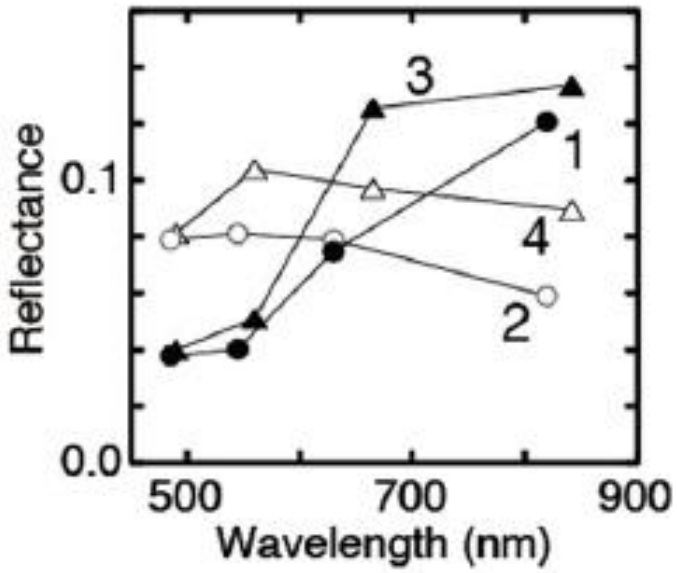

Figure 8. Reflectance of (1) coral-spawn slick in PlanetScope, (2) cloud in PlanetScope, (3) coral-spawn slick in Sentinel-2B, and (4) wave foam in Sentinel-2B (Yamano et al., 2020).

3.4 SAR for coral spawn slick detection

So far, there are two known studies on using SAR for detecting coral spawn slicks (Jones et al., 2006; Cresswell et al., 2019). Both studies utilised RADARSAT-1 data (Table 2), a Canadian commercial spaceborne SAR satellite that operated from November 1995 to March 2013. The payload consisted of a C-band single-polarization HH sensor with a spatial resolution between 8m and 100m, depending on the operation mode.

Jones et al. (2006) detected slick-like features in a RADARSAT-1 scene at Ashmore Reef in Western Australia that were presumed to be coral spawn slicks. No in-situ observations were recorded, so they integrated ancillary data, including ocean current, bathymetry and wind data, to aid their interpretation. The timing of the slicks coincided with predicted windows of coral reef mass spawning events in Western Australia, and the morphology of the slicks matched the shape of the nearby reef shoals and displayed a feathering pattern in the direction of the wind (Figure 10). The researchers theorised that slicks were not a result of other oceanographic phenomena, such as wind shadowing or accelerated current flow. It should be noted that dark features that match the morphology of reefs, unrelated to coral spawning, have been observed (McKinna et al., 2011). It is common in the GBR, where significant tidal differences create sheltered areas behind reef structures, resulting in an area of smooth water (McKinna et al., 2011).

Jones et al. (2006) also compared three alternative RADARSAT-1 scenes acquired outside coral spawning windows, and no slick-like features were noted. However, in two of these scenes, the inferred wind speed was below 2.5 m/s, less than the reported optimal thresholds for slick detection using SAR (Table 4). The other alternative scene is acquired at a different tide; the scene with the presumed coral spawn slick was acquired ~1 hour before low tide, whereas the alternative scene was acquired 1-2 hours before high tide. Therefore, it cannot be ruled out that the slicks are related to the bathymetry of the reef.

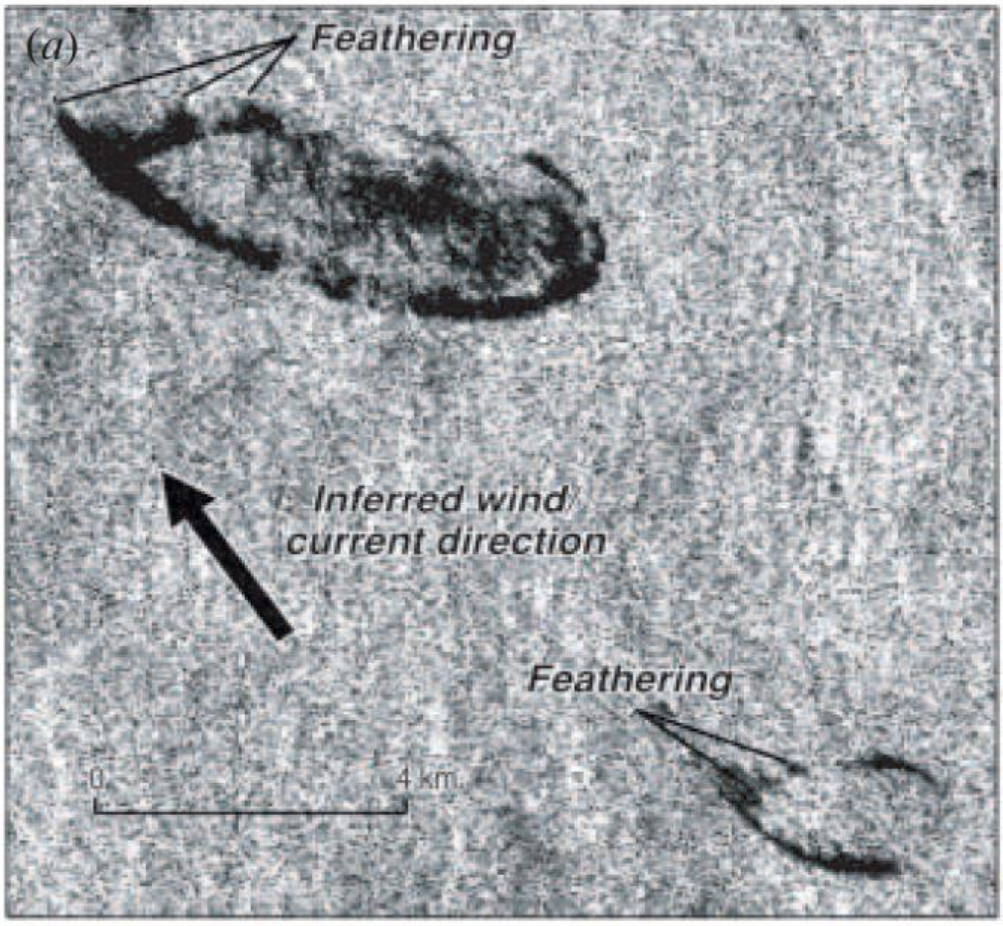

Figure 9. RADARSAT-1 image presumed to show coral spawn slicks from the study of Jones et al. (2006). The slicks show a feathering pattern that corresponds to the inferred wind direction, suggesting that the slick is from coral spawn and not a bathymetry related

Cresswell et al. (2019) also detected slick-like features in Western Australia that were interpreted as coral spawn slicks (Figure 10). The study used RADARSAT-1 images captured in "ScanSAR Wide" mode, which has a spatial resolution of 100m. The condition for coral spawning was ideal at the time of the image acquisition, specifically the phase of the moon, tide, and time of the day - image acquisition was 20 minutes after sunset. The slicks appeared to be dispersing in the direction of the inferred wind away from nearby reefs. However, some scepticism may be warranted in their interpretation. In particular, regarding the relatively low resolution of the SAR data they used compared to the size of coral slicks, which have only been reported to reach widths upwards of 20 to 30m in open oceans (Oliver & Willis, 1987; Yamano et al., 2020). Given the resolution of the SAR data and the observation that the slick spans several pixels in width, it can be inferred that the slick is several hundred meters wide.

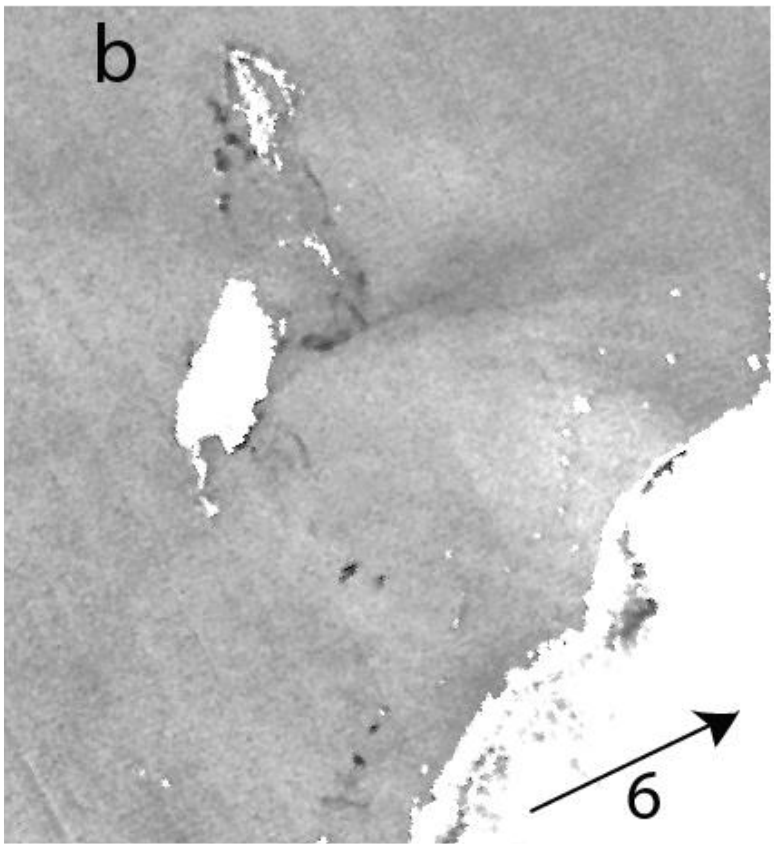

Figure 10. RADARSAT-1 scenes from the study of Cresswell et al. (2019). The vectors represent inferred wind direction and speed in m/s. The dark features in the Northern part of the image were interpreted as coral spawn slicks.

It is clear that SAR for coral spawn detection is in its early stages, and more research is required before it becomes a reliable method. The previous studies had no in-situ observations to confirm the presence of spawning slicks and instead relied on interpretation based on ancillary data for coral spawn slick identification. Therefore, the possibility of false detections cannot be ruled out, as phenomena like oil slicks, biogenic films, eddies, and low wind areas can all appear as dark slick-like features in a SAR image (Fingas & Brown, 1997; Jones et al., 2006; Alpers et al., 2017; Wu et al., 2018).

The two previous studies used single-polarization HH RADARSAT-1 data, presenting an opportunity to explore different polarizations, especially considering that VV polarization is the preferred polarization for sea-surface slick detection due to the tendency of electromagnetic energy to be vertically polarized when reflected from the sea surface (Migliaccio et al., 2015; Angelliaume et al., 2018). Moreover, polarimetric SAR methods could be explored, which have proven effective in oil spill detection (Migliaccio et al., 2015; Angelliaume et al., 2018; Li et al., 2021).

Until now, the integration of multispectral imagery and SAR for coral spawn slick detection has not been undertaken. Combining spectral information in multispectral imagery with SAR's all-weather and day and night capabilities will provide a more robust mechanism for detecting coral spawn slicks. The limitations of SAR in differentiating between different types of slicks could be mitigated by the detailed spectral information provided in multispectral imagery, helping confirm coral spawn slick detections.

3.5 Other look-alike features

A challenge for coral-spawn slick detection is that several other phenomena form slicks on the sea surface or may appear as look-alike features (LAF) in remote sensing imagery. These phenomena may be confused with coral-spawn slicks without appropriate measures, such as utilizing the different signals these features show in remote sensing images or using ancillary data. Three main categories of slicks occur as a film on the sea surface: (i) biogenic slicks, (ii) natural sea surface slicks, (ii) and oil slicks (Figure 11). In addition to these film slicks, other phenomena may appear as slick-like features in remote sensing data, such as suspended sediment, wave foam and debris (Yamano et al., 2020; Shao et al., 2021).

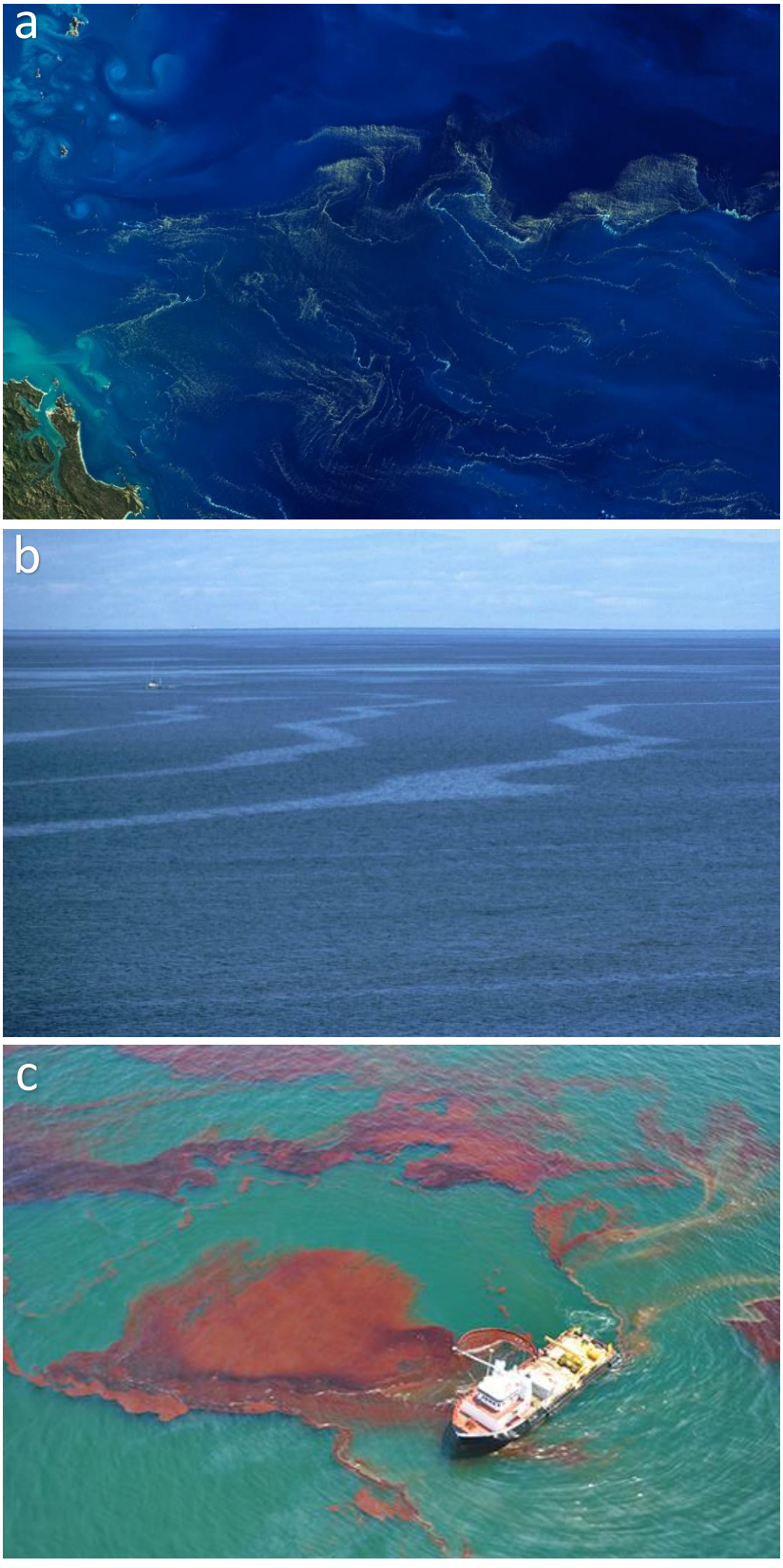

Figure 11. (a) Trichodesmium bloom (biogenic slick) in the Coral Sea in a Landsat 8 – OLI scene (Source: NASA). (b) Natural sea surface slick caused by a surface aggregation of surfactants produced by algae and cyanobacteria (Source: SEOS). (c) Oil slick from Gulf of Mexico oil spill in April 2010 (Source: NOAA).

3.5.1 Biogenic slicks

Biogenic slicks are mainly caused by surface aggregations of algae and phytoplankton. They commonly occur in nutrient-rich environments, such as those found in seas near river mouths (Qi et al., 2023). Remote sensing technologies, such as SAR and multispectral imagery, play a crucial role in detecting and monitoring these phenomena. Various biogenic slicks occur in the GBR, especially near the inshore reefs (Furnas, 1992; Vuki & Price, 1994; McKinna et al., 2011; Blondeau-Patissier et al., 2018). Hence, it is crucial to understand the signals they may exhibit in remote sensing imagery to differentiate them from coral spawn.

Cyanobacteria

Cyanobacteria blooms are common in the GBR, with the most common being those from *Trichodesmium spp*. (Hu et al., 2010; Qi et al., 2023). *Trichodesmium* is a genus of pelagic, nitrogen-fixing cyanobacterium abundant around the oceans of Australia (Capone et al., 1997; Qi et al., 2023). They tend to accumulate at the surface during extended periods of low wind (Capone et al., 1997), often forming extensive sea surface slicks, which have been reported to span areas over 52,000 km^2 in the Capricorn channel (Kuchler & Jupp, 1988; Furnas, 1992). *Trichodesmium* blooms most commonly occur between August and February in the GBR (Blondeau-Patissier et al., 2018). *Trichodesmium* slicks may occur alongside coral spawn slicks (Oliver & Willis, 1987), leading to a possibility of false detection in both multispectral and SAR imagery.

Subramaniam et al. (1999) and Dupouy et al. (2008) have measured the absorption spectra of *Trichodesmium*. Their results showed that absorption is influenced by Chlorophyll a, phycobilipigments, and carotenoids, which cause troughs at 440, 550, and 670nm (Dupouy et al., 2008). Optical satellite detection of *Trichodesmium* using Moderate Resolution Imaging Spectroradiometer (MODIS), the Coastal Zone Color Scanner (CZCS), the Sea-viewing Wide Field-of-View Sensor (SeaWiFS) and the Satellite Pour L'Observation de la Terre (SPOT) has been undertaken (Dupouy et al., 1988; Dupouy, 1992; Subramaniam & Carpenter, 1994; Subramaniam et al., 2001; McKinna et al., 2011). McKinna et al. (2011) devised an algorithm with 85% accuracy for *Trichodesmium* detection MODIS imagery based on three criteria. There is a lack of literature on detecting *Trichodesmium* using PlanetScope, so whether this sensor's radiometric properties are suitable is unclear.

The utilisation of SAR for the detection of *Trichodesmium* is limited. Qi et al. (2022) attempted to detect *Trichodesmium* but could find no correlation between slicks detected in optical imagery. SAR has successfully been employed for other types of cyanobacteria. However, these examples are mostly restricted to lakes and lagoons (Wang et al., 2014; Wang et al., 2017; Wu et al., 2018). In these studies, the cyanobacteria blooms corresponded with areas of reduced backscatter in the radar images.

Macroalgae

Macroalgae blooms are also common in the GBR (Burgess, 2006). They are often associated with increased levels of nutrient runoff from agricultural or urban land use but also occur naturally (Britta, 1999). Blooms of the genera *Hydroclathrus* (Phaeophyta / brown algae), *Sargassum* (Phaeophyta / brown algae) and *Ulva* (Chlorophyta / Green algae) have been recorded in the GBR (Burgess, 2006; Gower et al., 2008). *Sargassum* is especially common along the inshore reefs in the GBR (Vuki & Price, 1994).

Macroalgae reflectance is characterized by high NIR reflectance with a steep red-edge effect (Hu et al., 2015). The red edge effect is generally more pronounced in macroalgae compared to cyanobacteria like *Trichodesmium* (Hu et al., 2010; Hu et al., 2015). Accessory photosynthetic

pigments in Macroalgae algae equate to unique spectral responses (Hu et al., 2015). Green algae are characterized by Chlorophyll B pigments, whereas brown algae have Chlorophyll C pigments (Hu et al., 2015). Field measurements by Hu et al. (2015) analysed the spectral reflectance of *Sargassum* and *ulva.* Their results have a unique spectral response associated with chlorophyll C pigments between 600 and 650nm (Figure 12). *Ulva* had a similar response but lacked the reflectance curve between 600 and 650.

Hu et al. (2015) used the red/green band ratio (RGR) index to differentiate *Sargassum* from *Trichodesmium* and *Ulva* in optical satellite imagery because they have opposite RGR; *Sargassum* exhibits RGR > 1 due to high red band reflectance compared to green bands, whereas *Trichodesmium* and *Ulva* exhibit RGR < 1 (Figure 12). Wang and Hu (2021) developed a deep convolution neural network to extract *Sargassum* features in high-resolution satellite data. They achieved accuracy above 90% when the algorithm was applied to Multispectral Instrument (MSI), Operational Land Imager (OLI), and PlanetsSCope (Dove) sensor data.

The use of SAR for the detection of macroalgae is limited. In theory, macroalgae mats have the potential to have both positive and negative signal contrasts compared to the sea surface. Firstly, the macroalgae mats may dampen capillary waves, resulting in areas of reduced backscatter (Qi et al., 2022). In contrast, macroalgae are aquatic plants that have volumetric structures and, when exposed to the surface, may increase surface roughness, resulting in increased radar signal (Qi et al., 2022). So far, the literature points to the latter (Xinzhe et al., 2009; Shen et al., 2014; Chowdhury et al., 2023). Qi et al. (2022) detected the macroalgae's *Ulva* and *Sargassum* using Sentinel-1. These features exhibited positive backscatter intensity compared to the surrounding ocean. They also found that macroalgae blooms appeared thinner in SAR than in optical imagery. Shen et al. (2014) investigated the polarimetric properties of green macroalgae blooms using quad-polarized RADARSAT-2 data. The cross-polarized bands (VH or HV) showed the most contrast between the macroalgae mats and the surrounding ocean. Chowdhury et al. (2023) failed to detect submerged *Sargassum* mats with Sentinel-1.

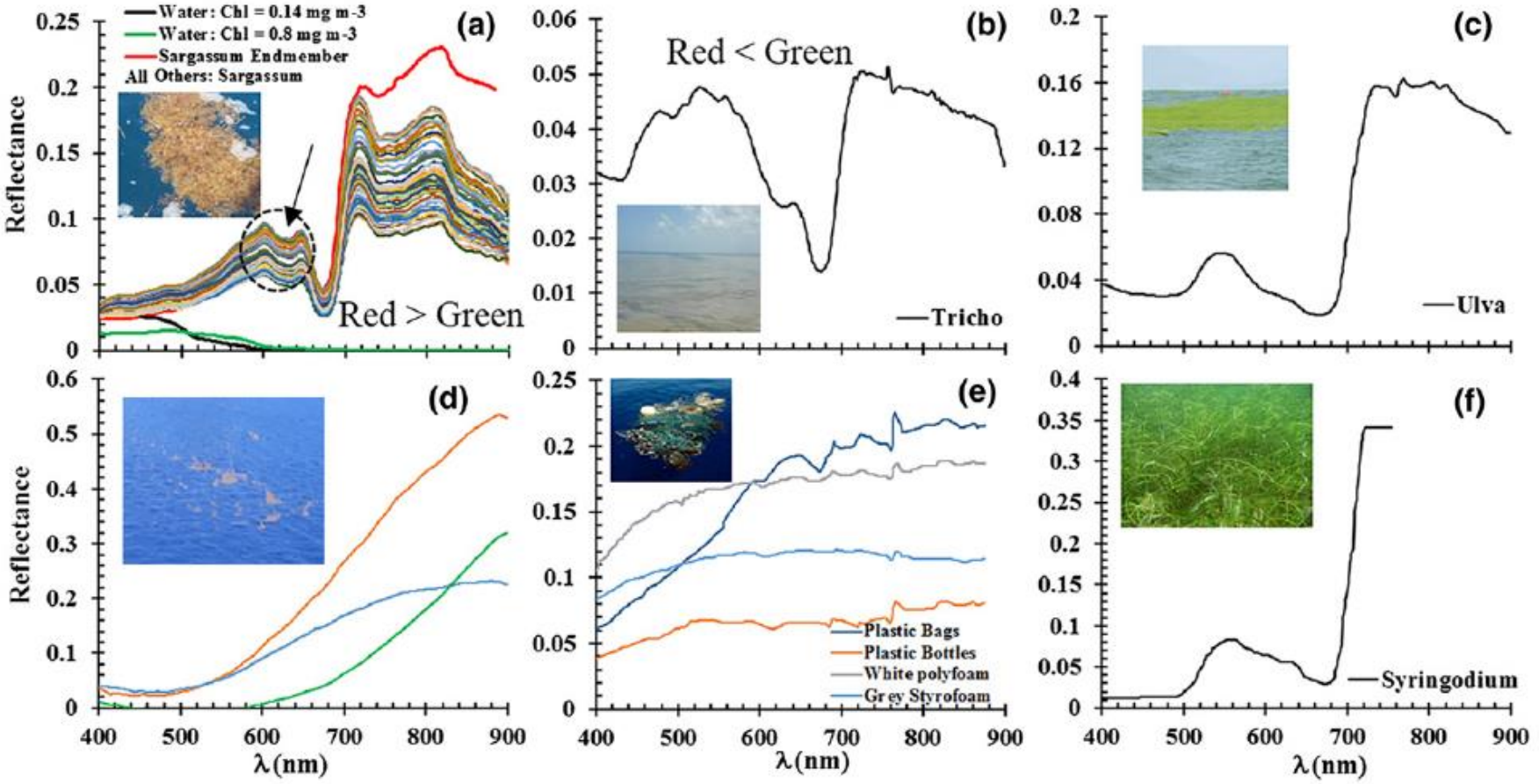

Fig. 2. (a) Surface reflectance spectra (*R*, dimensionless) of *Sargassum* mats and nearby waters measured in the GOM and off Bermuda. Note the local reflectance minimum around 632 nm (black arrow) due to the chlorophyll c pigment absorption, and the enhanced reflectance between 580 and 650 nm (dotted circle) as compared with the reflectance below 550 nm. Reflectance plotted in red was measured from field collected *Sargassum* aggregated in a bucket on the ship deck, thus representing pure *Sargassum* endmember. (b)–(f) Surface reflectance spectra for *Trichodesmium*, *Ulva prolifera*, emulsified oil, various garbage materials, and seagrass *Syringodium*. See text for more details on how these spectra were collected. For illustrative purpose, reprehensive photographs are inset in each panel. The oil spectra were collected by AVIRIS with spectral signature around 1.2 and 1.7 μm (Clark et al., 2010).

Figure 12. Reflectance spectra of various floating materials. Courtesy: Figure 2 from Hu et al. (2015). This article was published in Remote Sensing of the Environment, Volume 167, 15 September 2015, Chuanmin Hu, Lian Feng, Robert F. Hardy, Eric J. Hochberg, Spectral and spatial requirements of remote measurements of pelagic Sargassum macroalgae, 228-246, Copyright Elsevier (2024).

3.5.2 Natural sea surface slicks

Natural sea surface slicks are sometimes categorised as biogenic slicks but will be distinguished separately here. They may appear as smooth streaks on the ocean surface and are most common in coastal areas when wind speeds are less than 7 m/s (Romano & Marquet, 1991). They are mainly caused by an accumulation of surfactants (chemical compounds) produced by bacteria and algae (Voskuhl & Rahlff, 2022). The surfactants lower surface tension and dampen waves, leading to calm seas compared to the surrounding area (Voskuhl & Rahlff, 2022). Natural surface sea surface slicks tend to accumulate in current shears in fronts and eddies (Gade et al., 2013). They are an important biological habitat, hosting a variety of microbial organisms, and act as nurseries for larval fish and zooplankton (Whitney et al., 2021; Voskuhl & Rahlff, 2022). Natural sea surface slicks also affect the distribution of larvae, algae, and small fish (Voskuhl & Rahlff, 2022), and there is also a possibility that they could influence coral spawn slick dispersal (Willis & Oliver, 1990).

There is only a small body of work concerning detecting and monitoring natural sea surface slicks using multispectral and SAR data. In optical imagery, they may appear as smooth patches of the ocean (Voskuhl & Rahlff, 2022). Differences in bi-directional reflectance due to variations in surface smoothness make natural sea surface slicks most visible when optical satellite imagery is sunglint-saturated (Nichol et al., 2023). Hence, Whitney et al. (2021) and Nichol et al. (2023) monitored natural sea surface slicks using sunglint-saturated imagery from PlanetScope and Sentinel-2, respectively.

These film slicks may dampen short gravity-capillary waves (Hühnerfuss et al., 1981). When this happens, natural sea surface slicks may be visible in SAR imagery. Kurata et al. (2016) coordinated in-situ sampling with an overpass of RADARSAT-2 SAR satellite to successfully detect natural sea surface slicks using VV polarization. Nichol et al. (2023) also successfully detected these slicks using VV polarization Sentinel-1 imagery.

In multispectral imagery, these slicks are not too distinct from the surrounding ocean and have similar reflectance (Voskuhl & Rahlff, 2022). Coral spawn slicks should easily be distinguishable from them if the spatial resolution of the satellite data is sufficient. However, in SAR data, these slicks may pose a significant challenge when detecting coral-spawn slicks as there is less ability to differentiate between the two. They could be confused with coral-spawn slicks, or when coral-spawn slicks and natural sea surface slicks co-occur, the coral-spawn slicks may be hidden amongst the more extensive natural sea surface slicks.

3.5.3 Oil spills

Oil slicks can result from anthropogenic spills when human activity releases crude oil and other petroleum products into the ocean or from natural seeps on the sea floor (Wait, 2021). There is no oil exploration in the GBR, and ships must navigate with designated shipping areas and the General Use Zone unless a permit is acquired (GBRMPA). Therefore, there is a low chance of large-scale oil spill events. However, illegal discharge or spills from shipping accidents are still possible (Wait, 2021).

Oil spills typically have lower reflectance in the visible bands compared to seawater, particularly in the blue and green regions (Hu et al., 2009; Lu et al., 2012). On the other hand, their NIR reflectance is higher than water (Hu et al., 2009; Fingas & Brown, 2014). This red edge effect means oil spills could be confused with algal blooms or coral spawn slicks. The blue and green regions can help distinguish oil spills from algae and coral slicks, as oil has lower reflectance in these regions (Hu et al., 2015; Rajendran et al., 2021).

Pérez-García et al. (2022) constructed the Normalized Difference Oil Index (NDOI) for detecting oil spills. This index leverages the visible and NIR bands and has proved effective when applied to imagery from various commercial satellites (Haut et al., 2024). Lacava et al. (2017) presented a Robust Satellites Technique (RST) for detecting oil spills using MODIS imagery. Their multi-temporal approach uses visible wavelengths to identify oil spills while minimizing false detections from phenomena like cloud edges and ocean currents.

SAR is the predominant remote sensing technology used to monitor oil spills due to its all-weather, day and night capabilities (Alpers et al., 2017). It is the most established field for marine slick detection using SAR, with several decades of research behind it (Gade et al., 1998; Fingas & Brown, 2014). Oil has a significant dampening effect, which may reduce wave action, resulting in low backscatter in SAR imagery (Alpers et al., 2017; Holt & Jones, 2017).

Recently, the emergence of SAR polarimetry has proved valuable for oil spill detection. Migliaccio et al. (2015) explored polarimetric parameters for effectively monitoring oil slicks using fully polarimetric RADARSAT-2 data. Polarimetric parameters, such as the co-polarized phase difference, highlighted the departure from Bragg scattering observed in a slick-free sea surface. Their findings showcased the ability of polarimetry to differentiate between oil slicks and LAF.

3.5.4 Suspended sediment and river plumes

River plumes leading to high suspended sediment loads are common in coastal areas of the GBR (Devlin et al., 2013). They may be caused by fluvial flooding events and wind-driven resuspension (Wolanski, 1994; Fabricius et al., 2014). Suspended sediment tends to form extensive dense patches (Emiyati et al., 2017; Govindaraj et al., 2020), in contrast to the linear streaky patterns formed by coral spawn and biogenic slicks (Oliver & Willis, 1987).

River plumes can be put into three categories, each with varying colour and spectral properties (Brodie et al., 2010; M. J. Devlin et al., 2012; Álvarez-Romero et al., 2013):

(i) **Sediment-dominated:** Characterised by high concentrations of suspended sediment. They Have a distinct green-brown to beige colour and reflect highly in red to infrared wavelengths due to the scattering properties of suspended particles.

(ii) **Chlorophyll-a dominated:** Elevations in nutrient availability prompt phytoplankton growth. These plumes exhibit blueish-green waters, depending on the chlorophyll-a concentration—the presence of chlorophyll-a results in the absorption of red and blue wavelengths and the reflectance of green.

(iii) **CDOM-dominated.** Most influenced by the presence of Coloured dissolved organic matter (CDOM). These are typical for offshore plumes transitioning back to ambient conditions, characterized by distinct yellow water with high blue wavelength absorbance.

Satellite remote sensing methods have been applied to monitor river plumes in the GBR using MODIS, SeaWiFS and Landsat (Brodie et al., 2010; M. Devlin et al., 2012; Devlin et al., 2013). River plumes and suspended sediment usually reflect highly across visible and NIR bands compared to biogenic and coral spawn slicks (Yamano et al., 2020; Pisanti et al., 2022). However, they have caused false positives in *Trichodesmium* detection algorithms (Subramaniam et al., 2001)

The use of SAR for monitoring suspended sediment is in its early stages. Shao et al. (2021) assessed the characteristics of suspended sediment in Sentinel-1 SAR data. They found that suspended sediment alters the dielectric constant of the sea surface and may dampen wave action, indicating that SAR may be capable of measuring suspended sediment. Therefore, suspended sediment is a possible LAF for coral spawn detection.

3.5.5 Wave foam

Extensive aggregations of wave foam generated by wave action can form on the sea surface (Hauser et al., 2023). Wave foam may appear bright in optical imagery and could be confused with coral spawn (Yamano et al., 2020). Moore et al. (1998) measured the spectral reflectance of wave foam, which is characterised by high reflectance in the visible region and decreases with wavelength. There is a lack of research on how wave foam appears in SAR imagery.

4 STUDY AREA AND KNOWN CORAL SPAWNING EVENTS

The Great Barrier Reef (GBR) is the largest coral reef system in the world. It extends over 2300 kilometres, covers an area of approximately 340,000 square kilometres, and is visible from space (Figure 13b). Mass coral-spawning events occur throughout the entire region (Hock et al., 2019). The coral genus *Acropora* represents most coral species participating in mass-spawning here (Willis et al., 1985). Some other genera that undergo mass spawning in the GBR are *Montipora*, *Favia,* and *Pavona (Babcock et al., 1986)*. The study area of the following analysis is primarily confined to the Great Barrier Reef Marine Park area (Figure 13a). However, imagery extending slightly outside this area was also analysed in case coral spawn dispersed outside the GBR management area. The GBR management areas are within the Australian Eastern Standard Time (AEST) / UTC + 10 time zones.

All spatial files of reef features, names of reefs, GBR boundaries, and management areas used in this study come from GBRMPA Reef Geohub.

Recorded coral mass spawning observations and predictions were used to determine which date ranges and locations to focus on when searching for coral spawn slicks in the satellite imagery. Initially, finding recorded spawning observations would primarily involve searching for published literature on coral spawning events in the GBR. However, this was quickly found to be difficult and inefficient. Observations are often not reported until several years after an event, which makes it difficult to search for events that occurred relatively recently, and observations also frequently go unpublished (Baird et al., 2021). Instead, known events and predictions come from The Indo-Pacific Coral Spawning Database (CSD), Eyes on The Reef Sightings Network (EOTR), and media articles/websites reporting coral spawning events.

The Indo-Pacific Coral Spawning Database contains records of coral spawning observations throughout the Indo-Pacific region. The CSD provides species, timings, and spatial coordinates of spawning events. The CSD offers an incomplete picture of spawning events in the GBR. The CSD includes 119 observations for eight different Sites in GBR between 2016 and 2019 (Figure 14). Observations in the database may be recorded separately for individual coral species; multiple observations may belong to a single multi-species mass spawning event. There are no observations after 2019.

The Eye on The Reef Sighting Network program is a community-based web portal that can be used to share observations from the Great Barrier Reef. It is frequently used by divers, tour operators and members of the public to report various sightings, including those of coral spawn. The portal includes a map that shows the location, photos and videos, and descriptions of sightings—searching for Coral Spawn in the portal results in over 270 sightings since 22 Nov 2013 (Figure 14). A concern of using the EOTR data is that LAF, such as *Trichodesmium* blooms, could easily be mistaken as coral spawn, especially if the sightings are not from experts. The use of the EOTR data in this study is under a Creative Commons 4.0 Licence: © Commonwealth of Australia acting through the Great Barrier Reef Marine Park Authority - Eye on the Reef program.

Media articles were also used to find dates of known spawning events. The details of timings and locations within these sources can be limited. Google was used to search for Media articles reporting coral spawning events in the GBR between 2016 and 2022. Appendix 1 shows the media articles and websites that were used.

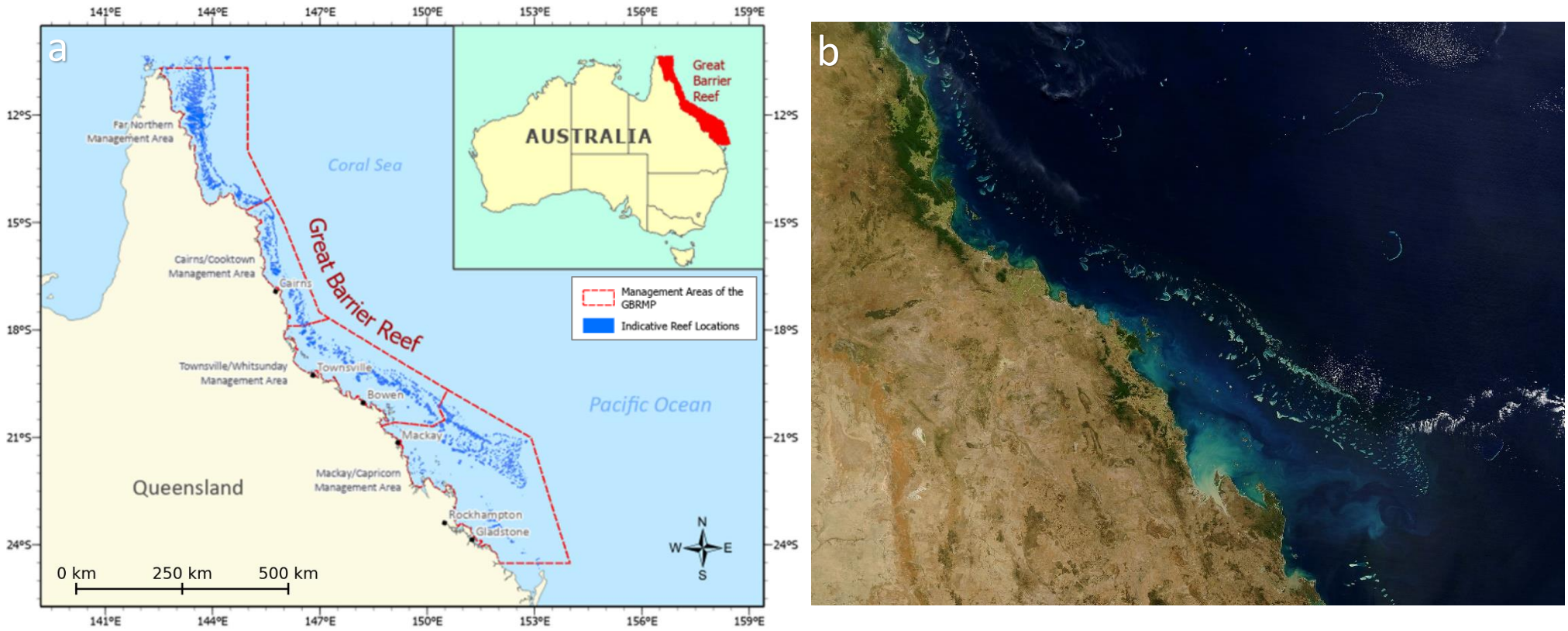

Figure 13. (a) Study area, reef locations, and management areas of the GBR. (b) MODIS Satellite image of the Great Barrier Reef. Credit: Jacques Descloitres, MODIS Rapid Response Team, NASA/GSFC.

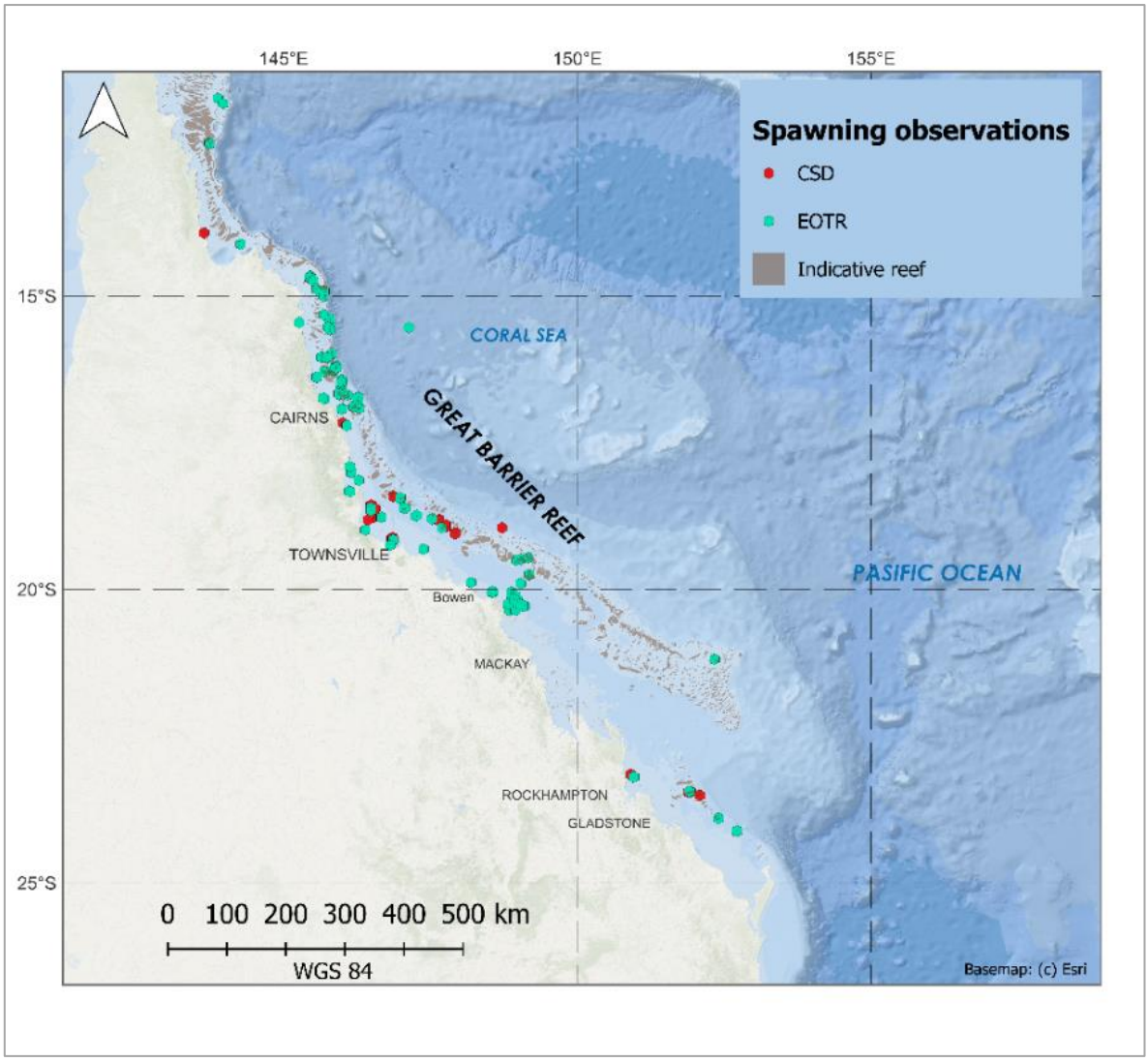

Figure 14. Locations of coral spawn sightings Indo-Pacific Coral Spawning Database (CSD) and the Eye On The Reef Sighting Network (EOTR). Credits © Commonwealth of Australia acting through the Great Barrier Reef Marine Park Authority - Eye on the Reef program.

5 Satellite data

The satellite data used for this project needed to achieve specific requirements. Firstly, it needs to have a spatial resolution that is high enough so that coral spawn slicks can be detected. Secondly, a relatively high temporal resolution is required to increase the chance that imagery is captured during a coral spawning event for a given location. For these reasons, PlanetScope and Sentinel-1 data were chosen.

5.1 PlanetScope

PlanetScope is a commercial constellation of CubeSat satellites named “Doves”. It comprises over 100 individual satellites equipped with high-resolution multispectral sensors with a spatial resolution of approximately 3 meters. The constellation consists of several generations of Doves, with new improvements being made each generation. The Dove sensors capture 8-bit imagery in blue, green, red, and NIR bands, with some additional bands in the new generations of Dove (Figure 15). The dimensions of individual PlanetScope scenes are about 25km x 8km.

The PlanetScope constellation generally achieves a revisit time of approximately one day over the world's landmass (Roy et al., 2021). PlanetScope imagery is not captured in many parts of the ocean, and revisit times may differ in coastal areas (Roy et al., 2021). The temporal coverage over GBR does not seem well understood in the literature. This study found that the revisit time for the GBR was several days in some instances, and significant gaps in coverage were observed on many days.

Different generations of Doves may have different spectral responses (Figure 15). Most noteworthy is that the response curves for the visible bands overlap in early generations (Huang & Roy, 2021). Therefore, consideration must be taken before directly comparing images acquired from different generations of PlanetScope. Later generations of PlanetScope sensors have more narrow bandwidths and are more suited to precisely capture the ~680nm absorption peak of chlorophyll-borne materials. Newer generation PlanetScope sensors may, therefore, have an improved ability to discriminate coral-spawn slicks from floating material like *Trichodesmium*, *Ulva* and *Sargassum.*

A trade-off for PlanetScope's strategy of numerous low-cost satellites is their relatively poor radiometric quality; radiometric inconsistencies have been reported between individual sensors, and imaging is variable under different illumination conditions (Roux et al., 2021).

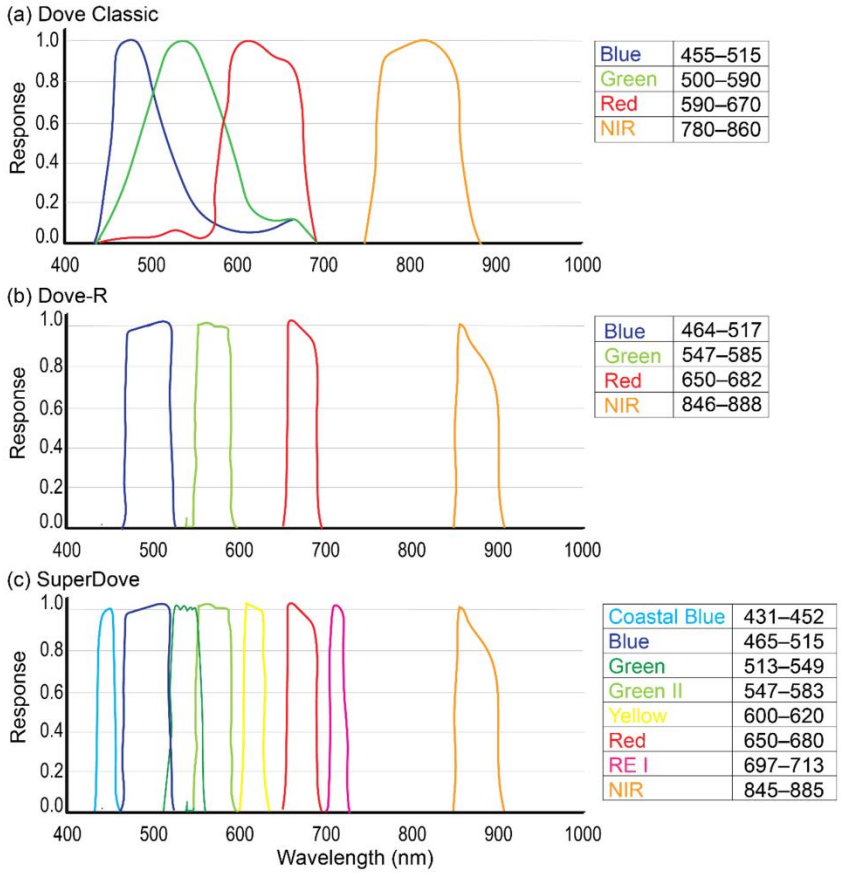

Figure 15. Spectral Response curves for different Planet scope sensors: (a) Dove Classic 'PS2', (b) Dove-R 'PS2.SD', and (c) SuperDove 'PSB.SD'. Courtesy of Frazier and Hemingway (2021).

5.2 Sentinel-1

The Sentinel-1 constellation is part of the Copernicus program of the European Space Agency (ESA). It consists of a pair of C-band SAR satellites, currently consisting of Sentinel-1A and Sentinel-2B. Sentinel-1A was launched in 2014, while Sentinel-2b was launched in April 2016. The central operating frequency of the Sentinel-1 sensors is 5.405 GHz, corresponding to a wavelength of approximately 5.55 cm. They are sun-synchronous polar-orbiting satellites that achieve a 6-day revisit time at the equator together. However, the revisit time over the GBR is approximately 12 days as scenes are primarily acquired from the Sentinel-1A sensor over Eastern Australia, with Sentinel-2B only representing a small proportion of the total scenes (Blondeau-Patissier et al., 2023). Sentinel-1A passes over the GBR in descending orbit at approximately 5:00 am local time (UTC+10).

This study uses Level-1 Ground Range Detected at High resolution (GRDH) Sentinel-1A imagery captured in Interferometric Wide (IW) swath mode, which is the primary operating mode over the GBR (Blondeau-Patissier et al., 2023). IW mode captures data at a 250km swath size with a spatial resolution of approximately 5m (before processing). GRDH products are where multi-looking has been performed, and the imagery has been projected onto ground range using an ellipsoidal model. The resulting product is square pixels displaying amplitude/intensity values with a loss of phase information. The data used in this study is captured in dual-polarization VV/VH mode, except for one scene captured in HH single polarization.

6 METHODS

6.1 Data collection and initial slick detection using Planet Explorer

The initial data collection involved using Planet Explorer to search for potential coral spawn slicks using images from the PlanetScope constellation. Planet Explorer is an online tool for searching, analysing, and downloading satellite imagery.

The primary cues for identifying slicks were distinct linear or patchy features characterised by a discoloured sea surface compared to the surrounding area. These were often irregular or elongated shapes in proximity to reef features. At this stage, all slick-like features were recorded, and there was no attempt to determine whether the slick was a coral spawn slick or if it had other look-alike features (LAF).

The data collection process can be summarized as follows:

1. **Search PlanetScope imagery in Planet Explorer**: Look for potential coral spawn slicks in the GBR region by filtering dates close to known spawning observations.
2. **Cross-reference Sentinel-1 SAR data**: Check the Copernicus Open Access Hub to see if Sentinel-1 SAR data is available at the same time and location.
3. **Data download:** If PlanetScope and Sentinel-1 data are available for a potential coral spawn slick, download the images. The Sentinel-1 data was downloaded from the Copernicus Open Access Hub.

The steps for detecting slicks in PlanetExplorer are demonstrated in Figure 16. Data was primarily if Sentinel-1 data was also available for the slicks detected in PlanetExplorer. However, some data was downloaded for analysis when the slicks displayed a solid resemblance to coral spawn slicks, regardless of Sentinel-1 availability. Cues for this exception included distinct pink or brown slicks adjacent to reefs.

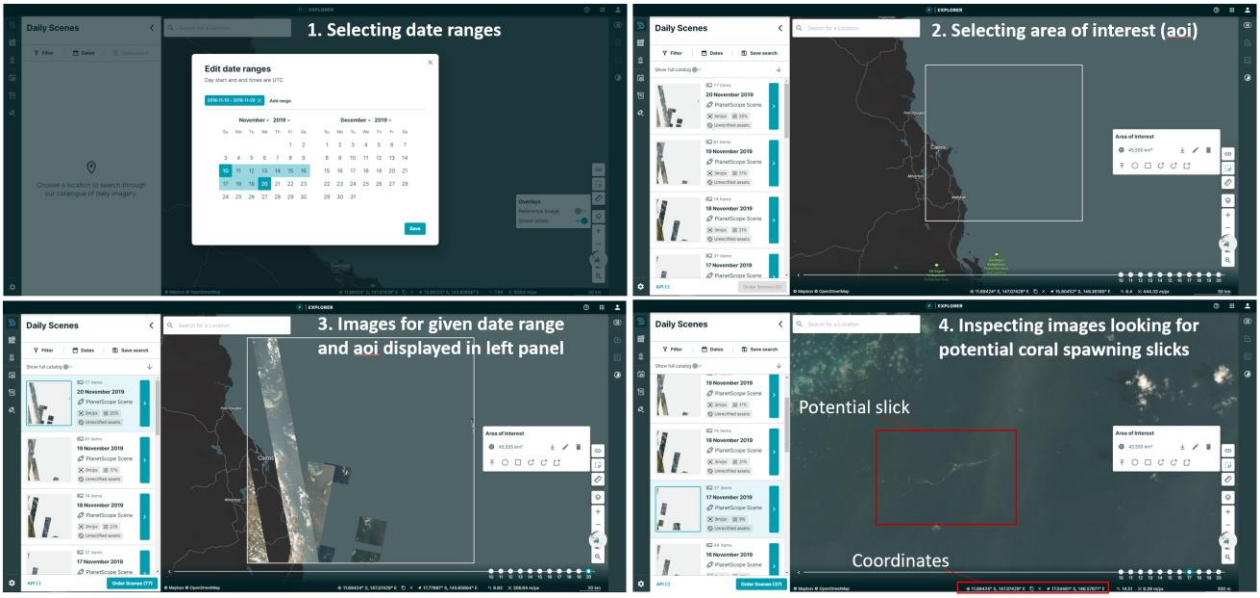

Figure 16. Steps for detecting potential coral spawning slicks using the Planet Explorer portal.

6.2 Multispectral imagery pre-processing

The PlanetScope images were primarily downloaded as surface reflectance products. Surface reflectance products were sometimes unavailable, and Top of Atmosphere (TOA) radiance products were acquired instead. The TOA radiance products were converted to TOA reflectance using the reflectance coefficients provided in the image metadata. The PlanetScope harmonization tool was also applied to the Dove imagery. The spectral bands used in this study were blue, green, red, and NIR.

PlanetScope images are captured in relatively small swaths, meaning a slick may span numerous image tiles. Hence, images were merged into mosaics. A Python script was used to mosaic images where the satellite ID, acquisition date, and product type matched (Appendix 3). This information was extracted from the image metadata.

6.3 SAR pre-processing

The Sentinel-1A SAR data was pre-processed using the SNAP (Sentinel Application Platform), an open-source software for analysing and processing remote sensing data. It is primarily designed to work with data from the ESA Copernicus program. The pre-processing was performed as a batch process with the graph model tool (Figure 17). The spatial resolution after processing was approximately 9 x 9m.

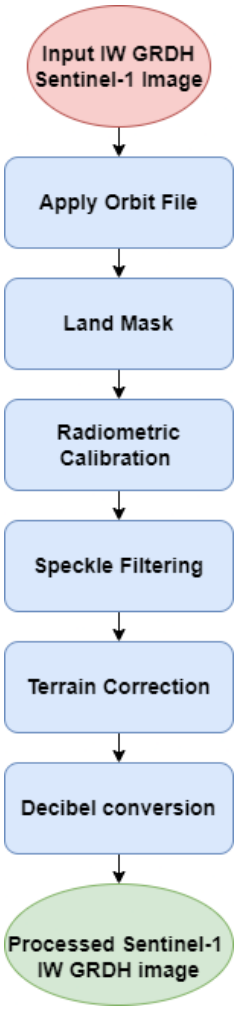

Figure 17. SAR processing steps in SNAP.

Apply orbit file – The default orbit vector information in the metadata of Sentinel-1 data can be relatively inaccurate. It can be improved with orbit files that contain more precise orbit path information. The orbit file is usually available days to weeks after a Sentinel-1 image has been acquired. It includes information from various sources, including gyroscope measurements, GNSS, and ground observations. The **Apply Orbit File** operator in SNAP downloads this information and applies the orbit state vectors to the image.

Calibration - SAR calibration is the process of calibrating a SAR image so that the image cells directly represent backscatter values (Small et al., 2009). This can be achieved by considering all the contributors that affect the radiometric values. The **Calibrate** module in SNAP was used to calibrate the data in this project using the Sigma Naught method. The relative angle between the ground target and the sensor and the distance influence the radiometric values in a SAR image. Because a SAR sensor is a side-looking instrument, the range and angle of cells vary significantly throughout a SAR image. The Sigma Naught method considers this and attempts to provide values independent of angle and distance.

Land mask- The land mask operator was used to mask out land areas from the SAR imagery, making it more straightforward to analyse the data without terrestrial interference from the islands throughout the GBR. The pre-defined land mask in SNAP was used.

Speckle-filter- Speckle noise appears as a 'salt and pepper' pattern of dark and light pixels in SAR imagery. Speckle noise is a result of random interference between coherent backscatter from multiple returns due to the complexity of the surface of the earth. (Lee et al., 1994) Because SAR uses a single wavelength, backscattered waves can interfere with each other constructively (resulting in high-intensity values) or destructively (resulting in low-intensity values) (Singh & Shree, 2016). Various filtering methods can be used to remove speckle from a SAR image. The **Single Product Speckle Filter** module in SNAP was used to clean the speckle using the Lee Sigma method.

Terrain-Correction - The side-looking nature of SAR systems and topographic variability can lead to geometric distortions throughout a SAR image, especially in areas that are not at NADIR to the sensor. **The Range Doppler Terrain Correction** method accounts for this by using orbit vector state information and slant-to-ground range conversions in relation to a DEM to geocode the image (Small & Schubert, 2008).

Decibel (dB) Conversion – dB conversion transforms the dynamic number (DN) radar intensity values into a logarithmic scale. It transforms the wide dynamic range of intensity values to a consistent scale, allowing relative differences in signal backscatter strength to be analysed and compared (Blondeau-Patissier et al., 2023).

6.4 High-scale slick detection and sample collection

Using QGIS, the PlaneteScope mosaics were analysed at high resolution to search for possible coral spawn slicks. The image histograms were adjusted as required to improve visual quality and interpretation. Polygon samples were digitized within the detected slicks so that spectral and location-based analysis could be undertaken (Figure 18). The entire slicks were not digitised due to their geometric complexity. The polygons representing slicks were organised into groups based on their geographical proximity.

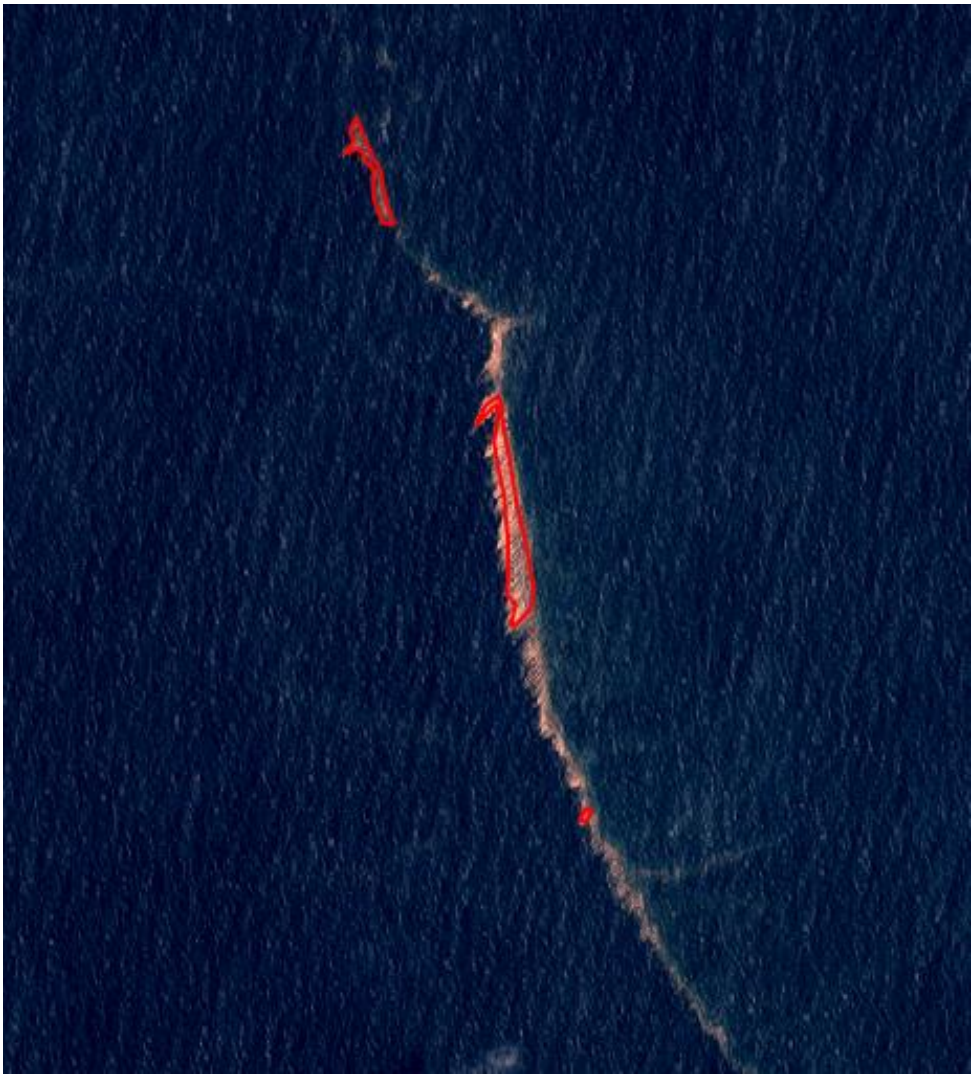

Figure 18. Example of polygon samples of detected slicks.

6.5 Proximity analysis of slick samples and coral spawning records

Utilising QGIS, A proximity analysis was undertaken to compare slick samples with EOTR and CSD coral spawning records to provide evidence on whether the slicks may be related to coral spawning. The minimum geographical distance between spawning records and the nearest slick sample in each image mosaic was calculated using a date filter (Figure 19). The time frame assessed was from 4 days earlier to 2 days after the satellite image acquisition date associated with the slick sample. The minimum distance was calculated for each date in the time frame.

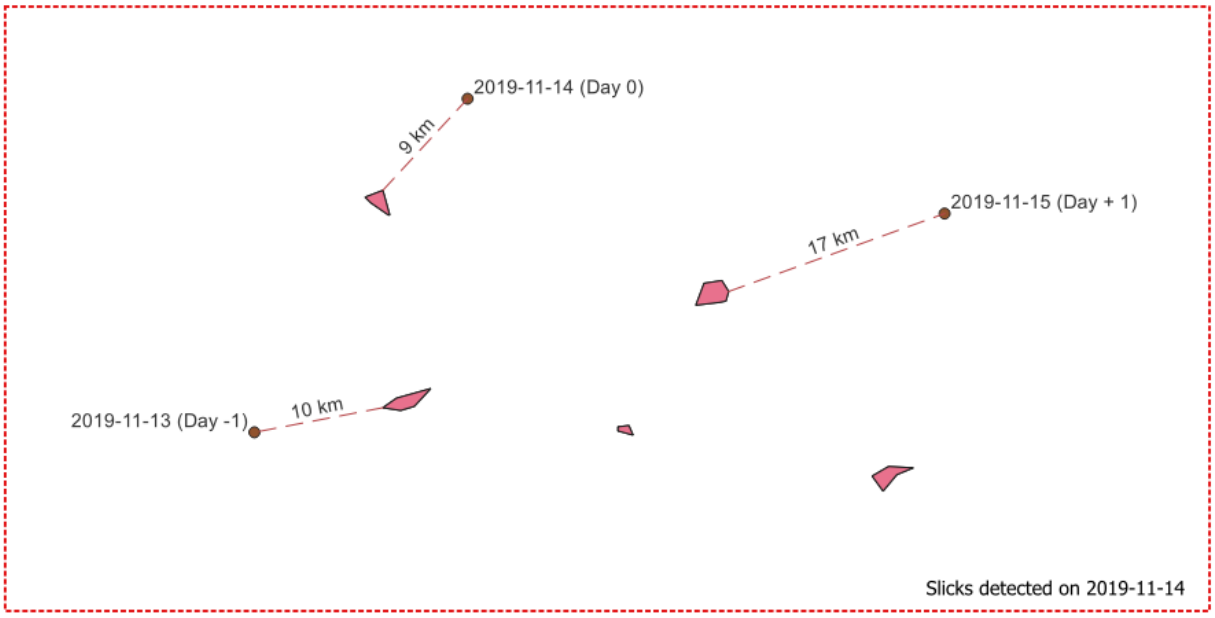

Figure 19. An example of the Proximity analysis methodology: The slicks in the PlanetScope image mosaic are dissolved into a single feature, and then the nearest distance is calculated from slick samples and EOTR/CSD observations from 4 days before until 2 days after the PlanetScope image acquisition date.

6.6 Spectral analysis

Several steps were taken to analyse the spectral characteristics of the identified slicks. First, red and green ratio (RGR) bands were generated for each PlanetScope image mosaic. This ratio was used as an indicator for coral-spawn slicks in a previous study by Yamano et al. (2020). Specifically, pixels with RGR values close to 1.8 in PlanetScope images were used to identify coral spawn slicks.

The mean reflectance for each band, including RGR, was calculated using the slick samples. The mean reflectance analysis was performed at two levels: at the slick group level and the image mosaic level. Calculating the mean reflectance at a group level enabled a more detailed analysis when required. At the image mosaic level, all the polygons within an image were aggregated before calculating the mean reflectance. The image mosaic level enabled a broader analysis that was more efficient to interpret due to the high number of slick groups detected. However, multiple types of slicks within an image could lead to misleading results.

The mean reflectance of water pixels in the image was calculated by digitizing polygons and extracting average water values per band. The mean reflectance of water pixels was plotted against the mean reflectance of slick pixels to provide insights into the distinctiveness of slick reflectance compared to background water pixels.

6.7 Weather data

ERA5 global atmospheric reanalysis data was used to see if optimal conditions for SAR slick detection were met and to assist image interpretation. Specifically, hourly single-level wind data measured 10 meters above the earth's surface, consisting of the 10m horizontal (u) and vertical (v) components of wind, which can be used to derive wind speed and direction. Using Python and the Climate Data Store (CDS) API, the 10m u and v wind components corresponding to the acquisition times of the SAR images were retrieved as NetCDF files. The Numpy Python module was used to derive wind speed and

direction from the u and v components using Equations 1 and 2. Rasters representing the wind speed and direction at a pixel for the specific time step were then generated. The mean windspeed was calculated using the wind speed rasters for each Sentinel-1A image extent (Figure 20).

$$W = \sqrt{u^2 + v^2}$$

Equation 1.

Where W is windspeed, u is the horizontal component of the wind, and v is the vertical component of the wind.

$$\theta = \arctan 2\,(v, u) \times \frac{180}{\pi}$$

Equation 2.

Where θ is the wind direction in degrees, v is the vertical component of wind, u is the horizontal component of the wind, the $arctan\ 2$ function is used to determine the angle in the correct quadrant based on the signs of u and v, the result is converted to degrees by multiplying by 180/π.

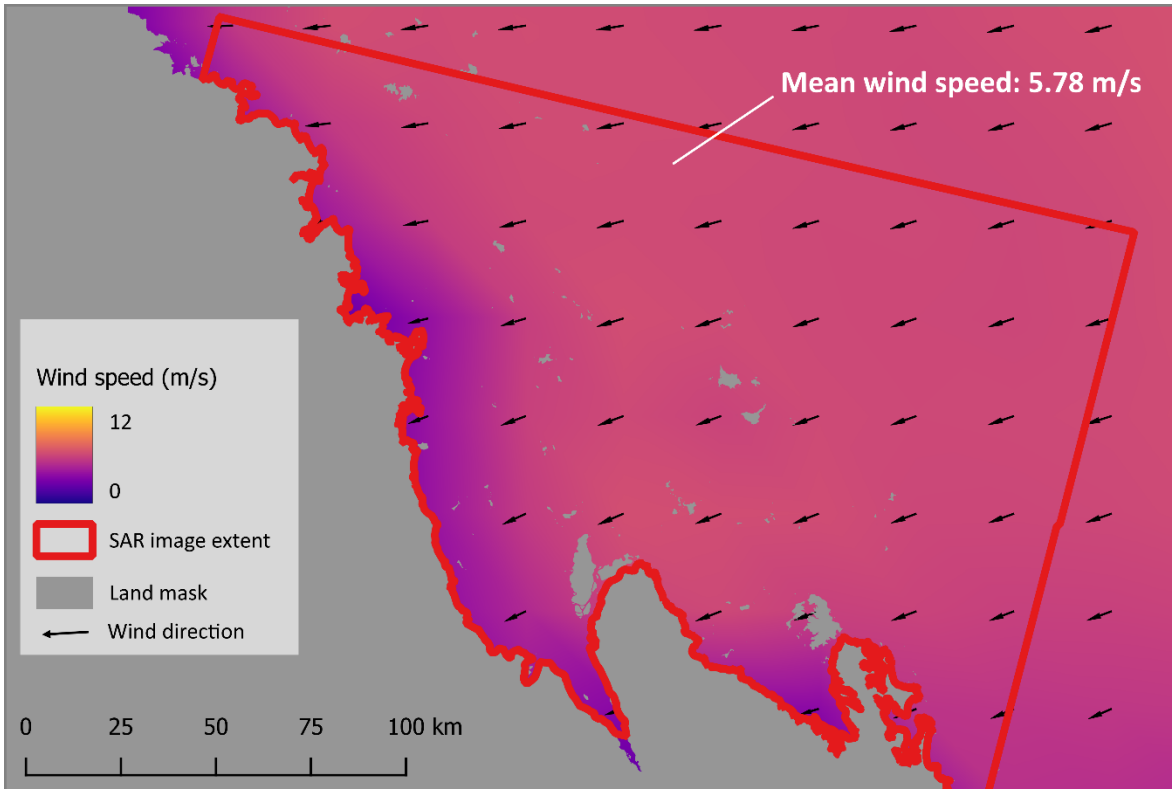

Figure 20. ERA5 hourly 10m wind speed and direction. The mean windspeed is calculated within the SAR extent.

6.8 Satellite imagery interpretation

The slicks initially detected in PlanetScope were assessed in conjunction with the spectral and proximity analysis results to see if there was any evidence that they were from coral spawning.

The criteria for identifying potential coral spawn slicks included:

- **Colouration**: Features exhibiting colours associated with coral spawn, such as pink, brown, and milky white
- **Geometry**: The dimensions and geometric characteristics were compared against typical sizes reported in the literature. Coral spawn slicks have been recorded at lengths of up to 5 to 10km and are usually between 10 to 30m wide (Oliver & Willis, 1987; Yamano et al., 2020; Gan et al., 2021). They typically form narrow linear patterns with occasional wider patches (Oliver & Willis, 1987).
- **Spectral properties**: Following the findings of Yamano et al. (2020), the spectral analysis results provided evidence of whether a slick was possibly from coral spawning. In particular, high RGR values near 1.8 are associated with coral spawn slicks. In contrast, low RGR values (e.g. less than 1) were considered to be more likely related to other biogenic phenomena, such as *Trichodesmium* blooms.
- **Temporal and spatial correlation with spawning observations:** The results of the proximity analysis were another line of evidence. If slicks had temporal alignment and were geographically near the EOTR and CSD records, it indicated that they might be the result of coral spawning.

Subsequently, any corresponding Sentinel-1A SAR imagery was investigated for possible slicks, which involved searching for dark areas representing areas of reduced backscattered compared to the surrounding sea surface. The search was concentrated within 20km of the optically detected slicks, assuming that slicks would not travel more than 20km in the approximate 3 hours between Sentinel-1A and PlanetScope scene acquisitions. The geometry of any slicks detected in SAR was cross-referenced with those optically detected to see if they could be linked between the images, with the help of the ERA5 wind data to see if their possible movement was consistent with the wind direction.

7 RESULTS

7.1 Optically detected slicks

Approximately 273 groups of slicks were detected and analysed in PlanetScope imagery on ten different days from 2016 to 2022. Only days near coral spawning periods (October to December) were investigated for slicks. The slicks spanned across 40 PlanetScope mosaics, consisting of data from several Dove generations (Table 5). Over the study period, the composition of PlanetScope satellite generations changed; from 2016 to 2019, it was mostly PS2 sensors, and then there were some from PS2.SD sensors, and from 2021 onwards, it is mostly PSB.SD. All the products are surface reflectance products except imagery captured on 2019-11-15 (UTC + 10), which were TOA radiance products. These were converted to TOA surface reflectance. The PlanetScope data from 2017 became corrupted after download and was discarded from the study due to time constraints, so there are no observations for this year.

Figure 21 shows the locations of the identified slick groups. The complete list of coordinates to these slicks is in Appendix 2. Most identified slicks were located near inshore reefs and coastal areas from K'gari to Bowen. A handful were located in the offshore reefs in the Mackay/Capricorn and Townsville/Whitsunday Management Areas. Two small groups are noted in outer offshore reefs in the Far Northern Management Area. None were detected in the Cairns/Cooktown Management Areas.

Table 5. Properties of PlanetScope mosaics where slicks were detected. Product types: Surface reflectance (SR), Top of Atmosphere (TOA) Radiance. Sensor generations: Dove Classic (PS2), Dove-R (PS2.SD), and SuperDove (PSB. SD). The date represents the acquisition time of the earliest image within the mosaic groups. All images within mosaic groups were captured within a few minutes of each other.

Image	Date (UTC)	Date (UTC+10)	Sattelite ID	Product Type	PS Generation
MS01	2016-12-21 T23:19:44	2016-12-22 T09:19:44	0e19	SR	PS2
MS02	2018-11-16 T23:35:23	2018-11-17 T09:35:23	0f35	SR	PS2
MS03	2018-11-16 T23:37:59	2018-11-17 T09:37:59	1003	SR	PS2
MS04	2018-11-16 T23:32:02	2018-11-17 T09:32:02	100c	SR	PS2
MS05	2018-11-16 T23:29:28	2018-11-17 T09:29:28	1010	SR	PS2
MS06	2018-11-16 T23:37:10	2018-11-17 T09:37:10	101f	SR	PS2
MS07	2018-11-16 T23:34:02	2018-11-17 T09:34:02	1021	SR	PS2
MS08	2019-11-11 T23:42:59	2019-11-12 T09:42:59	0f34	SR	PS2
MS09	2019-11-11 T23:24:30	2019-11-12 T09:24:30	104a	SR	PS2
MS10	2019-11-14 T00:07:35	2019-11-14 T10:07:35	1034	TOA Radiance	PS2
MS11	2019-11-14 T00:11:28	2019-11-14 T10:11:28	1105	TOA Radiance	PS2
MS12	2019-11-18 T23:53:19	2019-11-19 T09:53:19	1013	SR	PS2
MS13	2019-11-18 T23:47:54	2019-11-19 T09:47:54	1044	SR	PS2
MS14	2019-11-18 T23:21:01	2019-11-19 T09:21:01	0f3d	SR	PS2
MS15	2019-11-18 T23:41:25	2019-11-19 T09:41:25	1011	SR	PS2
MS16	2019-11-18 T23:39:27	2019-11-19 T09:39:27	101e	SR	PS2
MS17	2020-12-04 T23:20:30	2020-12-05 T09:20:30	2223	SR	PSB.SD
MS18	2021-11-19 T21:23:33	2021-11-20 T07:23:33	104e	SR	PS2
MS19	2021-11-19 T23:18:12	2021-11-20 T09:18:12	2276	SR	PSB.SD
MS20	2021-11-19 T23:52:23	2021-11-20 T09:52:23	241c	SR	PSB.SD
MS21	2021-11-19 T23:13:43	2021-11-20 T09:13:43	2429	SR	PSB.SD
MS22	2021-11-19 T23:04:39	2021-11-20 T09:04:39	2434	SR	PSB.SD
MS23	2021-11-19 T23:08:56	2021-11-20 T09:08:56	2455	SR	PSB.SD
MS24	2021-11-19 T23:13:20	2021-11-20 T09:13:20	2459	SR	PSB.SD
MS25	2021-11-19 T23:18:35	2021-11-20 T09:18:35	245d	SR	PSB.SD
MS26	2021-11-22 T23:27:20	2021-11-23 T09:27:20	2420	SR	PSB.SD
MS27	2021-11-22 T23:48:25	2021-11-23 T09:48:25	2423	SR	PSB.SD
MS28	2021-11-22 T23:27:20	2021-11-23 T09:27:20	2449	SR	PSB.SD
MS29	2021-11-22 T23:49:51	2021-11-23 T09:49:51	2458	SR	PSB.SD

MS30	2022-11-12 T23:43:50	2022-11-13 T09:43:50	247a	SR	PSB.SD
MS31	2022-11-12 T23:52:13	2022-11-13 T09:52:13	2486	SR	PSB.SD
MS32	2022-11-12 T23:45:45	2022-11-13 T09:45:45	248b	SR	PSB.SD
MS33	2022-11-12 T23:50:33	2022-11-13 T09:50:33	2490	SR	PSB.SD
MS34	2022-11-12 T23:48:08	2022-11-13 T09:48:08	249c	SR	PSB.SD
MS35	2022-11-14 T23:00:14	2022-11-15 T09:00:14	2421	SR	PSB.SD
MS36	2022-11-14 T23:31:01	2022-11-15 T09:31:01	2473	SR	PSB.SD
MS37	2022-11-14 T23:37:29	2022-11-15 T09:37:29	2492	SR	PSB.SD

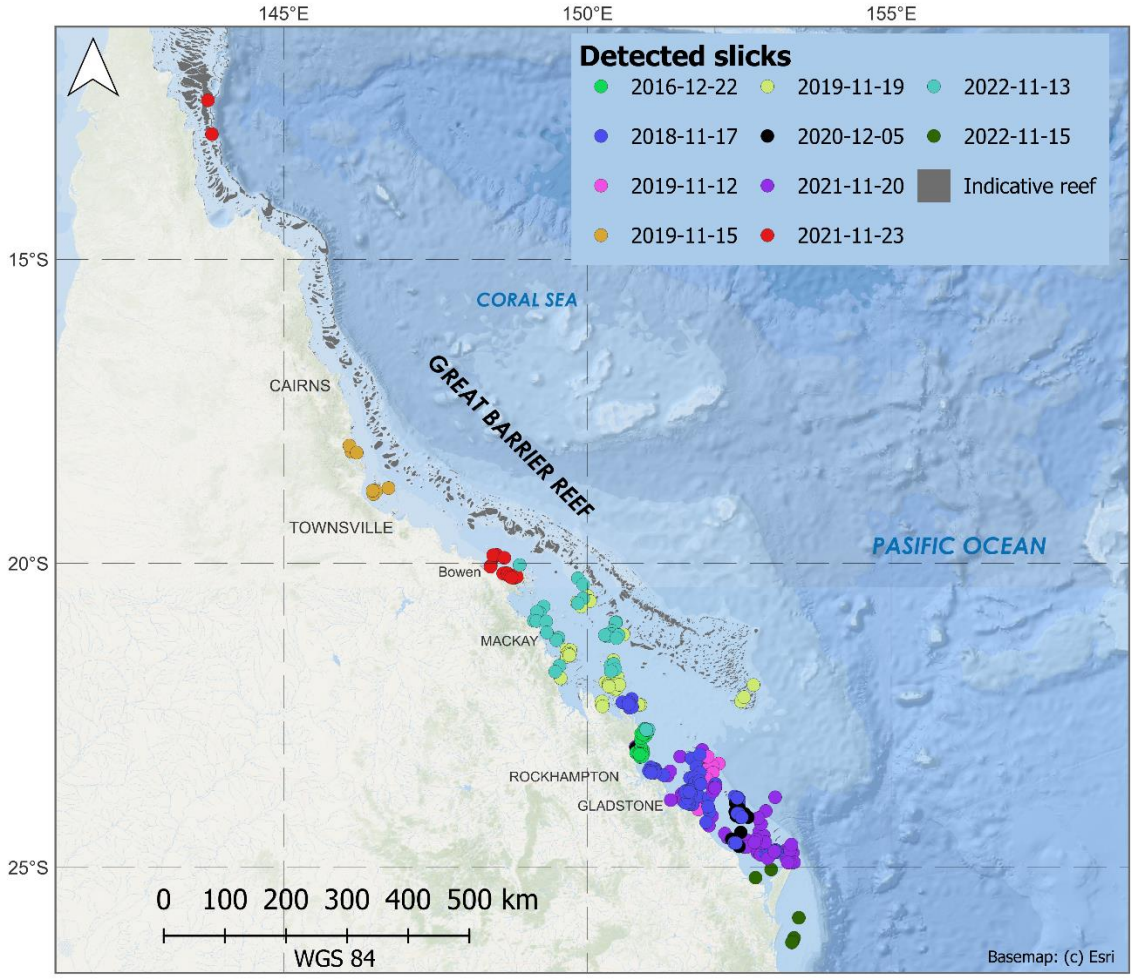

Figure 21. Detected slicks in high-detail analysis.

7.2 Proximity analysis

Table 6 presents the outcome of the proximity analysis conducted between the detected slicks and known spawning records from the EOTR and CSD databases. The minimum distance between an EOTR/CSD observation and slick samples is calculated daily from 4 days before to 2 days after the slick was detected (Figure 19). Out of the 10 days that slicks were identified, a match within the time frame was found on 8 days. No matches were detected for the slicks identified on 2016-12-22 and 2018-11-17. However, coral spawning was reported throughout the GBR on 2016-12-22 in supplementary data by Hock et al. (2019). As the PlanetScope data is captured in the morning, spawning observations on the same day likely occurred later that evening. The EOTR/CSD spawning records are sometimes timestamped, which could allow for a more precise comparison, but only days are compared here. Most spawning records are in the central region of the GBR (Figure 14), likely due to higher levels of human activity in these areas (Harriott, 2004). Slicks detected in more northern or southern regions are less likely to be near an observation due to this bias.

Table 6. The proximity analysis results between optically detected slicks and EOTR/CSD observations. Nearest distances are calculated for observations up to 4 days before and 2 days after the optically detected slicks. An empty value indicates there was no match on that date.

		Nearest distance to EOTR/CSD observation (km)						
Image	**Date(utc+10)**	**-4 day**	**-3 day**	**-2 day**	**-1 day**	**0 day**	**+1 day**	**+2 day**
MS01	2016-12-22							
MS02	2018-11-17							
MS03	2018-11-17							
MS04	2018-11-17							
MS05	2018-11-17							
MS06	2018-11-17							
MS07	2018-11-17							
MS08	2019-11-12		825.2		947.8	3.9		749
MS09	2019-11-12		811.5		932.3	2.3		735.1
MS10	2019-11-15	124.2	832.2		81.7	81.7	128.5	127.1
MS11	2019-11-15	217	746.6		5.7	5.5	214.2	208.8
MS12	2019-11-19	365.2	95.1	405	563.6		294.8	365.3
MS13	2019-11-19	279	191.1	318.8	660.3		208.5	279
MS14	2019-11-19	156.25	179.96	179.83	882.81		125.34	156.17
MS15	2019-11-19	188.17	208.97	208.82	877.35		154.56	188.08
MS16	2019-11-19	176.66	200.11	199.98	874.71		143.74	176.58
MS17	2020-12-05		910	376.3	376.1	10.1	75.7	939.8
MS18	2021-11-20						495.5	971.6
MS19	2021-11-20						573.2	1049.2
MS20	2021-11-20						628.3	1104.4
MS21	2021-11-20						419.2	895
MS22	2021-11-20						627	1103.1
MS23	2021-11-20						509.1	984.3
MS24	2021-11-20						416	892.1
MS25	2021-11-20						359	832.4
MS26	2021-11-23			67.1	406.6	51.9	81	509.9
MS27	2021-11-23			757.5	503	399.3	353.2	329.2
MS28	2021-11-23			19.6	420.9	10.6	73.5	523.9
MS29	2021-11-23			814.7	558.4	454.4	406.1	381.6
MS30	2022-11-13		379.4	231.7	231.7	340.4	192.2	577.5
MS31	2022-11-13		43.3	34.3	16.5	28.6	58.6	231
MS32	2022-11-13		189.6	160.6	180.4	167	224.9	420.3
MS33	2022-11-13		107.3	51.2	69	56.6	137.7	299.5
MS34	2022-11-13		88.3	79.9	95.7	85.3	123.3	335
MS35	2022-11-15	105.5	105.5	670.1	139.4	904		
MS36	2022-11-15	206.5	206.5	769.9	241.1	1000.4		
MS37	2022-11-15	116.6	116.6	667.1	145	896.9		

7.3 Spectral analysis

The results of the mean reflectance from the polygon samples are shown in Table 7. Plots that include the mean reflectance of water pixels are shown in Appendix 3; an example is shown in Figure 22.

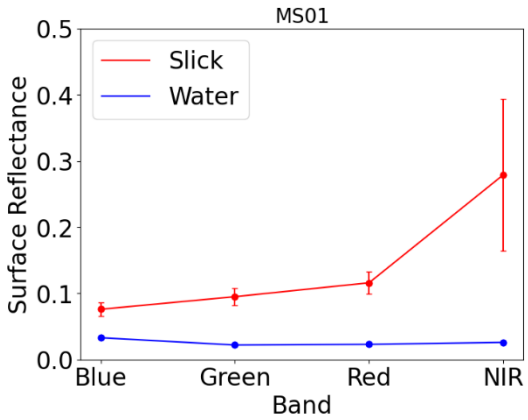

Figure 22. Example of reflectance plot for identified slicks.

NIR reflectance was generally higher than the visible bands. Visible reflectance often remained below 0.1. The High NIR reflectance indicates the slicks are distinct from the surrounding ocean because clear water absorbs nearly all NIR radiation (Mobley, 1994); the plots in Appendix 3 show low reflectance across all bands for water pixels. Low visible and high NIR reflectance suggest that the slicks have biological origins. It could indicate the presence of chlorophyll-born organisms, such as algae and cyanobacteria blooms, which strongly absorb visible radiation and strongly reflect NIR radiation(Hu et al., 2010; Chandler et al., 2023). Photosynthetic zooxanthellae that form symbiotic relationships with corals may also be found in coral spawn slicks (Yamano et al., 2020). The structural properties of coral spawn, such as the material and fluid surrounding the bundles, could also influence high NIR compared to water.

The mean red/green ratio (RGR) of slicks ranged from approximately 0.6 to 1.3. Typically, slicks with green hues had relatively low mean RGR values, while slicks with pink and brown hues had higher mean RGR values. The spectral analysis by Yamano et al. (2020) showed that coral spawn material mainly exhibits positive RGR. They used pixels with RGR above 1.8 to map coral spawn slicks using PlanetSope imagery, indicating that the slicks identified here with RGR values below 1 are unlikely to result from spawning corals. While the mean RGR values did not exceed 1.34 (Table 7), in pink-hued slicks, pixels in the centre of large patches ranged from 1.5 to 2.1. In contrast, the narrow regions displayed substantially lower RGR values, often falling below 1.

Reflectance often depended on the slick's width, especially for NIR and RGR bands, which showed increasing reflectance towards the centre (Figure 23). The trend of increasing reflectance tended to stabilize after approximately 30m from the edge of the slick. This effect may be due to surrounding water influencing the reflectance of pixels in the narrower regions of the slicks. PlanetScope Imagery may be less effective at discriminating coral spawn slicks when their widths are less than approximately 30m.

In some images, the mean reflectance values of slicks do not significantly differ from the background water pixels (Appendix 3), which may indicate that these features are not biogenic or coral spawn slicks and could be caused by coastal runoff, sediment resuspension or bottom interference (Hu et al., 2010).

Table 7. Mean reflectance (+ standard deviation) of slicks per image mosaic.

Image	Blue (sd)	Green (sd)	Red (sd)	NIR (sd)	RGR (sd)
MS01	0.076 ± 0.01	0.095 ± 0.013	0.116 ± 0.017	0.279 ± 0.115	1.214 ± 0.065
MS02	0.042 ± 0.007	0.047 ± 0.011	0.058 ± 0.015	0.097 ± 0.086	1.212 ± 0.07
MS03	0.059 ± 0.006	0.061 ± 0.008	0.059 ± 0.012	0.111 ± 0.047	0.961 ± 0.082
MS04	0.051 ± 0.015	0.061 ± 0.023	0.073 ± 0.028	0.155 ± 0.116	1.204 ± 0.057
MS05	0.059 ± 0.01	0.066 ± 0.015	0.074 ± 0.019	0.119 ± 0.08	1.12 ± 0.08
MS06	0.111 ± 0.01	0.133 ± 0.014	0.135 ± 0.017	0.225 ± 0.081	1.012 ± 0.037
MS07	0.06 ± 0.012	0.075 ± 0.019	0.088 ± 0.022	0.168 ± 0.098	1.18 ± 0.056
MS08	0.035 ± 0.008	0.038 ± 0.01	0.042 ± 0.014	0.053 ± 0.047	1.063 ± 0.151
MS09	0.028 ± 0.005	0.023 ± 0.006	0.028 ± 0.008	0.059 ± 0.034	1.205 ± 0.108
MS10	0.114 ± 0.007	0.116 ± 0.011	0.094 ± 0.015	0.106 ± 0.04	0.723 ± 0.05
MS11	0.108 ± 0.002	0.091 ± 0.002	0.067 ± 0.003	0.049 ± 0.005	0.667 ± 0.015
MS12	0.056 ± 0.019	0.056 ± 0.023	0.054 ± 0.016	0.107 ± 0.051	1.033 ± 0.224
MS13	0.054 ± 0.011	0.057 ± 0.018	0.06 ± 0.02	0.162 ± 0.085	1.058 ± 0.09
MS14	0.040 ± 0.008	0.038 ± 0.010	0.047 ± 0.013	0.091 ± 0.046	1.241 ± 0.265
MS15	0.028 ± 0.008	0.024 ± 0.009	0.030 ± 0.011	0.084 ± 0.053	1.262 ± 0.215
MS16	0.036 ± 0.008	0.033 ± 0.011	0.040 ± 0.014	0.061 ± 0.037	1.209 ± 0.199
MS17	0.084 ± 0.026	0.107 ± 0.04	0.074 ± 0.029	0.184 ± 0.09	0.692 ± 0.035
MS18	0.026 ± 0.004	0.034 ± 0.01	0.037 ± 0.012	0.059 ± 0.039	1.073 ± 0.115
MS19	0.036 ± 0.008	0.031 ± 0.013	0.026 ± 0.009	0.047 ± 0.029	0.849 ± 0.139
MS20	0.053 ± 0.018	0.057 ± 0.021	0.041 ± 0.016	0.108 ± 0.061	0.725 ± 0.142
MS21	0.039 ± 0.012	0.044 ± 0.016	0.031 ± 0.012	0.117 ± 0.066	0.719 ± 0.119
MS22	0.043 ± 0.01	0.039 ± 0.013	0.032 ± 0.01	0.048 ± 0.022	0.834 ± 0.057
MS23	0.069 ± 0.011	0.085 ± 0.019	0.058 ± 0.013	0.163 ± 0.078	0.675 ± 0.03
MS24	0.047 ± 0.009	0.054 ± 0.014	0.039 ± 0.01	0.099 ± 0.041	0.726 ± 0.072
MS25	0.072 ± 0.013	0.088 ± 0.016	0.06 ± 0.014	0.209 ± 0.113	0.675 ± 0.066
MS26	0.045 ± 0.015	0.055 ± 0.021	0.035 ± 0.012	0.172 ± 0.098	0.65 ± 0.077
MS27	0.048 ± 0.011	0.042 ± 0.012	0.058 ± 0.024	0.06 ± 0.026	1.344 ± 0.258
MS28	0.069 ± 0.013	0.085 ± 0.015	0.052 ± 0.011	0.292 ± 0.11	0.611 ± 0.098
MS29	0.037 ± 0.007	0.031 ± 0.01	0.042 ± 0.021	0.048 ± 0.026	1.327 ± 0.265
MS30	0.024 ± 0.011	0.036 ± 0.014	0.02 ± 0.012	0.152 ± 0.073	0.516 ± 0.191
MS31	0.042 ± 0.003	0.032 ± 0.004	0.022 ± 0.003	0.034 ± 0.011	0.689 ± 0.067
MS32	0.043 ± 0.008	0.049 ± 0.011	0.034 ± 0.007	0.153 ± 0.068	0.695 ± 0.085
MS33	0.058 ± 0.006	0.065 ± 0.01	0.04 ± 0.008	0.183 ± 0.08	0.609 ± 0.068
MS34	0.059 ± 0.017	0.067 ± 0.028	0.042 ± 0.017	0.204 ± 0.151	0.627 ± 0.08
MS35	0.042 ± 0.006	0.052 ± 0.011	0.023 ± 0.007	0.065 ± 0.026	0.448 ± 0.065
MS36	0.062 ± 0.012	0.085 ± 0.015	0.07 ± 0.011	0.205 ± 0.084	0.836 ± 0.049
MS37	0.071 ± 0.005	0.08 ± 0.009	0.046 ± 0.007	0.109 ± 0.033	0.579 ± 0.046

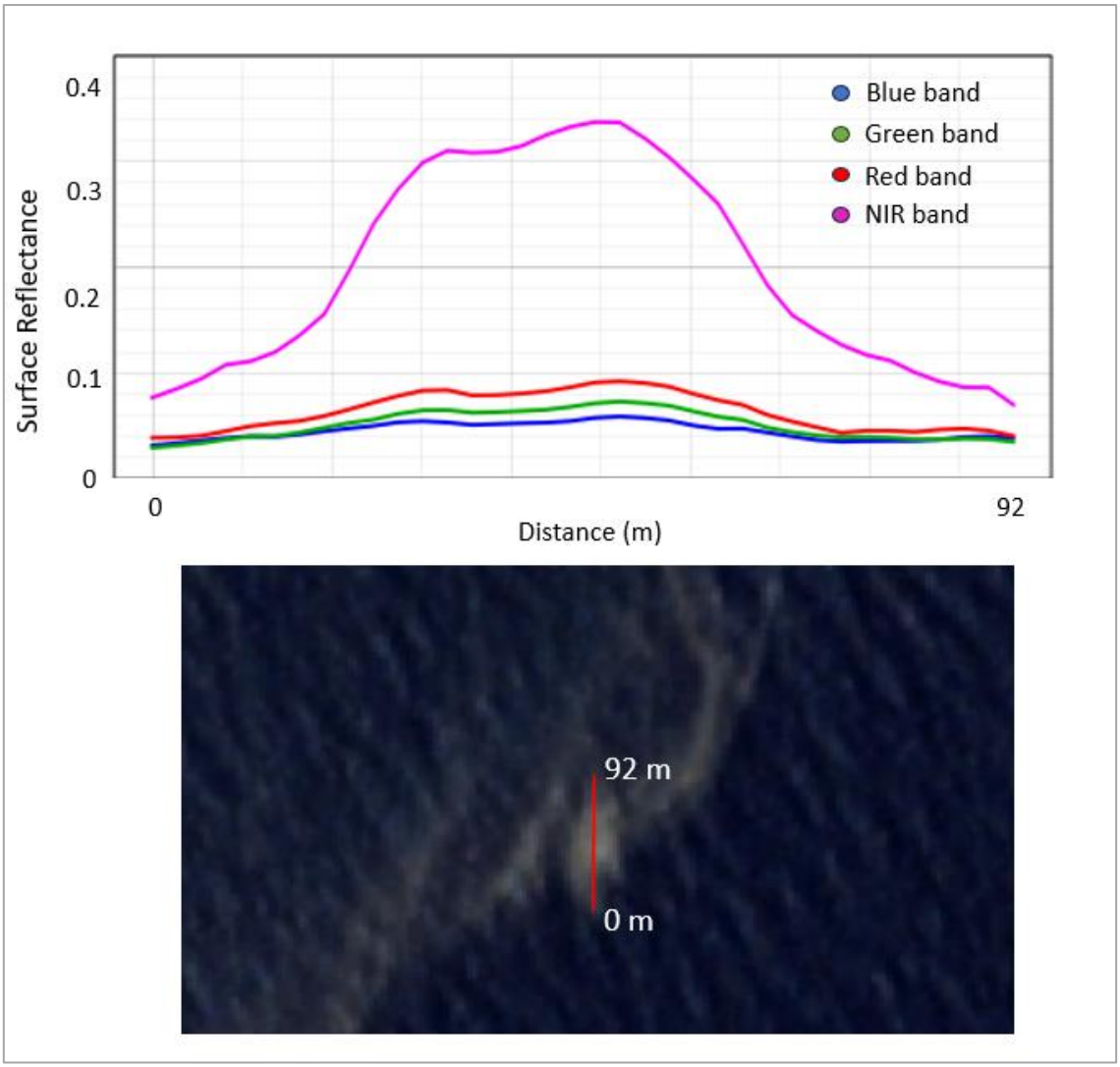

Figure 23. Profile plot showing how reflectance changes with the width of the slick.

7.4 SAR images and wind conditions

19 SAR images corresponding with optically detected slicks were analysed. The Sentinel-1 image names are in the standard naming convention used by ESA. Table 8 shows the list of Sentinel-1A scenes analysed and the corresponding wind conditions at acquisition time. The mean wind speeds were between 3 and 7 m/s and within the threshold for optimal oil-spill slick detection (Table 4). It should be noted that there are no studies on optimal thresholds for coral spawn detection, and the threshold may differ from those reported for oil slick detection. Thus, an inherent assumption in this work is that the optimal wind threshold for coral spawn slick detection is the same as for oil spills.

Table 8. List of Sentinel-1A images analysed in this study and corresponding ERA5 wind speed. The mean windspeed is calculated within the spatial extent (excluding landmass) of the Sentinel-1A image near acquisition time.

Image ID	Sentinel-1A image	Mean wind speed (m/s)
SAR01	S1A_IW_GRDH_1SDV_20181116T192018_20181116T192043_024617_02B431_6825	5.95
SAR02	S1A_IW_GRDH_1SDV_20181116T192043_20181116T192108_024617_02B431_3845	4.65
SAR03	S1A_IW_GRDH_1SDV_20191111T192050_20191111T192115_029867_036822_747A	6.36
SAR04	S1A_IW_GRDH_1SDV_20191111T192115_20191111T192140_029867_036822_8A8C	5.68
SAR05	S1A_IW_GRDH_1SDV_20191114T194413_20191114T194442_029911_0369A9_5D39	4.54
SAR06	S1A_IW_GRDH_1SDV_20191118T191231_20191118T191256_029969_036BAD_2379	4.09
SAR07	S1A_IW_GRDH_1SDV_20201204T192824_20201204T192853_035540_0427DB_7EEC	4.89
SAR08	S1A_IW_GRDH_1SDV_20201204T192853_20201204T192918_035540_0427DB_731F	4.56
SAR09	S1A_IW_GRDH_1SSH_20201204T083402_20201204T083430_035533_042794_D3F8	3.65
SAR10	S1A_IW_GRDH_1SDV_20211119T191243_20211119T191308_040644_04D26A_64E2	6.87
SAR11	S1A_IW_GRDH_1SDV_20211119T191308_20211119T191333_040644_04D26A_E297	5.66
SAR12	S1A_IW_GRDH_1SDV_20211119T191333_20211119T191358_040644_04D26A_5359	3.86
SAR13	S1A_IW_GRDH_1SDV_20211122T193626_20211122T193656_040688_04D3F6_1774	5.21
SAR14	S1A_IW_GRDH_1SDV_20221112T192836_20221112T192905_045865_057CCD_C1EE	6.15
SAR15	S1A_IW_GRDH_1SDV_20221112T192905_20221112T192930_045865_057CCD_C727	5.78
SAR16	S1A_IW_GRDH_1SDV_20221114T191220_20221114T191249_045894_057DB6_C151	3.18
SAR17	S1A_IW_GRDH_1SDV_20221114T191249_20221114T191314_045894_057DB6_30FF	5.60
SAR18	S1A_IW_GRDH_1SDV_20221114T191314_20221114T191339_045894_057DB6_0B78	5.89
SAR19	S1A_IW_GRDH_1SDV_20221114T191339_20221114T191404_045894_057DB6_72DD	6.28

7.5 Observations

In this section, the satellite imagery is analysed in depth. The spectral and proximity results are used to interpret optically detected slicks, and corresponding SAR imagery is assessed for potential slicks. The observation dates are based on the UTC+10 date of the PlanetScope images.

The summary of observations is as follows:

Slick characteristics

- **Colour variations and spatial extents**: The hues of slicks included green, brown and pink.
    - Green and brown slicks tended to be the most extensive, covering vast areas up to 70km long and were often hundreds of meters wide. *Trichodesmium and Sarragusm* surface aggregations are commonly green or brown and form extensive mats (Hu et al., 2010; Blondeau-Patissier et al., 2018; Wang et al., 2018),
    - The pink slicks tended to be smaller and more isolated. They reached lengths of approximately 5km and widths from 10 to 30m. These dimensions align with aerial observations of coral spawn slicks in the GBR by Oliver and Willis (1987).
- **Association with natural sea surface slicks:** The Identified slicks often aligned with apparent natural sea surface slicks, indicating the natural sea surface slicks may play an important role in coral spawn dispersal. It also raises the possibility that coral spawn slicks in SAR imagery may be hidden within natural sea surface slicks, making it difficult to assess their extent.

Slicks detected in SAR

- **Corresponding slicks**: In several cases, slicks could be matched between SAR and optical imagery. Some of these were likely biogenic slicks and not coral spawn.
    - 'Slicks' displayed either low or high backscatter compared to the surrounding sea. It is presumed that the slicks displaying high backscatter were macroalgae, whereas the ones displaying low backscatter were cyanobacteria blooms or coral spawn slicks.
    - There was one case where slicks in the SAR image roughly matched the geometry of a presumed coral spawn slick in the optical imagery; however, there is a significant presence of Look-Alike Features (LAF) in this image, making it challenging to make any assumptions confidently. Especially considering the coral spawn slicks are aligned with natural sea surface slicks in the corresponding optical data.
    - The optically detected slicks were not consistently detected in corresponding Sentinel-1A scenes, even though the wind conditions were mainly optimal. Temporal and spatial resolution differences may influence this; The Sentinel-1A imagery is captured ~ 3 hours earlier, and the spatial resolution of processed Sentinel-1A imagery is 10m compared to 3m for PlanetScope.
- **Presence of LAF in the GBR**: The results showed several types of LAF commonly occur in the GBR, which may complicate coral spawn detection.
    - Biogenic and natural sea surface slicks commonly occur near reefs and during spawning windows, increasing the potential for false detection.
    - Wind shadows caused large areas of SAR images to be masked. If a slick occurred within the wind shadow, it would be invisible.
    - Areas of low backscatter commonly occurred near reef features, including dark features displaying feathering patterns.
    - There is a possibility that previous research that presumed similar feathering patterns to be related to coral spawning may have made incorrect assumptions. Instead, this

pattern may be linked to reef bathymetry influencing sea surface smoothness. The SAR data here is captured near dawn, and it is unlikely that coral spawn slicks would still be directly on top of the reef.

7.5.1 Observations on 2016-12-22

Extensive brown slicks with slight pink hues were noted in the PlanetScope imagery between the Great Keppel Island and Flat Island Reef, measuring up to 12km long and mostly 10 to 30m wide with some occasional larger patches (Figure 24). The slicks exhibited positive RGR ratios of about 1.2 and relatively high NIR reflectance (Table 7), reaching up to NIR 0.5 reflectance in wide parts of the slicks. There are no recorded coral spawning observations within three days, and no overlapping Sentinel-1A imagery was available on this date.

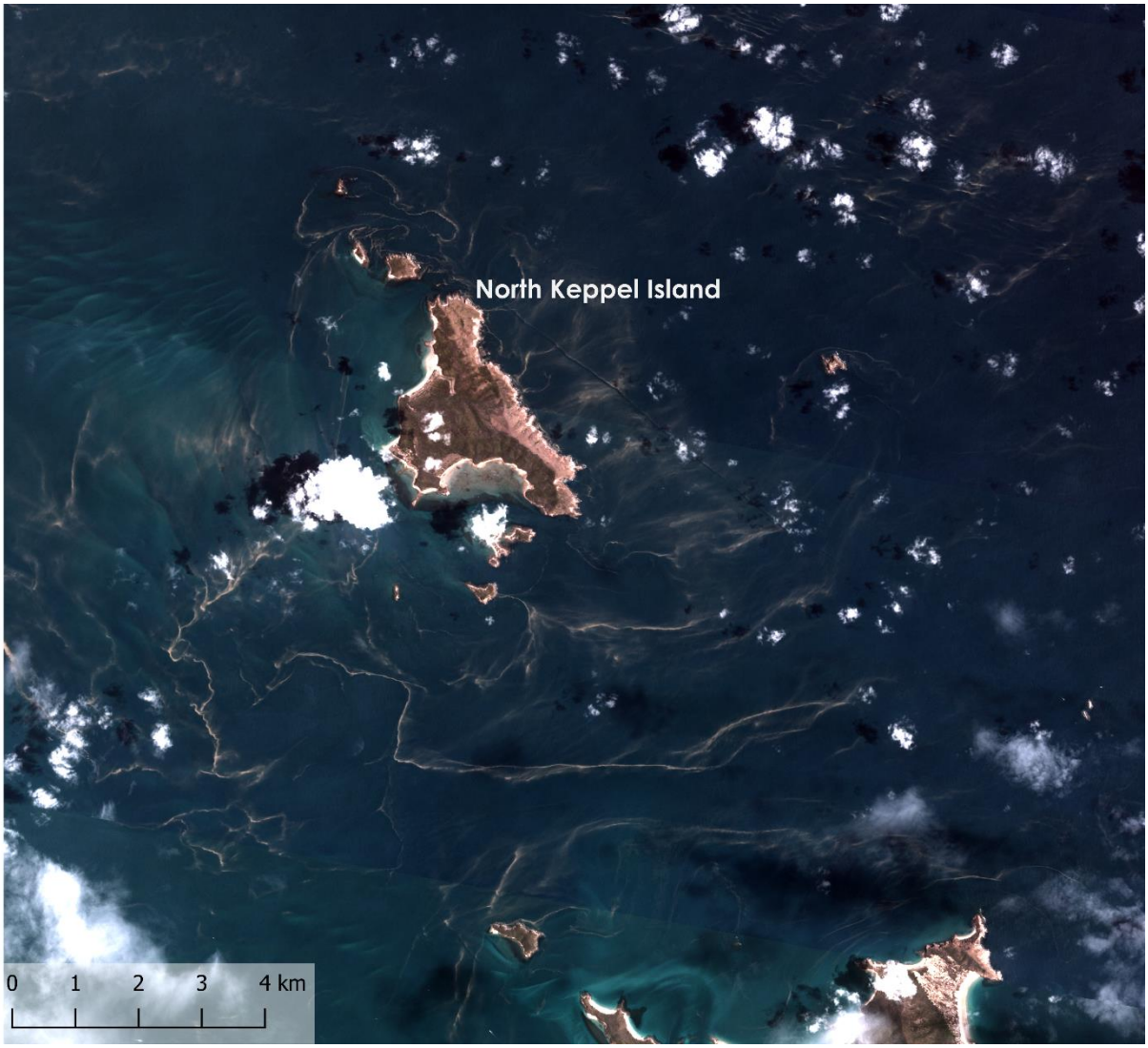

Figure 24. PlanetScope image in the Keppel Reef region with extensive biogenic slicks or possible coral spawn observed on 22 December 2016, 09:19 hours.

7.5.2 Observations on 2018-11-17

Slicks were detected along inshore reefs between K'gari Island and Townshend Island, with two distinct slick colours: green and brown with pink hues. The mean RGR were between 1 and 1.2 on this date (Table 7). There were no coral spawning observations within three days (Table 6).

The pinkish-brown collection of slicks was located near Lady Musgrave Reef, displaying feathering patterns in the direction of the wind (Figure 25a). The largest slick was approximately 15km long and 100m wide. The conditions for slick detection are met (Table 8), yet overlapping Sentinel-1A (SAR01 & SAR02) imagery showed no obvious slicks (Figure 25b).

The extent and colour of the green slicks indicate that they are *Trichodesmium* blooms. One of the slicks extends over 70km dispersed in a parallel linear pattern along the coast from Moore Park Beach to Agnes water. It is visible in PlanetScope and the corresponding Sentinel-1A imagery (Figure 25c-d). It appears to have travelled ~ 3km towards the coast between acquisition times, with light easterly winds (~3 m/s) inferred at SAR acquisition time.

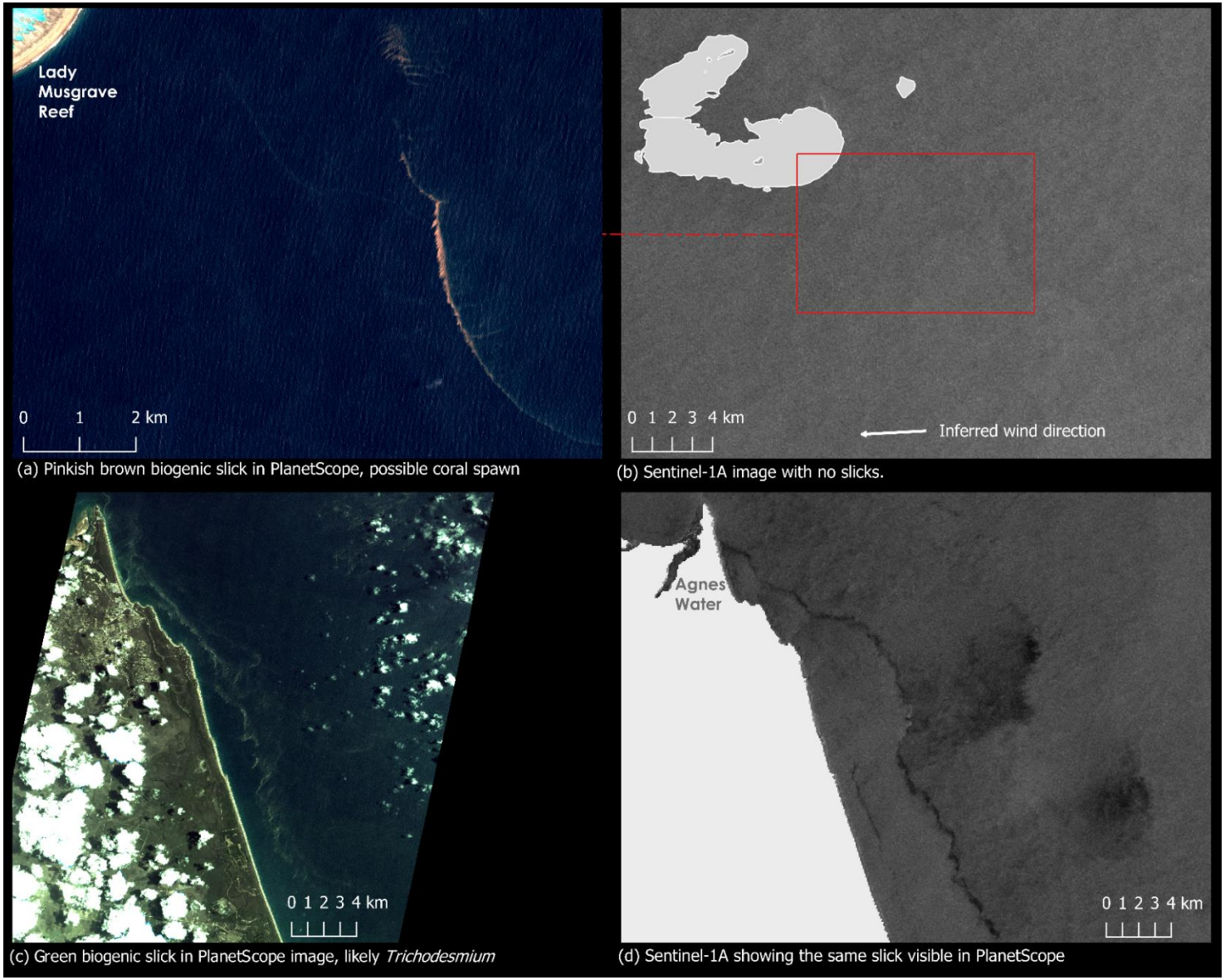

Figure 25. (a) A pinkish-brown slick visible in a PlanetScope image near Lady Musgrave Reef on 17 November 2018 at 09:32 hours. The slick displays a feathering pattern in the inferred wind direction (b) Sentinel-1A image with overlapping extent, showing no slicks, captured on 17 November 2018 at 05:21 hours. (c) A biogenic slick, likely Trichodesmium or another type of biogenic slick, in PlanetScope imagery on 17 November 2018 at 09:34 hours. (d) Sentinel-1A image showing the same slick in the PlanetScope image, captured on 17 November 2018 at 05:21 hours.

7.5.3 Observations on 2019-11-12

A group of brown slicks were detected around Heron Island, extending up to 12km long and 10 to 50m wide. In corresponding SAR data (SAR03 and SAR04), features displayed as bright pixels can be correlated to the slicks visible in the optical imagery (Figure 26). This contrast is consistent with previous observations of macroalgae, which appear as bright pixels compared to the surrounding sea due to volumetric scattering (Shen et al., 2014; Geng et al., 2020; Qi et al., 2022; Chowdhury et al., 2023). The colour and reflectance are consistent with *Sargassum* (Hu et al., 2015), with RGR values around 1.2 (Table 7).

There is a CSD record for spawning within 2km later that evening (Table 6). It is unclear if the CSD location is exact. The unpublished observation reported spawning from *Acropora hyacinthus*, *Acropora spathulata* and *Platygyra daedalea*. There is currently no spectra information for the spawning material of *Platygyra* corals.

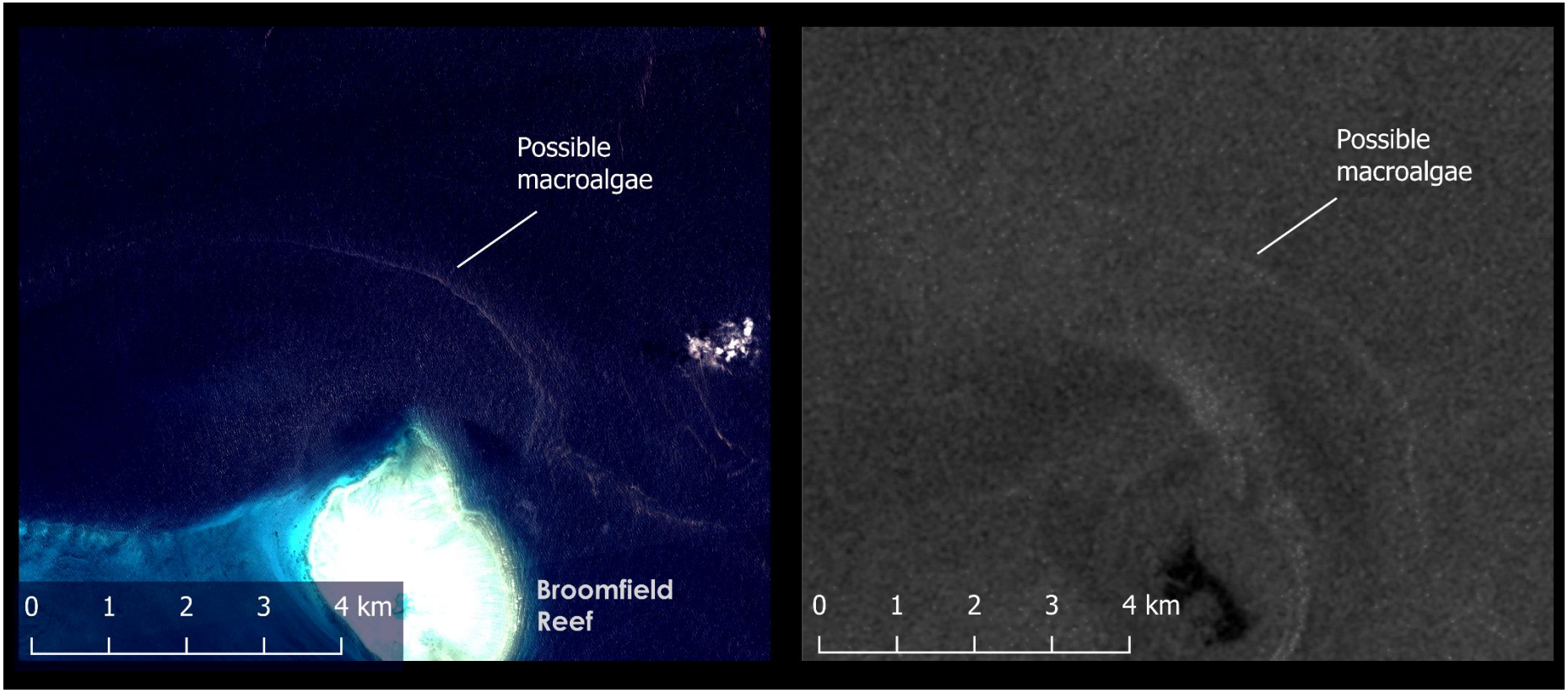

Figure 26. Presumed macro algae (possibly Sargassum) visible between PlanetScope (Left) and Sentinel-1 (right) imagery. The two images are displayed at the same extent and scale. PlanetScope image was acquired on 12 November 2019, 09:24 hours, and Sentinel-1A image on 12 November 2019, 05:20 hours.

7.5.4 Observations on 2019-11-14

Groups of slicks were detected along inshore areas from Great Palm Island to Tully Heads. They measured up to 10km in length and were between 10 and 50m wide. The slicks show relatively flat reflectance across the bands with RGR values less than 1 (Table 7), indicating that they are most likely *Trichodesmium* blooms or another type of biogenic slick. Possible natural sea surface slicks are also visible, which appear as darker smooth areas.

Slicks with similar geometry and curve shapes can be seen between SAR05 and MS10 (Figure 27). The SAR imagery is captured 19 hours 36 minutes after the PlanetScope imagery. The radar data is complicated by possible LAF, particularly in the eastern side of the image, possibly caused by wind shadows or natural sea surface slicks.

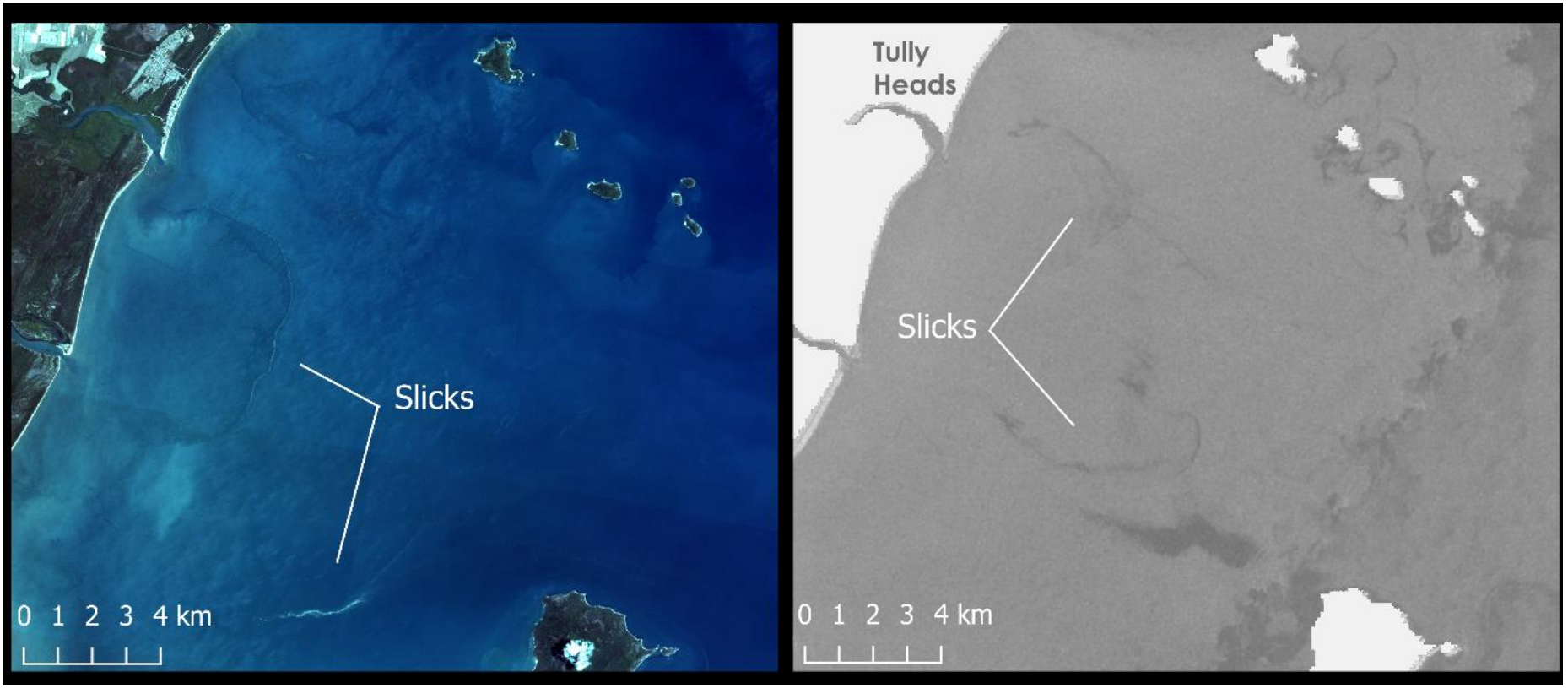

Figure 27. (left) Biogenic slick visible in PlanetScope on 14 November 2019, 10:07 hours and (right) Sentinel-1A on 15 November 2019, 05:44 hours. The images are at the same extent and scale. Some of the dark features in the Senintel-1A on the right half are likely LAF, possibly Low winds areas or natural sea surface slicks.

7.5.5 Observations on 2019-11-19

Clusters of brown slicks throughout the Northumberland Islands region (Figure 28), with another group at Credlins Reef (~100km offshore from Mackay), were detected on this date. They measured up to 12km long and up to 80m wide. These slicks exhibited RGR values between 0.8 and 1.2. The slicks were often aligned with apparent natural sea surface slicks. There was no corresponding Sentinel-1A imagery in this area.

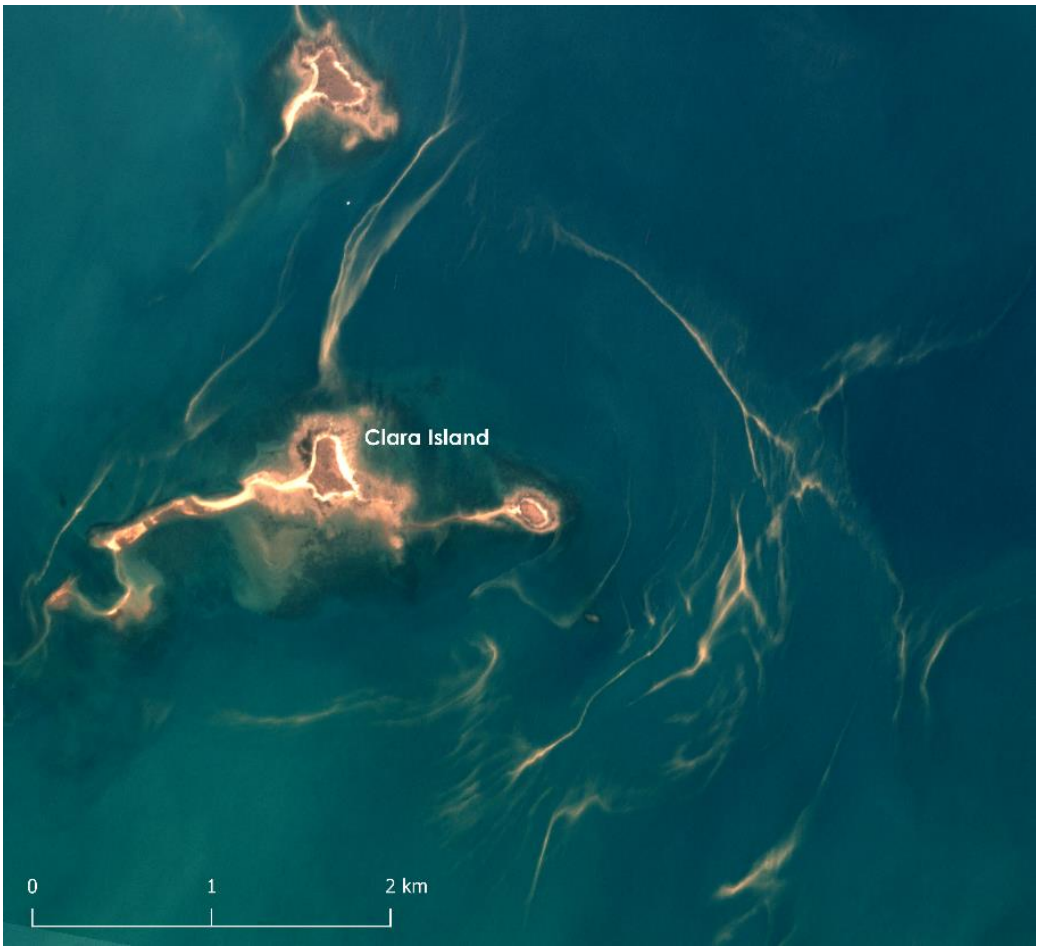

Figure 28. Biogic slick or possible coral spawn in PlanetScope imagery near Clara Island on 19 November 2019, 09:48 hours.

Pink-hued slicks were identified in the Swains Reef Region (MS14-16), extending upwards of ~5km long and typically ranging from 10 to 20m wide. These geometric characteristics correspond strongly with previous aerial surveys of coral spawn slicks in the GBR, as Oliver and Willis (1987) reported. The slicks mostly displayed positive RGR values around 1.3, with some pixels In the widest parts of slicks reaching up to 1.5. Additionally, coral spawning observations are reported multiple times within three days, with the closest being ~125km away (Table 6). Therefore, relatively strong evidence suggests they are coral spawn slicks.

Sunglint significantly affects some images, accentuating apparent natural sea surface slicks with which the identified coral spawn slicks are frequently aligned (Figure 29a). This observation indicates that natural sea surface slicks may influence the dispersal of coral spawn.

Some of the slicks overlap with Sentinel-1A imagery (SAR06). The conditions for slick detection are met with light easterlies (4.09 m/s) at acquisition time. Faint slicks are visible in the same region as the presumed coral spawn slick identified in the Planet Scope (Figure 29c). These slicks roughly match the geometry of those identified in PlanetScope. However, whether they are coral spawn slicks or the natural sea surface slicks visible in the optical imagery is unclear. If the coral spawn slicks are aligned with the natural sea surface slicks, they may be impossible to discriminate in the SAR imagery. Moreover, the broader extent reveals extensive slicks and dark patches from wind shadows (Figure 29d). These slicks span a vast area and are sometimes over 100m wide, suggesting they are mostly LAF.

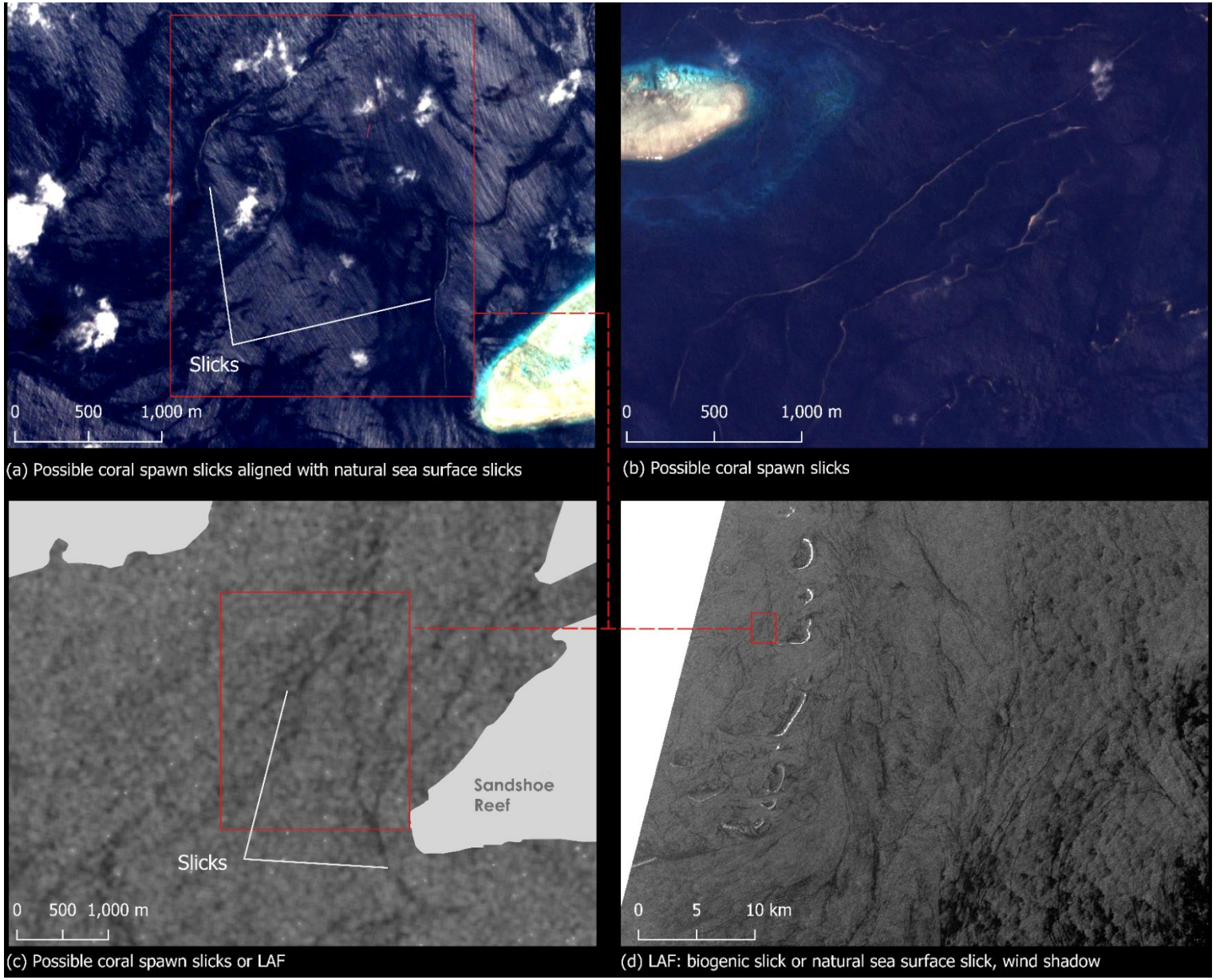

Figure 29. Possible coral spawning slicks and/or LAF in PlanetScope (a-b) and Sentinel-1A images (c-d). The red boundary shows equal geometry between images. Acquisition dates: (a) PlanetScope image captured on 19 November 2019 at 09:41 hours, (b) PlanetScope image captured on 19 November 2019 at 09:39 hours, (c-d) Sentinel-1A images captured on 19 November 2019 at 05:12 hours.

7.5.6 Observations on 2020-12-05

On this day, green slicks were detected in Southern GBR from Burnnet River to North Keppel Island, and there was an aggregation between Lady Musgrave Reef and Herald Patches. The slicks are up to 10km long and 200m wide and have RGR less than 1, indicating that they are most likely *Trichodesmium* blooms. Sentinel-1A imagery in the area shows numerous slicks (SAR07 and SAR08). One of the Sentinel-1A images here is HH single-polarization (SAR09), and no slicks are visible even though extensive slicks are visible in the overlapping area in PlanetScope.

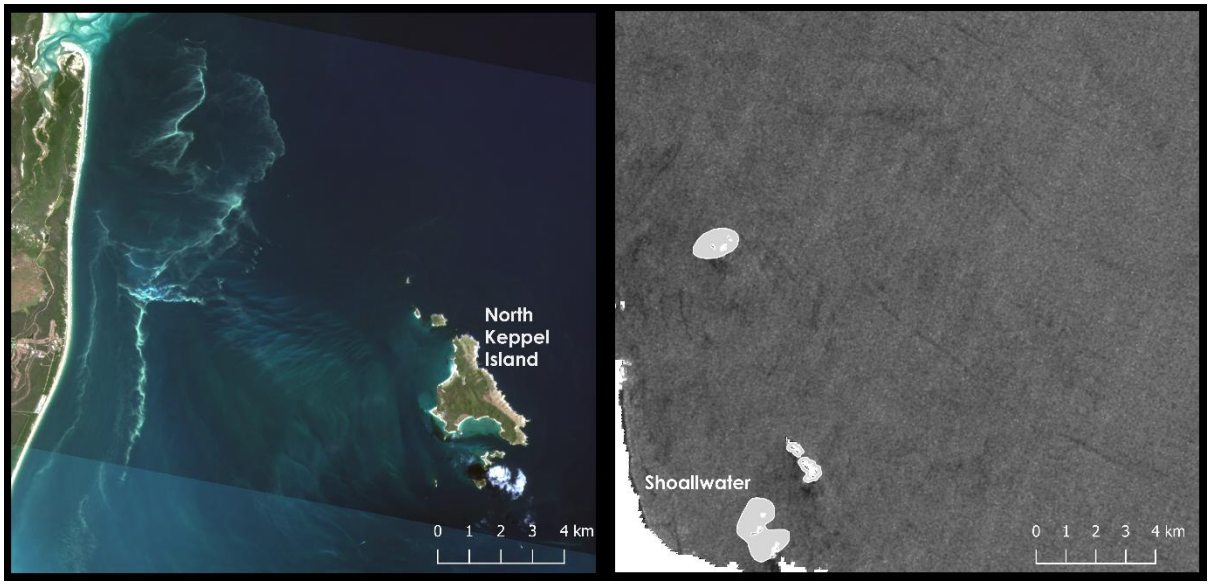

Figure 30. (left) Possible biogenic slick (Trichodesmium) in PlanetScope image on 5 December 2020 at 09:46 hour. (right) Several slick-like linear features are visible in the Sentinel-1A on 5 December 2020 at 05:28 hours. This area is slightly north of the extent of the PlanetScope image.

7.5.7 Observations on 2021-11-20

On this day, extensive Green slicks were detected from Rockhampton to K'gari, extending up to 30km long, with large patches over 500m wide. The slick mainly exhibited higher NIR reflectance than visible bands and had RGR values less than 1 (Table 7). There are Sentinel-1A images with overlapping geometry with many of the slicks on this date (SAR10-12). Conditions for slick detection are met (Table 8), yet no distinct slicks are detected in proximity to optically detected slicks. The reflectance and extent of the slicks suggest that they are algal blooms, possibly *Trichodosium.*

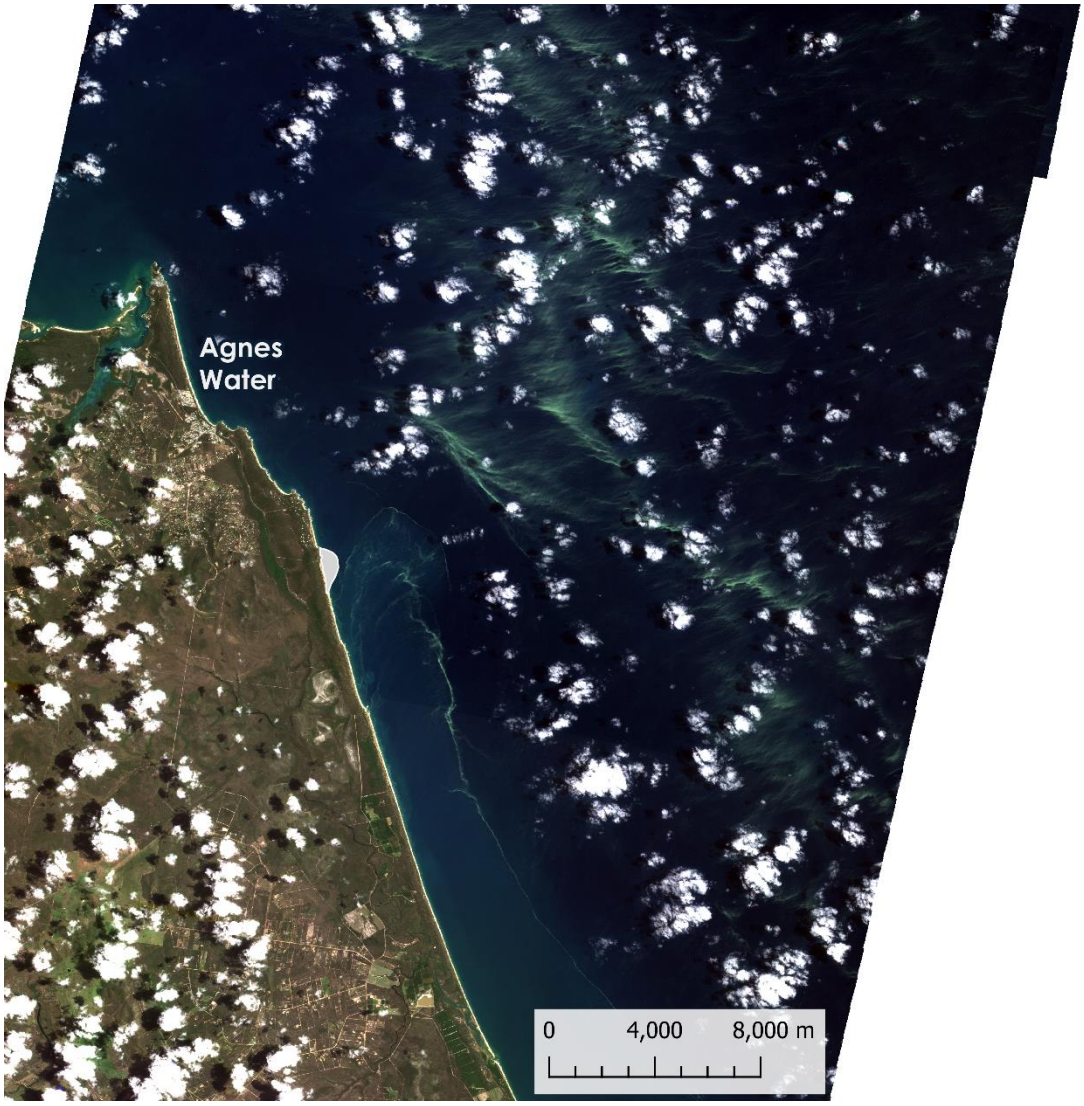

Figure 31. Extensive biogenic slicks (likely Trichodesmium) in PlanetScope image on 20 November 2021, 09:09 hours.

7.5.8 Observations on 2021-11-23

Two groups of distinctly pink-hued slicks were detected in the Far Northern Management area, specifically at Lagoon Reef and another 5km north of Cat Reef (MS27 and MS29). The slicks ranged from 1.5km to 4km in length and were approximately 10m wide, with larger patches up to 30m wide. The mean RGR of these slicks was approximately 1.3 (Table 7). Pixels in the centre of wide patches exhibited RGR values up to 2.1 (Figure 32).In contrast, narrower sections displayed decreasing RGR values, often below 1, rendering significant portions of the slick invisible when using an RGR threshold of 1. There are coral spawning observations within the period several hundred km away, which is expected due to the remoteness of these locations. The spectral reflectance, geometry, and proximity to the reef of the slicks confidently indicate that they are from coral spawning. No corresponding Sentinel-1A imagery was available at these locations on this date.

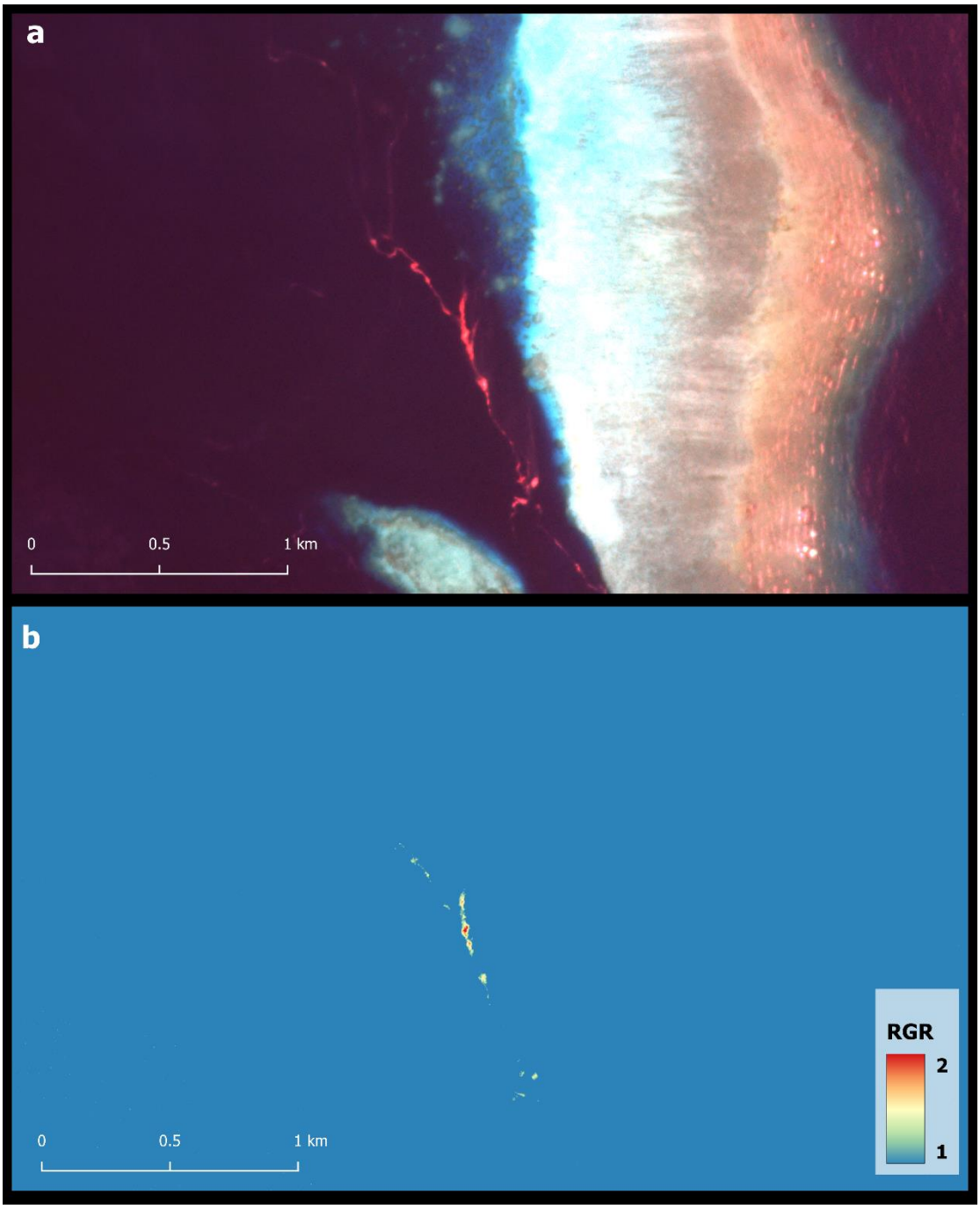

Figure 32. (a) PlanetScope RGB imagery of possible coral-spawn slick. (b) The same area mapped using a red/green band ratio (RGR) index. RGR increases with the width of the slick, with narrow parts of the slick having RGR less than 1. Approximate location: -12.9404808°, 143.818421°. Observed on 23 December 2021, 09:48 hours.

In images MS26 and MS28, wide-ranging green slicks are visible between Whitsunday Island and Bowen, extending up to 30km long and 300m wide (Figure 33). These have pixels with low RGR and are likely *Trichodesmium* blooms. They are not visible in the corresponding Sentinel-1A imagery captured in this area on the same day.

Offshore from Bowen, numerous dark features are visible in Sentinel-1A (SAR13) between Circular Quay Reef and Bowl Reef. These include dark patches, which may be attributed to the reef structures influencing sea surface smoothness (Blondeau-Patissier et al., 2023). Some dark features exhibit feathering in the approximate direction of the wind (Figure 33b). The feathering patterns are similar to features identified by Jones et al. (2006) that were presumed to be the early stages of coral spawning. Here, the Sentinel-1A data is captured at 5:36 am. Coral spawning generally occurs shortly after dusk (Harrison & Wallace, 1990). Therefore, a coral spawn slick would likely be dispersed further away from the reef by the following morning (Harrison & Wallace, 1990; Willis & Oliver, 1990), suggesting that the feathering patterns may be related to the reef bathymetry rather than coral spawn slicks.

Linear slick features are also visible in this area (Figure 33b). Smooth streaks of water, possibly representing natural sea surface slicks, are visible in the PlanetScope imagery in this area. No biogenic or coral spawn slicks are visible.

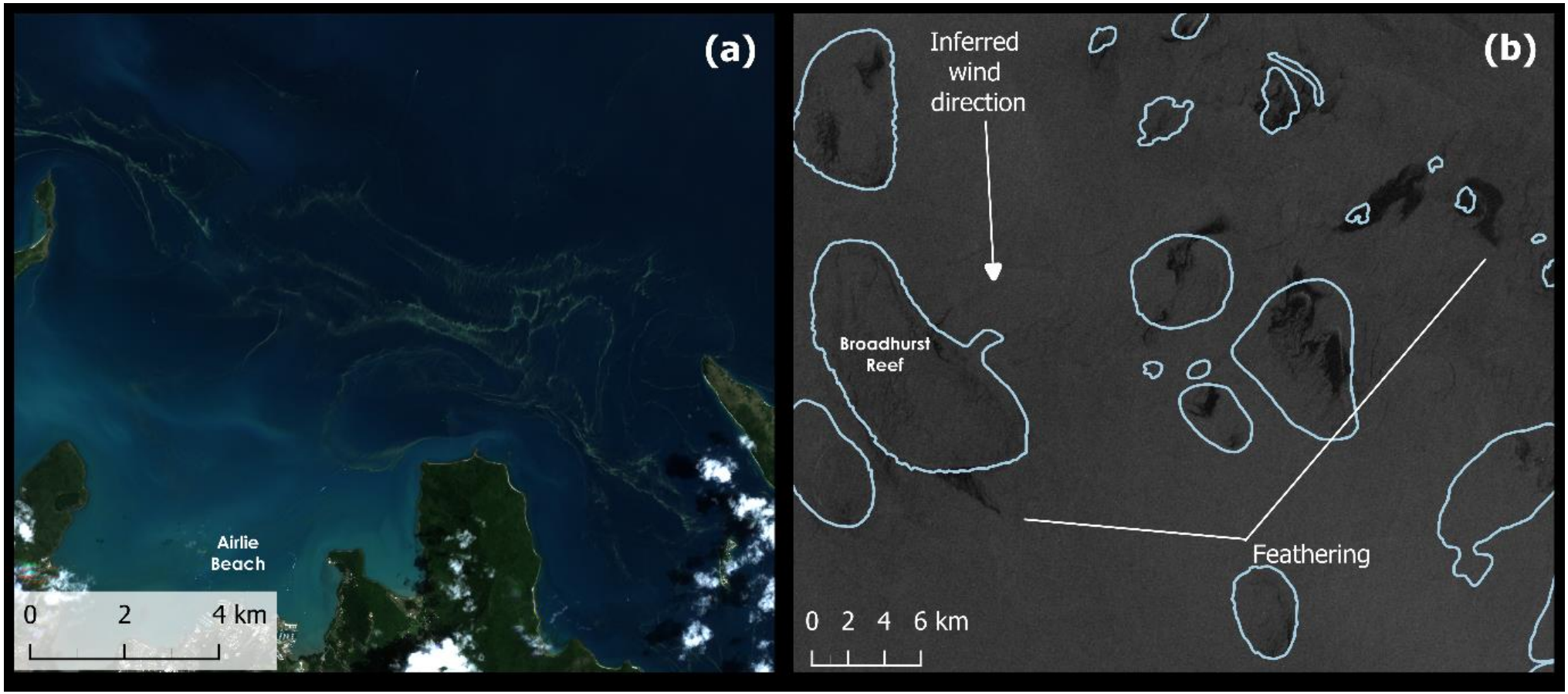

Figure 33. (a) Biogenic slicks in a PlanetScope image near Airlie Beach on 23 November 2021, 09:25 hours (b) A possible LAF is exhibiting feathering patterns in Sentinel-1A on 23 November 2021, 05:36 hours. The blue lines represent GBRMPA reef outlines.

7.5.9 Observations on 2022-11-13

Wide-spread green-hued slicks were detected between Rockhampton and 100km north of Mackay. Some slicks were over 10km long and up to 150m wide. Two Sentinel-1A (SAR14-15) images from the same day have matching geometry. The SAR imagery found no distinct slicks within 10km of optically detected slicks. Numerous dark features associated with reef structures and islands were present, including features displaying feathering patterns in the same direction as the wind (Figure 34) and, again, resembling what Jones et al. (2006) described as the early stages of coral spawn slicks.

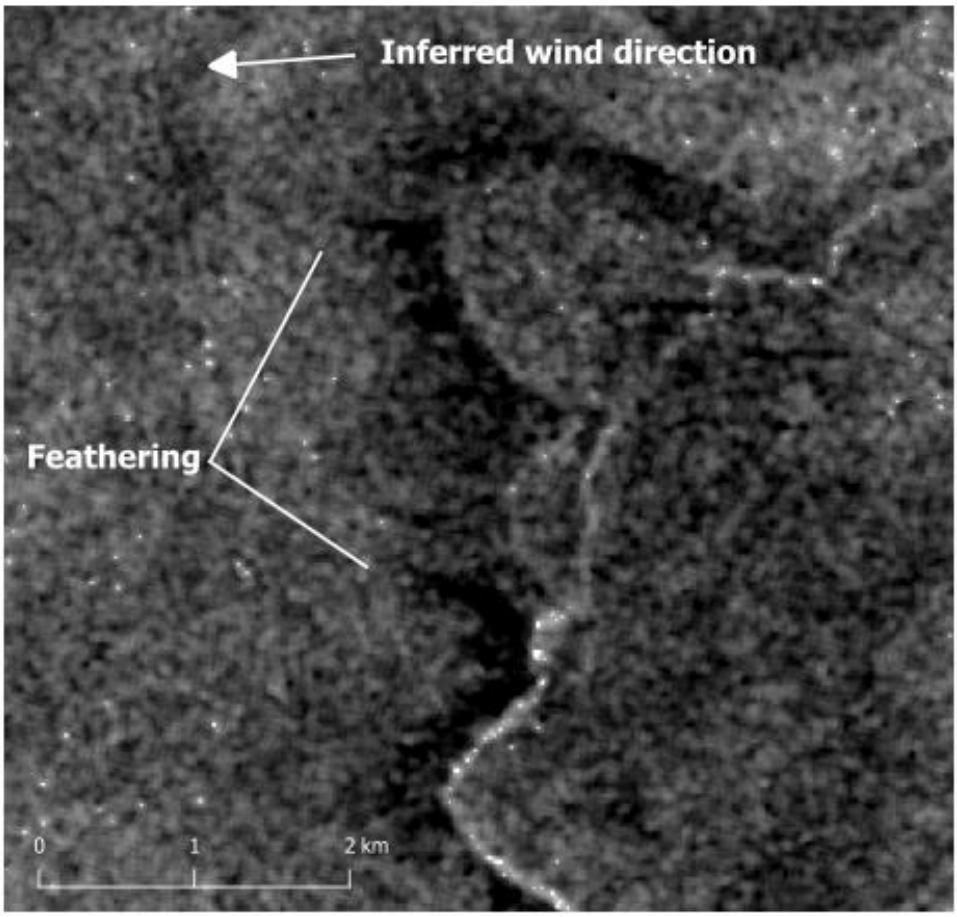

Figure 34. SAR image with dark features displaying feathering patterns adjacent to a reef structure, observed on 13 November 2022, 05:28 hours

7.5.10 Observations on 2022-11-15

On this date, clusters of green-hued slicks were detected around Hervey Bay and K'gari Island, reaching up to 5km long and between 10 and 30m wide. All the slicks on this date displayed RGR less than 1, and considering green-coloured coral spawn slicks have not been reported, they are likely *Trichodesmium* blooms. Sentinel-1A (SAR16-19) imagery from the same day has matching geometry, yet no slicks were detected even though conditions for slick detection were met (Table 8).

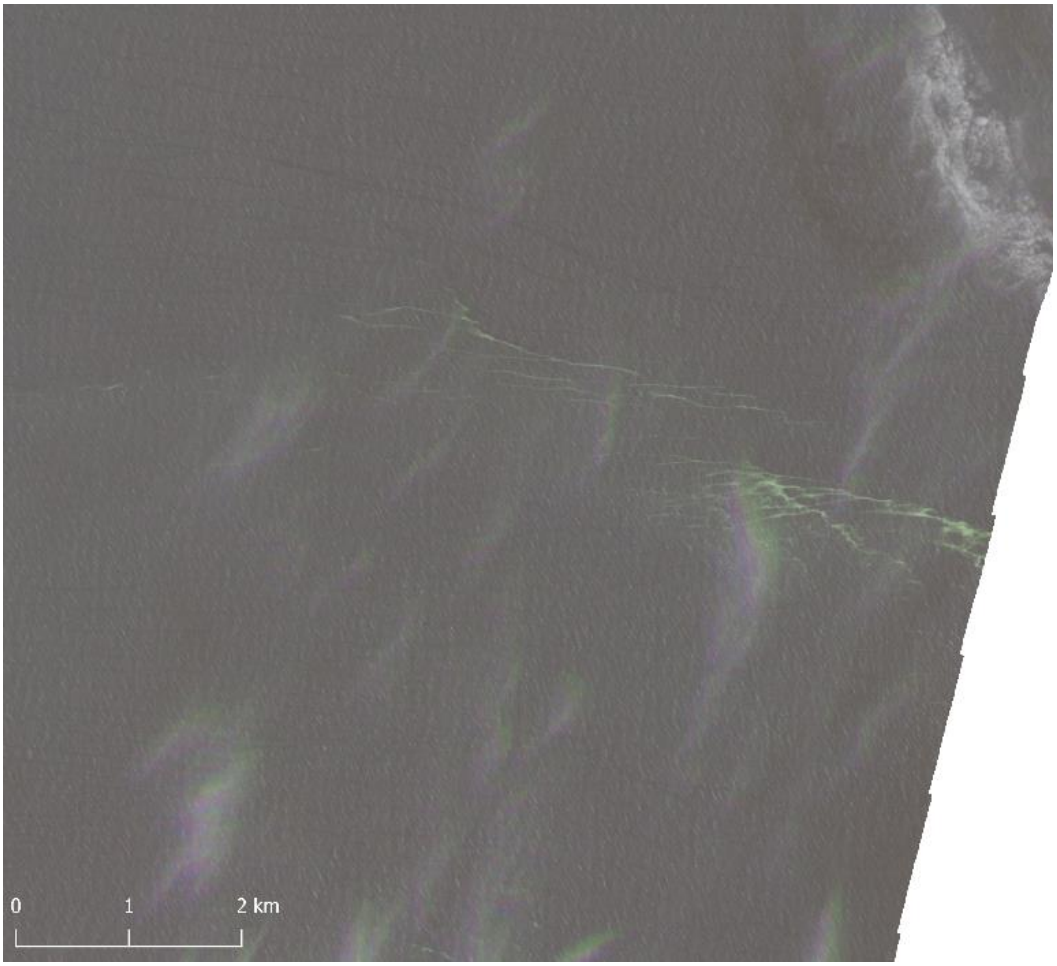

n

Figure 35. Probable biogenic slicks in PlanetScope image on 15 November 2022, 09:31 hours. Approximate location: -26.1462°, 153.4333°.

8 DISCUSSION

This study is the first attempt to compare multispectral and SAR imagery for detecting coral spawn slicks. The research addresses the limitations of both data types and suggests areas of focus for future research. Moreover, a database of slicks in the GBR has been generated and made freely available for further study.

Detection and identification of slicks

Slicks with a solid resemblance to coral spawn were detected on two days, supported by the spectral and proximity analysis. These slicks had pink hues, and their morphology matched previous descriptions of coral spawn slicks in the GBR (Oliver & Willis, 1987). These were close to reefs and were approximately 10 to 30m wide with lengths up to 5km. They displayed high Red / Green reflectance ratios (RGR) of around 1.5 to 2.1 and a distinct 'red edge' effect.

Many of the slicks extended to vast areas well beyond the sizes reported for coral spawn slicks. These were possibly *Trichodesmium* blooms or other biogenic slicks. The reflectance of the slicks often agreed with that of *Trichodesmium* (Hu et al., 2010; McKinna et al., 2011; Hu et al., 2015; Rousset et al., 2018), i.e., higher blue/green reflectance compared to red and increased NIR reflectance (as shown in Figure 12).

RGR was adequate for identifying coral spawn but was limited by the spatial resolution of PlanetScope. Only regions wider than ~30m exhibited high RGR values that met the threshold Yamano et al. (2020) used to discriminate coral spawn, which is a significant limiting factor, considering coral spawn slicks are generally about 10 to 20m wide (Oliver & Willis, 1987; Jamodiong et al., 2018; Yamano et al., 2020). In the narrower parts, minimal spectral differences distinguish them from other observed slicks in the four PlanetScope bands used in this study. Similar findings have been observed where low-resolution MODIS data was ineffective at mapping *Trichodesmium* blooms due to weak spectral signals from mixing with adjacent water pixels (Hu et al., 2010; McKinna et al., 2011; Rousset et al., 2018).

A limitation of the spectral analysis is that the Yamano et al. (2020) study used TOA reflectance products and employed their own image correction methods (dark-pixel corrections). In contrast, most of the images here were surface reflectance products, and the PlanetScope images came as pre-processed products with corrections already applied using standard Planet algorithms. Here, data from multiple PlantScope generations, whereas Yamano et al. (2020) only used PS2. Therefore, there are limitations in making direct comparisons between these two studies.

Slicks could be matched between PlanetScope and Sentinel-1 in several cases, though not consistently. These were primarily associated with areas of low backscatter (e.g., Figure 25, Figure 27, Figure 29 and Figure 30) or high backscatter in contrast to the surrounding sea surface in one case (Figure 26).

In one case, a slick matched the geometry of a probable coral spawn slick visible in PlanetScope (Figure 29). However, in the optical imagery, there was a significant presence of natural sea surface slicks, and the coral spawn slicks were often contained within them. Oliver and Willis (1987) observed that coral spawn slicks were frequently associated with fronts between water parcels, and wakes and eddies behind reefs. Their findings and those in this study suggest that coral spawn slicks may often be hidden within other wave-dampening features in SAR imagery, making them virtually undetectable.

There were some examples where large green-hued slicks could be matched between SAR and optical imagery (Figure 25, Figure 27, and Figure 30). They were visible as areas of low backscatter compared to the surrounding sea surface. These slicks exhibited low RGR values in corresponding optical imagery

(Table 7). The evidence points towards these being cyanobacteria blooms, such as *Trichodesmium,* forming as films on the sea surface and dampening capillary waves.

Previous research has shown that macroalgae will generally appear as bright pixels compared to the ambient sea surface in SAR images due to their volumetric properties when exposed above the sea surface (Shen et al., 2014; Geng et al., 2020; Qi et al., 2022; Chowdhury et al., 2023). Therefore, the floating material that displayed a high backscatter is most likely *Sargassum* or another type of macroalgae.

The discrepancy between slicks in PlanetScope not being visible in Sentinel-1A could be influenced by several factors, including temporal differences, macroalgae submergence, and resolution issues. The Sentinel-1A data tended to be acquired 3 hours earlier than the PlanetScope in this study due to PlanetScope and Sentinel-1A having sun-synchronous orbits. *Trichodesmium* can alter their buoyancy and most commonly aggregate at the surface during clear days with calm seas (Ani et al., 2023). In cases where *Trichodesmium* slicks were visible in PlanetScope but not in Sentinel-1A, it is possible that the *Trichodesmium* had not aggregated at the surface at SAR acquisition time. Additionally, macroalgae may be submerged beneath the sea surface, making it undetectable in SAR (Chowdhury et al., 2023). Furthermore, it could be that the resolution of the Sentinel-1 data was not sufficient. These inconsistencies are also reported by Qi et al. (2022), who also did not consistently detect various species of algae using Sentinel-1 data.

Revaluation of prior research

The evidence that two previous studies detected coral spawn slicks using SAR may be insufficient:

(i) The phenomena Jones et al. (2006) described as early stages of coral spawning could instead be attributed to reef features influencing radar backscatter. Similar features were observed in this study, and no slicks were visible in the corresponding optical imagery. Additionally, the SAR data used here was captured at dawn, and it is unlikely that coral spawning would be in its early stages, as corals spawn shortly after dusk (Babcock et al., 1986). Dark features were frequently observed near reef formations, likely caused by eddies behind reefs, highlighting the challenge of look-alike features (LAF) when detecting coral spawn slicks using SAR.

(ii) Cresswell et al. (2019) used coarse resolution (100m) RADARSAT-1 data, suggesting the observed features were several hundreds of meters wide. These sizes are unusual for coral spawn slicks. Such magnitudes have only been reported at Coral Bay, where slicks failed to disperse and were trapped in the bay (Simpson et al., 1993; Baird et al., 2023). What Cresswell et al. (2019) observed was possibly a biogenic slick or a bathymetry-related phenomenon instead.

Coral spawn spectra

More research into the spectral characteristics of coral spawn slicks is required. Research similar to Yamano et al. (2020) could combine field measurements with satellite observations, focusing on finding spectral differences between coral spawn slicks and other floating materials. In the GBR, finding key spectral differences from *Trichodesmium* is a priority.

The results of this study, and that of Yamano et al. (2020), show that PlanetScope data has limitations for coral spawn slick detection, especially regarding its spatial and spectral resolution (Table 1). Higher-resolution sensors could improve coral spawn slick discrimination, particularly those with multiple narrow, non-visible bands, such as Worldview-3, which has a resolution of 1.24m and several bands in the non-visible spectral. Furthermore, a multi-sensor approach may be needed to capture spawning events fully due to their widespread and remote nature.

The RGR as a spectral index is promising, but it is unclear if it would be effective for slicks from species other than *Acropora spp*. Brown-hued coral spawn slicks may be made up of *Montipora* bundles (Yamano et al., 2020), whose eggs generally contain symbiotic algae (Hirose et al., 2001), and relatively low RGR values may be shown due to the absorption peak of chlorophyll at 680nm. The spectral properties change as the coral spawn decays and becomes a milky white colour (Oliver & Willis, 1987; Yamano et al., 2020). Therefore, further development of the spectral library of coral spawn slicks is needed and to investigate various indicies that may improve detection.

Moreover, hyperspectral imagery could also enhance the detection of coral-spawn slicks by enabling the differentiation between the coral species represented in a slick based on the subtle spectral differences observed in laboratory measurements. Identification at a species level could provide significant ecological insights for more targeted conservation strategies. Underwater hyperspectral imagery has successfully been used to classify the benthic communities of coral reef ecosystems (Mills et al., 2023; Teague et al., 2023).

Multispectral and SAR integration

The integration of SAR and multispectral imagery is shown here to have some advantages. When used in conjunction, the ability of multispectral imagery to measure unique spectral signatures and SAR's sensitivity to surface structure should improve coral spawn slick detection. Future applications could employ a decision tree method combining SAR and multispectral data to help discriminate slicks. For instance, if a slick displays positive backscatter, it can be ruled out from being coral spawn.

SAR limitations

This study highlights that coral spawn detection in the GBR using SAR is challenged by several phenomena that may cause LAF, including biogenic slicks, natural sea surface slicks, bathymetry, reef features and low wind regions. The main limiting factor for studies on detecting coral spawn slicks with SAR is a lack of ground truth. An ideal future step would be to combine in-situ measurements with the simultaneous acquisition of SAR and multispectral data from either aircraft or satellite-mounted systems. This would provide a robust analysis of remote sensing methods for monitoring coral spawning events and help rule out the possibility of false detections.

The spatial resolution of Sentinel-1 may be too coarse to effectively detect coral spawn slicks, which are usually only a few meters wide. The spatial resolution after processing was 9m. At this resolution, the slicks may be invisible or appear as faint linear features. SAR systems with higher resolution should be explored, such as ICEYE, which has a resolution down to 0.5m.

Automatic detection of coral spawn slicks

The rapid advance in artificial intelligence (AI) has proved effective in marine monitoring applications, so the automatic detection of coral spawn slicks is increasingly feasible. For example, machine learning and deep learning algorithms have increased the accuracy of oil spill detection using SAR compared to traditional techniques (Matkan et al., 2013; Qi et al., 2023). Traditional methods include thresholding algorithms, which involve setting a specific backscatter threshold used to classify pixels in the image (Alpers et al., 2017; Wu et al., 2018). These techniques are simple but susceptible to false detections (Alpers et al., 2017). On the other hand, machine-learning algorithms can analyse complex patterns in the data to find subtle differences between features (Blondeau-Patissier et al., 2023). Machine learning algorithms generally require significant training data for high accuracy (Blondeau-Patissier et al., 2023). The slicks identified in this study could be used as training data in future studies.

9 CONCLUSIONS

The research objectives were met through a structured approach combining extensive literature review, data collection, and analysis. The literature review provided a solid understanding of summarising remote sensing methods for detecting coral spawn slicks and differentiating similar phenomena. Numerous slicks were detected in PlanetScope imagery between 2016 and 2022 in the GBR. These locations are provided as a database and can be explored in future research.

There is relatively high confidence that these belonged to coral spawn on two dates. These slicks had pink hues, were localised near reefs, and had smaller geometry than the other identified slicks. The Red / Green ratio (RGR) index effectively discriminated coral spawn slicks. However, it was hindered by the spatial resolution of PlanetScope imagery. Narrower parts of the slicks exhibited low RGR values, with minimal spectral differences compared to the identified algal blooms. The geometry and reflectance of most other slicks suggest that they are likely cyanobacteria blooms or macroalgae, such as *Trichodesmium* and *Sargassum*. The findings highlight that algal blooms are common during coral spawning periods. Another critical observation was that slicks were often aligned within natural sea surface slicks, suggesting this phenomenon may play a role in coral spawn dispersal.

On one occasion, a Sentinel-1A scene overlapped with presumed coral spawn slicks identified in PlanetScope, and slick features could be matched between the images. However, the presence of apparent natural sea surface slicks containing coral spawn slicks in the optical imagery raised uncertainty about the nature of the slicks detected in Sentinel-1A. Presumed algae blooms could occasionally be linked between SAR and optical imagery. Green slicks, possibly *Trichodesmium* blooms, were associated with negative backscatter compared to the surrounding sea surface. In one scene, a brown slick was related to positive backscatter; it is theorised that this was a macroalgae mat, possibly *Sargassum.*

The integration of multispectral and SAR is promising, and this study shows how these technologies can complement each other. Multispectral imagery may be preferred due to its higher ability to differentiate features based on spectral properties. The main limitation of SAR is the high presence of LAF and the lack of ability to distinguish between them. However, SAR can fill the gaps, i.e. when multispectral data is unavailable or there is cloud cover. When combined with multispectral imagery, SAR can provide insights into the surface structure and aid in discriminating cora spawn slicks. For example, features that display positive backscatter can be ruled out from coral spawn.

.

10 REFERENCES

Alavipanah, S. K., Matinfar, H. r., Rafiei Emam, A., Khodaei, K., Bagheri, R., & Panah, A. (2008). Criteria of selecting satellite data for studying land resources.

Alpers, W., Holt, B., & Zeng, K. (2017). Oil spill detection by imaging radars: Challenges and pitfalls. *Remote Sensing of Environment*, *201*, 133-147. https://doi.org/https://doi.org/10.1016/j.rse.2017.09.002

Álvarez-Romero, J., Devlin, M., Silva, E., Petus, C., Ban, N., Pressey, R., Kool, J., Roberts, J., Cerdeira-Estrada, S., Wenger, A., & Brodie, J. (2013). A novel approach to model exposure of coastal-marine ecosystems to riverine flood plumes based on remote sensing techniques. *Journal of Environmental Management*, *119C*, 194-207. https://doi.org/10.1016/j.jenvman.2013.01.036

Angelliaume, S., Dubois-Fernandez, P. C., Jones, C. E., Holt, B., Minchew, B., Amri, E., & Miegebielle, V. (2018). SAR imagery for detecting sea surface slicks: Performance assessment of polarization-dependent parameters [Periodical]. *IEEE Transactions on Geoscience and Remote Sensing, Geoscience and Remote Sensing, IEEE Transactions on, IEEE Trans. Geosci. Remote Sensing*, *56*(8), 4237-4257. https://doi.org/10.1109/TGRS.2018.2803216

Ani, C. J., Smithers, S. G., Lewis, S., Baird, M., & Robson, B. (2023). eReefs modelling suggests Trichodesmium may be a major nitrogen source in the Great Barrier Reef. *Estuarine, Coastal and Shelf Science*, *285*, 108306. https://doi.org/https://doi.org/10.1016/j.ecss.2023.108306

Babcock, R. C., Bull, G. D., Harrison, P. L., Heyward, A. J., Oliver, J. K., Wallace, C. C., & Willis, B. L. (1986). Synchronous spawning of 105 scleractinian coral species on the Great Barrier Reef. *Mar Biol*, *90*, 379–394 https://doi.org/https://doi.org/10.1007/BF00428562

Bair, E. H., Dozier, J., Rittger, K., Stillinger, T., Kleiber, W., & Davis, R. E. (2023). How do tradeoffs in satellite spatial and temporal resolution impact snow water equivalent reconstruction? *The Cryosphere*, *17*(7), 2629-2643. https://doi.org/10.5194/tc-17-2629-2023

Baird, A., Crosbie, A., Mera, H., Gudge, S., & Ross, C. (2023). High coral mortality following coral spawning in Coral Bay, Western Australia. *Galaxea, Journal of Coral Reef Studies*, *25*, 35-36. https://doi.org/10.3755/galaxea.G26-5

Baird, A., & Guest, J. (2009). Spawning synchrony in scleractinian corals: Comment on Mangubhai & Harrison (2008). *Marine Ecology Progress Series*, *374*, 301-304. https://doi.org/10.3354/meps07838

Baird, A., Guest, J., Edwards, A., Bauman, A., Bouwmeester, J., Mera, H., Abrego, D., Alvarez-Noriega, M., Babcock, R., Barbosa, M., Bonito, V., Burt, J., Cabaitan, P., Chang, C.-F., Chavanich, S., Chen, C., Chen, C., Chen, W.-J., Chung, F., & Yusuf, S. (2021). An Indo-Pacific coral spawning database. *Scientific Data*, *8*. https://doi.org/10.1038/s41597-020-00793-8

Blondeau-Patissier, D., Brando, V. E., Lønborg, C., Leahy, S. M., & Dekker, A. G. (2018). Phenology of Trichodesmium spp. blooms in the Great Barrier Reef lagoon, Australia, from the ESA-MERIS 10-year mission. *Plos One*, *13*(12), e0208010. https://doi.org/10.1371/journal.pone.0208010

Blondeau-Patissier, D., Schroeder, T., Suresh, G., Li, Z., Diakogiannis, F. I., Irving, P., Witte, C., & Steven, A. D. L. (2023). Detection of marine oil-like features in Sentinel-1 SAR images by supplementary use of deep learning and empirical methods: Performance assessment for the Great Barrier Reef marine park. *Marine Pollution Bulletin*, *188*, 114598. https://doi.org/https://doi.org/10.1016/j.marpolbul.2023.114598

Brekke, C., & Solberg, A. H. S. (2005). Oil spill detection by satellite remote sensing. *Remote Sensing of Environment*, *95*(1), 1-13. https://doi.org/https://doi.org/10.1016/j.rse.2004.11.015

Britta, S. (1999). Short-term nutrient pulses as tools to assess responses of coral reef macroalgae to enhanced nutrient availability. *Marine Ecology Progress Series*, *182*, 305-310. https://www.int-res.com/abstracts/meps/v182/p305-310/

Brodie, J., Schroeder, T., Rohde, K., Faithful, J., Masters, B., Dekker, A., Brando, V., & Maugham, M. (2010). Dispersal of suspended sediments and nutrients in the Great Barrier Reef lagoon during river-discharge events: Conclusions from satellite remote sensing and concurrent

flood-plume sampling. *Marine and Freshwater Research*, *61*, 651-664. https://doi.org/10.1071/MF08030

Burgess, S. C. (2006). Algal blooms on coral reefs with low anthropogenic impact in the Great Barrier Reef. *Coral Reefs*, *25*(3), 390-390. https://doi.org/10.1007/s00338-006-0108-7

Capone, D. G., Zehr, J. P., Paerl, H. W., Bergman, B., & Carpenter, E. J. (1997). Trichodesmium, a globally significant marine cyanobacterium. *Science*, *276*(5316), 1221-1229. https://doi.org/10.1126/science.276.5316.1221

Chandler, C. J., Ávila-Mosqueda, S. V., Salas-Acosta, E. R., Magaña-Gallegos, E., Mancera, E. E., Reali, M. A. G., de la Barreda-Bautista, B., Boyd, D. S., Metcalfe, S. E., Sjogersten, S., van Tussenbroek, B., Silva, R., & Foody, G. M. (2023). Spectral characteristics of beached Sargassum in response to drying and decay over time. *Remote Sensing*, *15*(17), 4336. https://www.mdpi.com/2072-4292/15/17/4336

Cheung, M. W. M., Hock, K., Skirving, W., & Mumby, P. J. (2021). Cumulative bleaching undermines systemic resilience of the Great Barrier Reef. *Current Biology*, *31*(23), 5385-5392.e5384. https://doi.org/https://doi.org/10.1016/j.cub.2021.09.078

Chowdhury, S., Rashid, A., Yang, C.-S., & Daewoon, S. (2023). Detection of Macroalgal Bloom from Sentinel−1 Imagery. *Remote Sensing*, *15*, 4764. https://doi.org/10.3390/rs15194764

Cresswell, A., Tildesley, P., & Cresswell, G. (2019). Synthetic Aperture Radar scenes of the North West Shelf, Western Australia, suggest this is an underutilised method to remotely study mass coral spawning. *Journal of the Royal Society of Western Australia*, *102*, 45-51.

Devlin, M., Schroeder, T., McKinna, L., Brodie, J., Brando, V., & Dekker, A. (2012). Monitoring and mapping of flood plumes in the Great Barrier Reef based on in situ and remote sensing observations. In (pp. 147-188). https://doi.org/10.1201/b11702-10

Devlin, M. J., McKinna, L. W., Álvarez-Romero, J. G., Petus, C., Abott, B., Harkness, P., & Brodie, J. (2012). Mapping the pollutants in surface riverine flood plume waters in the Great Barrier Reef, Australia. *Marine Pollution Bulletin*, *65*(4), 224-235. https://doi.org/https://doi.org/10.1016/j.marpolbul.2012.03.001

Devlin, M. J., Wenger, A., Petus, C., da Silva, E. T., DeBose, J., & Álvarez-Romero, J. (2013). *Reef Rescue Marine Monitoring Program: Final report of JCU activities 2011/12: flood plumes and extreme weather monitoring for the Great Barrier Reef Marine Park Authority*. http://hdl.handle.net/11017/2803

Dupouy, C. (1992). Discoloured waters in the Melanesian Archipelago (New Caledonia and Vanuatu). The value of the NIMBUS-7 Coastal Zone Colour Scanner observations. *Marine pelagic cyanobacteria*. https://doi.org/10.1007/978-94-015-7977-3_11

Dupouy, C., Neveux, J., Dirberg, G., Rottgers, R., Tenorio, M. M. B., & Ouillon, S. (2008). Bio-optical properties of the marine cyanobacteria Trichodesmium spp. *Journal of Applied Remote Sensing*, *2*(1), 023503. https://doi.org/10.1117/1.2839036

Dupouy, C., Petit, M., & Dandonneau, Y. (1988). Satellite detected cyanobacteria bloom in the southwestern tropical Pacific Implication for oceanic nitrogen fixation. *International Journal of Remote Sensing*, *9*(3), 389-396. https://doi.org/10.1080/01431168808954862

Emiyati, Manoppo, A. K. S., & Budhiman, S. (2017). Estimation on the concentration of total suspended matter in Lombok Coastal using Landsat 8 OLI, Indonesia. *IOP Conference Series: Earth and Environmental Science*, *54*, 012073. https://doi.org/10.1088/1755-1315/54/1/012073

Fabricius, K. E., Logan, M., Weeks, S., & Brodie, J. (2014). The effects of river run-off on water clarity across the central Great Barrier Reef. *Marine Pollution Bulletin*, *84*(1), 191-200. https://doi.org/https://doi.org/10.1016/j.marpolbul.2014.05.012

Fingas, M., & Brown, C. (2014). Review of oil spill remote sensing. *Marine Pollution Bulletin*, *83*(1), 9-23. https://doi.org/https://doi.org/10.1016/j.marpolbul.2014.03.059

Fingas, M. F., & Brown, C. E. (1997). Review of oil spill remote sensing. *Spill Science & Technology Bulletin*, *4*(4), 199-208. https://doi.org/https://doi.org/10.1016/S1353-2561(98)00023-1

Frazier, A. E., & Hemingway, B. L. (2021). A technical review of Planet smallsat data: Practical considerations for processing and using PlanetScope imagery. *Remote Sensing*, *13*(19), 3930. https://www.mdpi.com/2072-4292/13/19/3930

Furnas, M. J. (1992). Pelagic Trichodesmium (=Oscillatoria) in the Great Barrier Reef region. In E. J. Carpenter, D. G. Capone, & J. G. Rueter (Eds.), *Marine Pelagic Cyanobacteria: Trichodesmium and other Diazotrophs* (pp. 265-272). Springer Netherlands. https://doi.org/10.1007/978-94-015-7977-3_17

Gade, M., Alpers, W., Hühnerfuss, H., Masuko, H., & Kobayashi, T. (1998). Imaging of biogenic and anthropogenic ocean surface films by the multifrequency/multipolarization SIR-C/X-SAR. *Journal of Geophysical Research: Oceans*, *103*(C9), 18851-18866. https://doi.org/https://doi.org/10.1029/97JC01915

Gade, M., Byfield, V., Ermakov, S., Lavrova, O., & Mitnik, L. (2013). Slicks as indicators for marine processes. *Oceanography (Washington D.C.)*, *26*, 138-149.

Gan, S. H., Waheed, Z., Chung, F. C., Spiji, D. A., Sikim, L., Saleh, E., & Tan, C. H. (2021). In situ observations of coral spawning and spawn slick at Lankayan Island, Sabah, Malaysia. *Marine Biodiversity*, *51*(1), 10. https://doi.org/10.1007/s12526-020-01158-5

Garcia-Pineda, O., Zimmer, B., Howard, M., Pichel, W., Li, X., & MacDonald, I. R. (2009). Using SAR images to delineate ocean oil slicks with a texture-classifying neural network algorithm (TCNNA) [Article]. *Canadian Journal of Remote Sensing*, *35*(5), 411-421. https://doi.org/10.5589/m09-035

Geng, X., Li, P., Yang, J., Shi, L., Li, X.-m., & Zhao, J. (2020). Ulva prolifera detection with dual-polarization GF-3 SAR data. *IOP Conference Series: Earth and Environmental Science*, *502*(1), 012026. https://doi.org/10.1088/1755-1315/502/1/012026

Govindaraj, S., Saravanakumar, A., & Machendiranathan, M. (2020). Study on sentinel 3-OLCI sensor validation for chlorophyll a and total suspended matter in coast waters of parangipettai, Bay of Bengal, Southeast coast of India [Article]. *Indian Journal of Ecology*, *47*(2), 303-307. https://www.scopus.com/inward/record.uri?eid=2-s2.0-85086275449&partnerID=40&md5=9a6134fba299ce7be16964a15e3d8d9e

Gower, J., King, S., & Goncalves, P. (2008). Global monitoring of plankton blooms using MERIS MCI. *International Journal of Remote Sensing*, *29*, 6209-6216. https://doi.org/10.1080/01431160802178110

Guan, H., Huang, J., Li, L., Li, X., Miao, S., Su, W., Ma, Y., Niu, Q., & Huang, H. (2023). Improved Gaussian mixture model to map the flooded crops of VV and VH polarization data. *Remote Sensing of Environment*, *295*, 113714. https://doi.org/https://doi.org/10.1016/j.rse.2023.113714

Harriott, V. (2004). Marine tourism impacts on the Great Barrier Reef. *Tourism in Marine Environments*, *1*, 29-40. https://doi.org/10.3727/154427304774865850

Harrison, P. L., Babcock, R. C., Bull, G. D., Oliver, J. K., Wallace, C. C., & Willis, B. L. (1984). Mass spawning in tropical reef corals. *Science*, *223*(4641), 1186-1189. https://doi.org/doi:10.1126/science.223.4641.1186

Harrison, P. L., & Wallace, C. C. (1990). Reproduction, dispersal and recruitment of scleractinian corals. In Z. Dubinsky (Ed.), *Coral Reefs* (Vol. 25, pp. 133-207). Elsevier.

Hauser, D., Abdalla, S., Ardhuin, F., Bidlot, J.-R., Bourassa, M., Cotton, D., Gommenginger, C., Evers-King, H., Johnsen, H., Knaff, J., Lavender, S., Mouche, A., Reul, N., Sampson, C., Steele, E. C. C., & Stoffelen, A. (2023). Satellite remote sensing of surface winds, waves, and currents: Where are we now? *Surveys in Geophysics*, *44*(5), 1357-1446. https://doi.org/10.1007/s10712-023-09771-2

Haut, J. M., Moreno-Alvarez, S., Pastor-Vargas, R., Perez-Garcia, A., & Paoletti, M. E. (2024). Cloud-Based Analysis of Large-Scale Hyperspectral Imagery for Oil Spill Detection. *IEEE Journal of Selected Topics in Applied Earth Observations and Remote Sensing*, *17*, 2461-2474. https://doi.org/10.1109/JSTARS.2023.3344022

Hedley, J. D., Roelfsema, C. M., Chollett, I., Harborne, A. R., Heron, S. F., Weeks, S., Skirving, W. J., Strong, A. E., Eakin, C. M., Christensen, T. R. L., Ticzon, V., Bejarano, S., & Mumby, P. J. (2016). Remote sensing of coral reefs for monitoring and management: A review. *Remote Sensing*, *8*(2).

Hirose, M., Kinzie, R., & Hidaka, M. (2001). Timing and process of entry of zooxanthellae into oocytes of hermatypic corals. *Coral Reefs*, *20*, 273-280. https://doi.org/10.1007/s003380100171

Hock, K., Doropoulos, C., Gorton, R., Condie, S., & Mumby, P. (2019). Split spawning increases robustness of coral larval supply and inter-reef connectivity. *Nature Communications*, *10*. https://doi.org/10.1038/s41467-019-11367-7

Hoegh-Guldberg, O., Poloczanska, E. S., Skirving, W., & Dove, S. (2017). Coral reef ecosystems under climate change and ocean acidification [Review]. *Frontiers in Marine Science*, *4*. https://doi.org/10.3389/fmars.2017.00158

Holt, B., & Jones, C. (2017, 23-28 July 2017). Detection of marine slicks with SAR: Scientific and experimental legacy of werner alpers, his students and colleagues. 2017 IEEE International Geoscience and Remote Sensing Symposium (IGARSS),

Holzman, M. E., Rivas, R. E., & Bayala, M. I. (2021). Relationship between TIR and NIR-SWIR as indicator of vegetation water availability. *Remote Sensing*, *13*(17).

Hu, C., Cannizzaro, J., Carder, K. L., Muller-Karger, F. E., & Hardy, R. (2010). Remote detection of Trichodesmium blooms in optically complex coastal waters: Examples with MODIS full-spectral data. *Remote Sensing of Environment*, *114*(9), 2048-2058. https://doi.org/https://doi.org/10.1016/j.rse.2010.04.011

Hu, C., Feng, L., Hardy, R. F., & Hochberg, E. J. (2015). Spectral and spatial requirements of remote measurements of pelagic Sargassum macroalgae. *Remote Sensing of Environment*, *167*, 229-246. https://doi.org/https://doi.org/10.1016/j.rse.2015.05.022

Hu, C., Li, X., Pichel, W. G., & Muller-Karger, F. E. (2009). Detection of natural oil slicks in the NW Gulf of Mexico using MODIS imagery. *Geophysical Research Letters*, *36*(1). https://doi.org/https://doi.org/10.1029/2008GL036119

Hühnerfuss, H., Alpers, W., Jones, W. L., Lange, P. A., & Richter, K. (1981). The damping of ocean surface waves by a monomolecular film measured by wave staffs and microwave radars. *Journal of Geophysical Research: Oceans*, *86*(C1), 429-438. https://doi.org/https://doi.org/10.1029/JC086iC01p00429

Jackson, C. (2004). *Synthetic Aperture Radar marine user's manual*.

Jafarbiglu, H., & Pourreza, A. (2022). A comprehensive review of remote sensing platforms, sensors, and applications in nut crops. *Computers and Electronics in Agriculture*, *197*, 106844. https://doi.org/https://doi.org/10.1016/j.compag.2022.106844

Jamodiong, E. A., Maboloc, E. A., Leriorato, J. C., Tañedo, M. C. S., Diaz, L. A., Tabalanza, T. D., Cabaitan, P. C., & Villanueva, R. D. (2018). Coral spawning and spawn-slick observation in the Philippines. *Marine Biodiversity*, *48*(4), 2187-2192. https://doi.org/10.1007/s12526-017-0680-9

Janga, B., Asamani, G. P., Sun, Z., & Cristea, N. (2023). A Review of Practical AI for Remote Sensing in Earth Sciences. *Remote Sensing*, *15*(16).

Jenkins, A. D., & Jacobs, S. J. (1997). Wave damping by a thin layer of viscous fluid. *Physics of Fluids*, *9*(5), 1256-1264. https://doi.org/10.1063/1.869240

Jensen, J. R. (1996). *Introductory digital image processing: a remote sensing perspective. Second edition* [Book]. https://www.scopus.com/inward/record.uri?eid=2-s2.0-0030318229&partnerID=40&md5=61545dffa9920432291477a91f59df9a

Jesus, J., & Kuplich, T. (2020). Applications of SAR data to the estimate of forest biophysical variables in Brazil. *Cerne*, *26*, 88. https://doi.org/10.1590/01047760202026012656

Jones, A. T., Thankappan, M., Logan, G. A., Kennard, J. M., Smith, C. J., Williams, A. K., & Lawrence, G. M. (2006). Coral spawn and bathymetric slicks in Synthetic Aperture Radar (SAR) data from

the Timor Sea, north-west Australia. *International Journal of Remote Sensing*, *27*(10), 2063-2069. https://doi.org/10.1080/01431160500445308
Kuchler, D. A., & Jupp, D. L. B. (1988). Shuttle photograph captures massive phytoplankton bloom in the Great Barrier Reef. *International Journal of Remote Sensing*, *9*(8), 1299-1301. https://doi.org/10.1080/01431168808954937
Kurata, N., Vella, K., Hamilton, B., Shivji, M., Soloviev, A., Matt, S., Tartar, A., & Perrie, W. (2016). Surfactant-associated bacteria in the near-surface layer of the ocean. *Scientific reports*, *6*(1), 19123. https://doi.org/10.1038/srep19123
La, T. V., Messager, C., Honnorat, M., & Channelliere, C. (2018). Detection of convective systems through surface wind gust estimation based on Sentinel-1 images: A new approach. *Atmospheric Science Letters*, *19*(12), e863. https://doi.org/https://doi.org/10.1002/asl.863
Lacava, T., Ciancia, E., Coviello, I., Di Polito, C., Grimaldi, C. S. L., Pergola, N., Satriano, V., Temimi, M., Zhao, J., & Tramutoli, V. (2017). A MODIS-Based Robust Satellite Technique (RST) for Timely Detection of Oil Spilled Areas. *Remote Sensing*, *9*(2).
Lee, J., Jurkevich, L., Dewaele, P., Wambacq, P., & Oosterlinck, A. (1994). Speckle filtering of synthetic aperture radar images: A Review. *Remote Sensing Reviews*, *8*. https://doi.org/10.1080/02757259409532206
Li, G., Li, Y., Hou, Y., Wang, X., & Wang, L. (2021). Marine oil slick detection using improved polarimetric feature parameters based on polarimetric Synthetic Aperture Radar data. *Remote Sensing*, *13*(9), 1607. https://www.mdpi.com/2072-4292/13/9/1607
Lu, Y., Li, X., Tian, Q., & Han, W. (2012). An optical remote sensing model for estimating oil slick thickness based on two-beam interference theory. *Optics Express*, *20*, 24496-24504. https://doi.org/10.1364/OE.20.024496
Luo, Q., Perissin, D., Zhang, Y., & Jia, Y. (2014). L- and X-Band multi-temporal InSAR analysis of Tianjin subsidence. *Remote Sensing*, *6*(9), 7933-7951.
Matkan, A., Hajeb, M., & Azarakhsh, Z. (2013). Oil spill detection from SAR image using SVM based classification. *International Archives of the Photogrammetry, Remote Sensing and Spatial Information Sciences - ISPRS Archives*, *40*, 55-60. https://doi.org/10.5194/isprsarchives-XL-1-W3-55-2013
McKinna, L. I. W., Furnas, M. J., & Ridd, P. V. (2011). A simple, binary classification algorithm for the detection of Trichodesmium spp. within the Great Barrier Reef using MODIS imagery. *Limnology and Oceanography: Methods*, *9*(2), 50-66. https://doi.org/https://doi.org/10.4319/lom.2011.9.50
Migliaccio, M., Nunziata, F., & Buono, A. (2015). SAR polarimetry for sea oil slick observation. *International Journal of Remote Sensing*, *36*(12), 3243-3273. https://doi.org/10.1080/01431161.2015.1057301
Migliaccio, M., Nunziata, F., & Buono, A. (2018, 12-15 June 2018). SAR polarimetry for effective sea oil slick observation. 2018 IEEE/OES Baltic International Symposium (BALTIC),
Mills, M. S., Ungermann, M., Rigot, G., den Haan, J., Leon, J. X., & Schils, T. (2023). Assessment of the utility of underwater hyperspectral imaging for surveying and monitoring coral reef ecosystems. *Scientific reports*, *13*(1), 21103. https://doi.org/10.1038/s41598-023-48263-6
Mobley, C. (1994). *Light and water: Radiative transfer in natural waters*. Academic Press. Available from: https://www.oceanopticsbook.info/view/introduction/level-2/other-web-resources
Moore, K., Voss, K., & Gordon, H. (1998). Spectral reflectance of whitecaps: Instrumentation, calibration, and performance in coastal waters. *Journal of Atmospheric and Oceanic Technology*, *15*, 496-509. https://doi.org/10.1175/1520-0426(1998)015<0496:SROWIC>2.0.CO;2
Naz, S., Iqbal, M. F., Mahmood, I., & Allam, M. (2021). Marine oil spill detection using Synthetic Aperture Radar over Indian Ocean. *Marine Pollution Bulletin*, *162*, 111921. https://doi.org/https://doi.org/10.1016/j.marpolbul.2020.111921

Nichol, J. E., Antonarakis, A. S., & Nazeer, M. (2023). Monitoring the sea surface microlayer (SML) on Sentinel images. *Science of the Total Environment*, *872*, 162218. https://doi.org/https://doi.org/10.1016/j.scitotenv.2023.162218

Oliver, J. K., & Willis, B. L. (1987). Coral-spawn slicks in the Great Barrier Reef: preliminary observations. *Marine Biology*, *94*, 521-529.

Pérez-García, Á., Horstrand, P., & López, J. F. (2022, 13-16 Sept. 2022). Ndoi, A novel oil spectral index: Comparisons and results. 2022 12th Workshop on Hyperspectral Imaging and Signal Processing: Evolution in Remote Sensing (WHISPERS),

Phillips, O. M. (1988). Radar Returns from the Sea Surface—Bragg Scattering and Breaking Waves. *Journal of Physical Oceanography*, *18*(8), 1065-1074. https://doi.org/https://doi.org/10.1175/1520-0485(1988)018<1065:RRFTSS>2.0.CO;2

Pisanti, A., Magrì, S., Ferrando, I., & Federici, B. (2022). Sea water turbidity analysis from Sentinel-2 images: Atmospheric correction and bands correlation. *The International Archives of the Photogrammetry, Remote Sensing and Spatial Information Sciences*, *XLVIII-4/W1-2022*, 371-378. https://doi.org/10.5194/isprs-archives-XLVIII-4-W1-2022-371-2022

Pourshamsi, M., Xia, J., Yokoya, N., Garcia, M., Lavalle, M., Pottier, E., & Balzter, H. (2021). Tropical forest canopy height estimation from combined polarimetric SAR and LiDAR using machine-learning. *ISPRS Journal of Photogrammetry and Remote Sensing*, *172*, 79-94. https://doi.org/https://doi.org/10.1016/j.isprsjprs.2020.11.008

Qi, L., Wang, M., Hu, C., Capone, D. G., Subramaniam, A., Carpenter, E. J., & Xie, Y. (2023). Trichodesmium around Australia: A view from space. *Geophysical Research Letters*, *50*(16), e2023GL104092. https://doi.org/https://doi.org/10.1029/2023GL104092

Qi, L., Wang, M., Hu, C., & Holt, B. (2022). On the capacity of Sentinel-1 synthetic aperture radar in detecting floating macroalgae and other floating matters. *Remote Sensing of Environment*, *280*, 113188. https://doi.org/10.1016/j.rse.2022.113188

Rajendran, S., Vethamony, P., Sadooni, F. N., Al-Kuwari, H. A.-S., Al-Khayat, J. A., Govil, H., & Nasir, S. (2021). Sentinel-2 image transformation methods for mapping oil spill – A case study with Wakashio oil spill in the Indian Ocean, off Mauritius. *MethodsX*, *8*, 101327. https://doi.org/https://doi.org/10.1016/j.mex.2021.101327

Romano, J.-C., & Marquet, R. (1991). Occurrence frequencies of sea-surface slicks at long and short time-scales in relation to wind speed. *Estuarine, Coastal and Shelf Science*, *33*(5), 445-458. https://doi.org/https://doi.org/10.1016/0272-7714(91)90083-N

Rousset, G., De Boissieu, F., Menkes, C., Lefèvre, J., Frouin, R., Rodier, M., Ridoux, V., Laran, S., Bonnet, S., & Dupouy, C. (2018). Remote sensing of Trichodesmium spp. mats in the western tropical South Pacific. *Biogeosciences*, *15*, 5203-5219. https://doi.org/10.5194/bg-15-5203-2018

Roux, J. L., Christopher, S., & Maskey, M. (2021). Exploring the use of planetscope data for particulate matter air quality research [Article]. *Remote Sensing*, *13*(15), Article 2981. https://doi.org/10.3390/rs13152981

Roy, D., Huang, H., Houborg, R., & Martins, V. (2021). A global analysis of the temporal availability of PlanetScope high spatial resolution multi-spectral imagery. *Remote Sensing of Environment*, *264*, 112586. https://doi.org/10.1016/j.rse.2021.112586

Shao, W., Zhao, C., Jiang, X., Sun, Z., Wang, X., Wang, J., & Cai, L. (2021). Characteristics of suspended sediment in Sentinel-1 synthetic aperture radar observations. *Remote Sensing Letters*, *12*(11), 1167-1179. https://doi.org/10.1080/2150704X.2021.1974119

Shen, H., Perrie , W., Liu, Q., & He, Y. (2014). Detection of macroalgae blooms by complex SAR imagery. *Marine Pollution Bulletin*, *78*. https://doi.org/10.1016/j.marpolbul.2013.10.044

Simpson, C. J. (1991). Mass spawning of corals on Western Australian reefs and comparisons with the Great Barrier Reef. *J R Soc W Aust*, *74*.

Simpson, C. J., Cary, J. L., & Masini, R. J. (1993). Destruction of corals and other reef animals by coral spawn slicks on Ningaloo Reef, Western Australia. *Coral Reefs*, *12*(3), 185-191. https://doi.org/10.1007/BF00334478

Singh, P., & Shree, R. (2016, 30 Sept.-1 Oct. 2016). Analysis and effects of speckle noise in SAR images. 2016 2nd International Conference on Advances in Computing, Communication, & Automation (ICACCA) (Fall),

Skrunes, S., Brekke, C., & Eltoft, T. (2012, 22-27 July 2012). Oil spill characterization with multi-polarization C- and X-band SAR. 2012 IEEE International Geoscience and Remote Sensing Symposium,

Small, D., Miranda, N., & Meier, E. (2009, 12-17 July 2009). A revised radiometric normalisation standard for SAR. 2009 IEEE International Geoscience and Remote Sensing Symposium,

Small, D., & Schubert, A. (2008). Guide to ASAR geocoding. *RSL-ASAR-GC-AD*(1.0).

Subramaniam, A., Brown, C. W., Hood, R. R., Carpenter, E. J., & Capone, D. G. (2001). Detecting Trichodesmium blooms in SeaWiFS imagery. *Deep Sea Research Part II: Topical Studies in Oceanography*, *49*(1), 107-121. https://doi.org/https://doi.org/10.1016/S0967-0645(01)00096-0

Subramaniam, A., & Carpenter, E. J. (1994). An empirically derived protocol for the detection of blooms of the marine cyanobacterium Trichodesmium using CZCS imagery. *International Journal of Remote Sensing*, *15*(8), 1559-1569. https://doi.org/10.1080/01431169408954191

Subramaniam, A., Carpenter, E. J., Karentz, D., & Falkowski, P. G. (1999). Bio-optical properties of the marine diazotrophic cyanobacteria Trichodesmium spp. I. Absorption and photosynthetic action spectra. *Limnology and Oceanography*, *44*(3), 608-617. https://doi.org/https://doi.org/10.4319/lo.1999.44.3.0608

Teague, J., Day, J. C. C., Allen, M. J., Scott, T. B., Hochberg, E. J., & Megson-Smith, D. (2023). A Demonstration of the Capability of Low-Cost Hyperspectral Imaging for the Characterisation of Coral Reefs. *Oceans*, *4*(3), 286-300. https://www.mdpi.com/2673-1924/4/3/20

Thenkabail, P. S., Smith, R. B., & Pauw, E. D. (2000). Hyperspectral vegetation indices and their relationships with agricultural crop characteristics. *Remote Sensing of Environment*, *71*, 158-182.

Valenzuela, G. R. (1978). Theories for the interaction of electromagnetic and oceanic waves: A review. *Boundary-Layer Meteorology*, *13*(1), 61-85. https://doi.org/10.1007/BF00913863

Voskuhl, L., & Rahlff, J. (2022). Natural and oil surface slicks as microbial habitats in marine systems: A mini review. *Frontiers in Marine Science*, *9*. https://doi.org/10.3389/fmars.2022.1020843

Vuki, V. C., & Price, I. R. (1994). Seasonal changes in the Sargassum populations on a fringing coral reef, Magnetic Island, Great barrier reef region, Australia. *Aquatic Botany*, *48*(2), 153-166. https://doi.org/https://doi.org/10.1016/0304-3770(94)90082-5

Wait, A. D. (2021). The importance of data reliability and usability when assessing impacts of marine mineral oil Spills. *Toxics*, *9*(11). https://doi.org/10.3390/toxics9110302

Wang, G., Li, J., Cai, Z., Zhang, F., & Shen, Q. (2017). Synthetic aperture radar detection and characteristic analysis of cyanobacterial scum in Lake Taihu. *Journal of Applied Remote Sensing*, *11*, 012006. https://doi.org/10.1117/1.JRS.11.012006

Wang, G., Li, J., Shen, Q., & Zhang, F. (2014). Monitoring cyanobacteria-dominant algal blooms in eutrophicated Taihu Lake in China with synthetic aperture radar images. *Chinese Journal of Oceanology and Limnology*, *33*, 139-148. https://doi.org/10.1007/s00343-015-4019-8

Wang, M., & Hu, C. (2021). Satellite remote sensing of pelagic Sargassum macroalgae: The power of high resolution and deep learning. *Remote Sensing of Environment*, *264*, 112631. https://doi.org/https://doi.org/10.1016/j.rse.2021.112631

Wang, M., Hu, C., Cannizzaro, J., English, D., Han, X., Naar, D., Lapointe, B., Brewton, R., & Hernandez, F. (2018). Remote sensing of Sargassum biomass, nutrients, and pigments. *Geophysical Research Letters*, *45*(22), 12,359-312,367. https://doi.org/https://doi.org/10.1029/2018GL078858

Whitney, J. L., Gove, J. M., McManus, M. A., Smith, K. A., Lecky, J., Neubauer, P., Phipps, J. E., Contreras, E. A., Kobayashi, D. R., & Asner, G. P. (2021). Surface slicks are pelagic nurseries for diverse ocean fauna. *Scientific reports*, *11*(1), 3197. https://doi.org/10.1038/s41598-021-81407-0

Willis, B. L., Babcock, R. C., Harrison, P. L., Oliver, J. K., & Wallace, C. C. (1985). *Patterns in the mass spawning of corals on the Great Barrier Reef from 1981 to 1984* Moorea, French Polynesia.

Willis, B. L., & Oliver, J. K. (1990). Direct tracking of coral larvae: Implications for dispersal studies of planktonic larvae in topographically complex environments. *Ophelia*, *32*(1-2), 145-162. https://doi.org/10.1080/00785236.1990.10422029

Wolanski, E. (1994). Physical oceanographic processes of the Great Barrier Reef. *CRC Press*. https://doi.org/https://doi.org/10.1201/9781351075602

Wu, L., Wang, L., Min, L., Hou, W., Guo, Z., Zhao, J., & Li, N. (2018). Discrimination of algal-bloom using spaceborne SAR observations of Great Lakes in China. *Remote Sensing*, *10*(5), 767. https://www.mdpi.com/2072-4292/10/5/767

Xinzhe, Y., Jianqiang, L., Chunhua, X., Tao, Z., & Xingai, S. (2009, 26-30 Oct. 2009). Application of spaceborne SAR imagery in monitoring green algae. 2009 2nd Asian-Pacific Conference on Synthetic Aperture Radar,

Yamano, H., Sakuma, A., & Harii, S. (2020). Coral-spawn slicks: Reflectance spectra and detection using optical satellite data. *Remote Sensing of Environment*, *251*, 112058. https://doi.org/https://doi.org/10.1016/j.rse.2020.112058

Zhang, Y., Li, Y., & Lin, H. (2014). Oil-Spill Pollution Remote Sensing by Synthetic Aperture Radar. In. https://doi.org/10.5772/57477

Zheng, H., Zhang, Y., Yunhua, W., Zhang, X., & Meng, J. (2017). The polarimetric features of oil spills in full polarimetric synthetic aperture radar images. *Acta Oceanologica Sinica*, *36*, 105-114. https://doi.org/10.1007/s13131-017-1065-4

Ziemann, A. (2015). *A manifold learning approach to target detection in high-resolution hyperspectral imagery* Thesis. Rochester Institute of Technology. Accessed from: https://repository.rit.edu/.

11 APPENDICES

Appendix 1. Media articles and websites reporting coral reef spawning events in the Great Barrier Reef.

Year	determined date	Source
2016	Nov 17-18-19th	https://cairnsdiveadventures.com.au/2016/10/great-barrier-reef-coral-spawning-2016/
2016	Nov 21	https://www.sciencealert.com/the-full-moon-just-triggered-one-of-the-largest-mass-spawning-events-of-2016 https://mybestplace.com/en/article/the-night-of-the-corals-the-reproductive-phenomenon-of-the-great-barrier-reef
2016	November 19	https://australian.museum/blog-archive/amri-news/meagre-coral-spawning-following-the-2016-mass-bleaching/
2017	November (not specific)	https://theconversation.com/explainer-mass-coral-spawning-a-wonder-of-the-natural-world-87253
2018	Fourth, fifth and sixth night after the full moon in December.	https://www.gbrbiology.com/2022/05/30/coral-larval-project/
2018	Nov 27-28	https://www.whitsundayescape.com/news/coral-spawning/
2018	Roughly Nov 27th-29th	https://www.ecovoice.com.au/good-g-reef-coral-spawning-signals-new-life-as-great-barrier-reef-gears-up-for-tomorrows-big-climax/
2019	Fitzroy Island- 3rd and 4th night after the full moon in October. Moore Reef- 4th, 5th and 6th night after the full moon in November. Moore Reef-5th and 16th night after the full moon in December.	https://www.gbrbiology.com/2022/05/30/coral-larval-project/
2019	About Nov 18	https://news.cgtn.com/news/2019-11-18/Great-Barrier-Reef-annual-mass-coral-spawning-begins-LH6iVkHhmw/index.html
2021	Nov 19	https://earth.org/the-great-barrier-reef-gives-birth-in-massive-coral-spawning-event/
2022	Nov 11-12	https://australian.museum/blog/amri-news/news-from-lirs-big-coral-spawning-event-in-2022/

Appendix 2. Locations of identified slicks.

date	slick id	longitude	latitude
2016-12-21	0e19_AnalyticMS-SR_20161221-207	150.855796	-23.111236
2016-12-21	0e19_AnalyticMS-SR_20161221-209	150.821865	-23.105257
2016-12-21	0e19_AnalyticMS-SR_20161221-210	150.800970	-23.111699
2016-12-21	0e19_AnalyticMS-SR_20161221-203	150.917629	-23.124868
2016-12-21	0e19_AnalyticMS-SR_20161221-204	150.911601	-23.071262
2016-12-21	0e19_AnalyticMS-SR_20161221-206	150.880716	-23.040398
2016-12-21	0e19_AnalyticMS-SR_20161221-211	150.842713	-23.126668
2016-12-21	0e19_AnalyticMS-SR_20161221-214	150.903750	-23.140563
2016-12-21	0e19_AnalyticMS-SR_20161221-212	150.865793	-23.184407
2016-12-21	0e19_AnalyticMS-SR_20161221-213	150.899812	-23.175677
2016-12-21	0e19_AnalyticMS-SR_20161221-208	150.858340	-23.140742
2016-12-21	0e19_AnalyticMS-SR_20161221-201	150.880716	-22.909350
2016-12-21	0e19_AnalyticMS-SR_20161221-202	150.884486	-22.870762
2016-12-21	0e19_AnalyticMS-SR_20161221-200	150.953519	-22.835415
2016-12-21	0e19_AnalyticMS-SR_20161221-197	150.937417	-22.804259
2016-12-21	0e19_AnalyticMS-SR_20161221-196	150.947352	-22.776860
2016-12-21	0e19_AnalyticMS-SR_20161221-192	150.938872	-22.750074
2016-12-21	0e19_AnalyticMS-SR_20161221-195	150.990878	-22.769259
2016-12-21	0e19_AnalyticMS-SR_20161221-193	150.977849	-22.742239
2016-12-21	0e19_AnalyticMS-SR_20161221-199	150.884183	-22.796185
2016-12-21	0e19_AnalyticMS-SR_20161221-194	150.941480	-22.720420
2016-12-21	0e19_AnalyticMS-SR_20161221-198	150.917382	-22.808396
2018-11-16	100c_AnalyticMS-SR_20181116-164	152.491589	-23.942477
2018-11-16	100c_AnalyticMS-SR_20181116-165	152.494469	-23.879758
2018-11-16	100c_AnalyticMS-SR_20181116-167	152.420083	-23.834397
2018-11-16	100c_AnalyticMS-SR_20181116-166	152.475027	-23.854216
2018-11-16	100c_AnalyticMS-SR_20181116-151	151.771483	-23.959514
2018-11-16	0f35_AnalyticMS-SR_20181116-127	151.709710	-23.208407
2018-11-16	0f35_AnalyticMS-SR_20181116-136	151.848652	-23.145621
2018-11-16	0f35_AnalyticMS-SR_20181116-129	151.788647	-23.345661
2018-11-16	0f35_AnalyticMS-SR_20181116-128	151.848672	-23.437335
2018-11-16	0f35_AnalyticMS-SR_20181116-131	151.685823	-23.530163
2018-11-16	0f35_AnalyticMS-SR_20181116-132	151.759532	-23.521322
2018-11-16	0f35_AnalyticMS-SR_20181116-134	151.787995	-23.764257
2018-11-16	0f35_AnalyticMS-SR_20181116-133	151.699411	-23.734500
2018-11-16	0f35_AnalyticMS-SR_20181116-135	151.719220	-23.904187
2018-11-16	1003_AnalyticMS-SR_20181116-137	150.574115	-22.284456
2018-11-16	1003_AnalyticMS-SR_20181116-138	150.727507	-22.228142
2018-11-16	1003_AnalyticMS-SR_20181116-140	150.688282	-22.322464
2018-11-16	1003_AnalyticMS-SR_20181116-143	150.713024	-22.320439
2018-11-16	1003_AnalyticMS-SR_20181116-141	150.693025	-22.375961
2018-11-16	1003_AnalyticMS-SR_20181116-142	150.735245	-22.361536
2018-11-16	1003_AnalyticMS-SR_20181116-144	150.675931	-22.284854
2018-11-16	1003_AnalyticMS-SR_20181116-139	150.673654	-22.316060
2018-11-16	100c_AnalyticMS-SR_20181116-146	151.770480	-23.606650
2018-11-16	100c_AnalyticMS-SR_20181116-148	151.743191	-23.751097
2018-11-16	100c_AnalyticMS-SR_20181116-163	151.684311	-23.726387
2018-11-16	100c_AnalyticMS-SR_20181116-162	151.621019	-23.742853
2018-11-16	100c_AnalyticMS-SR_20181116-149	151.744307	-23.797253
2018-11-16	100c_AnalyticMS-SR_20181116-152	151.719490	-23.955579
2018-11-16	100c_AnalyticMS-SR_20181116-156	151.729845	-23.961037
2018-11-16	100c_AnalyticMS-SR_20181116-155	151.673153	-23.957718
2018-11-16	100c_AnalyticMS-SR_20181116-153	151.662937	-23.930464
2018-11-16	100c_AnalyticMS-SR_20181116-157	151.615355	-23.937178
2018-11-16	100c_AnalyticMS-SR_20181116-150	151.828147	-23.824166
2018-11-16	100c_AnalyticMS-SR_20181116-169	152.492383	-24.115622
2018-11-16	100c_AnalyticMS-SR_20181116-168	152.466896	-24.112677
2018-11-16	100c_AnalyticMS-SR_20181116-170	152.539298	-24.176123
2018-11-16	100c_AnalyticMS-SR_20181116-276	152.465821	-23.859057
2018-11-16	100c_AnalyticMS-SR_20181116-288	152.415261	-24.595890
2018-11-16	100c_AnalyticMS-SR_20181116-171	152.443206	-24.599521
2018-11-16	100c_AnalyticMS-SR_20181116-158	151.651645	-23.865054
2018-11-16	100c_AnalyticMS-SR_20181116-159	151.700540	-23.779893
2018-11-16	100c_AnalyticMS-SR_20181116-161	151.611409	-23.757896
2018-11-16	100c_AnalyticMS-SR_20181116-160	151.676450	-23.755102
2018-11-16	100c_AnalyticMS-SR_20181116-145	151.839996	-23.578386
2018-11-16	100c_AnalyticMS-SR_20181116-147	151.865527	-23.629787
2018-11-16	1010_AnalyticMS-SR_20181116-174	153.095432	-24.713690
2018-11-16	1010_AnalyticMS-SR_20181116-172	153.118088	-24.747877
2018-11-16	1010_AnalyticMS-SR_20181116-175	153.023732	-24.739004
2018-11-16	1010_AnalyticMS-SR_20181116-177	152.938458	-24.776860
2018-11-16	1010_AnalyticMS-SR_20181116-176	152.977829	-24.746023
2018-11-16	1010_AnalyticMS-SR_20181116-173	153.092907	-24.731728
2018-11-16	101f_AnalyticMS-SR_20181116-178	151.095715	-23.440345
2018-11-16	101f_AnalyticMS-SR_20181116-179	151.036568	-23.433721
2018-11-16	101f_AnalyticMS-SR_20181116-293	151.029618	-23.435624
2018-11-16	101f_AnalyticMS-SR_20181116-184	151.086585	-23.375423
2018-11-16	101f_AnalyticMS-SR_20181116-183	151.112181	-23.381920
2018-11-16	101f_AnalyticMS-SR_20181116-182	151.094941	-23.393667
2018-11-16	101f_AnalyticMS-SR_20181116-185	151.039669	-23.354680
2018-11-16	101f_AnalyticMS-SR_20181116-180	151.034536	-23.416414
2018-11-16	101f_AnalyticMS-SR_20181116-181	151.009981	-23.411485
2018-11-16	101f_AnalyticMS-SR_20181116-186	151.248720	-23.483375
2018-11-16	101f_AnalyticMS-SR_20181116-292	151.106140	-23.441139
2018-11-16	101f_AnalyticMS-SR_20181116-294	151.042720	-23.417538
2018-11-16	101f_AnalyticMS-SR_20181116-295	151.045879	-23.441742
2018-11-16	1021_AnalyticMS-SR_20181116-191	152.106344	-23.628644
2018-11-16	1021_AnalyticMS-SR_20181116-190	151.996738	-23.848553
2018-11-16	1021_AnalyticMS-SR_20181116-188	152.009300	-24.086844
2018-11-16	1021_AnalyticMS-SR_20181116-189	151.985119	-23.999221
2018-11-16	1021_AnalyticMS-SR_20181116-187	151.952701	-24.258537
2019-11-11	0f34_AnalyticMS-SR_20191111-117	151.954129	-23.390038
2019-11-11	0f34_AnalyticMS-SR_20191111-119	152.057823	-23.441901
2019-11-11	0f34_AnalyticMS-SR_20191111-118	152.066547	-23.340883
2019-11-11	0f34_AnalyticMS-SR_20191111-300	152.158636	-23.294325
2019-11-11	0f34_AnalyticMS-SR_20191111-120	152.159935	-23.293313
2019-11-11	0f34_AnalyticMS-SR_20191111-121	151.824200	-24.045918
2019-11-11	104a_AnalyticMS-SR_20191111-122	151.958284	-23.395953
2019-11-11	104a_AnalyticMS-SR_20191111-124	152.061735	-23.333449
2019-11-11	104a_AnalyticMS-SR_20191111-123	151.980559	-23.179823
2019-11-11	104a_AnalyticMS-SR_20191111-125	152.064248	-23.442290
2019-11-11	104a_AnalyticMS-SR_20191111-126	151.962862	-23.544501
2019-11-14	100d_AnalyticMS_20191114-1	146.476887	-18.860773
2019-11-14	100d_AnalyticMS_20191114-2	146.503531	-18.802898
2019-11-14	100d_AnalyticMS_20191114-3	146.522652	-18.810603
2019-11-14	100d_AnalyticMS_20191114-4	146.464915	-18.803995
2019-11-14	1034_AnalyticMS_20191114-82	146.116342	-18.165564
2019-11-14	1034_AnalyticMS_20191114-81	146.082316	-18.064084
2019-11-14	1034_AnalyticMS_20191114-83	146.201883	-18.179109
2019-11-14	1105_AnalyticMS_20191114-84	146.726647	-18.760751
2019-11-18	1013_AnalyticMS-SR_20191118-88	149.999388	-20.534918
2019-11-18	1013_AnalyticMS-SR_20191118-89	150.044030	-20.620980
2019-11-18	1013_AnalyticMS-SR_20191118-87	149.825873	-20.645571
2019-11-18	1013_AnalyticMS-SR_20191118-90	149.897519	-20.710508
2019-11-18	1013_AnalyticMS-SR_20191118-91	149.652624	-21.418272
2019-11-18	1013_AnalyticMS-SR_20191118-93	149.717691	-21.426443
2019-11-18	1013_AnalyticMS-SR_20191118-92	149.675239	-21.472018
2019-11-18	1013_AnalyticMS-SR_20191118-95	149.693686	-21.493702
2019-11-18	1013_AnalyticMS-SR_20191118-94	149.660654	-21.534422
2019-11-18	1013_AnalyticMS-SR_20191118-96	149.701558	-21.511634
2019-11-18	1013_AnalyticMS-SR_20191118-97	149.557970	-21.886421
2019-11-18	1044_AnalyticMS-SR_20191118-114	150.589935	-21.170650
2019-11-18	1044_AnalyticMS-SR_20191118-98	150.427566	-21.594700
2019-11-18	1044_AnalyticMS-SR_20191118-113	150.400163	-21.824721
2019-11-18	1044_AnalyticMS-SR_20191118-112	150.489711	-21.857231
2019-11-18	1044_AnalyticMS-SR_20191118-99	150.295197	-21.957031
2019-11-18	1044_AnalyticMS-SR_20191118-100	150.346494	-21.976663
2019-11-18	1044_AnalyticMS-SR_20191118-101	150.440838	-21.981919
2019-11-18	1044_AnalyticMS-SR_20191118-104	150.406229	-22.007484
2019-11-18	1044_AnalyticMS-SR_20191118-105	150.462233	-22.076769
2019-11-18	1044_AnalyticMS-SR_20191118-106	150.477760	-22.061203
2019-11-18	1044_AnalyticMS-SR_20191118-107	150.524004	-21.995516
2019-11-18	1044_AnalyticMS-SR_20191118-102	150.345672	-22.006440
2019-11-18	1044_AnalyticMS-SR_20191118-103	150.351789	-22.024121
2019-11-18	1044_AnalyticMS-SR_20191118-109	150.226517	-22.301539
2019-11-18	1044_AnalyticMS-SR_20191118-108	150.248375	-22.318084
2019-11-18	1044_AnalyticMS-SR_20191118-110	150.238852	-22.273122
2019-11-18	1044_AnalyticMS-SR_20191118-111	150.246040	-22.351760
2019-11-18	1063_AnalyticMS-SR_20191118-116	150.870065	-22.325496
2019-11-18	1063_AnalyticMS-SR_20191118-115	150.840410	-22.320888
2019-11-18	0f3d_AnalyticMS-SR_20191118-1	152.482149	-22.203851
2019-11-18	0f3d_AnalyticMS-SR_20191118-2	152.589812	-22.284193
2019-11-18	0f3d_AnalyticMS-SR_20191118-3	152.634977	-22.491196

2019-11-18	1011_AnalyticMS-SR_20191118-1	152.734220	-22.189845
2019-11-18	1011_AnalyticMS-SR_20191118-2	152.727742	-21.848791
2019-11-18	1011e_AnalyticMS-SR_20191118-1	152.617686	-22.292836
2019-11-18	1011e_AnalyticMS-SR_20191118-2	152.539989	-22.177438
2019-11-18	1011e_AnalyticMS-SR_20191118-3	152.595081	-22.096211
2019-11-18	1011e_AnalyticMS-SR_20191118-4	152.471663	-22.072056
2020-12-4	1057_AnalyticMS-SR_20201204-85	151.915581	-23.909323
2020-12-4	1057_AnalyticMS-SR_20201204-86	151.745574	-23.923303
2020-12-4	2223_AnalyticMS-SR_20201204-283	152.585081	-24.120060
2020-12-4	2223_AnalyticMS-SR_20201204-279	152.496592	-24.032696
2020-12-4	2223_AnalyticMS-SR_20201204-278	152.436661	-23.938089
2020-12-4	2223_AnalyticMS-SR_20201204-277	152.456202	-23.905997
2020-12-4	2223_AnalyticMS-SR_20201204-281	152.448693	-24.150506
2020-12-4	2223_AnalyticMS-SR_20201204-284	152.640021	-24.175937
2020-12-4	2223_AnalyticMS-SR_20201204-282	152.505789	-24.176472
2020-12-4	2223_AnalyticMS-SR_20201204-280	152.430676	-24.084093
2020-12-4	2223_AnalyticMS-SR_20201204-287	152.522089	-24.424646
2020-12-4	2223_AnalyticMS-SR_20201204-285	152.372294	-24.536043
2020-12-4	2223_AnalyticMS-SR_20201204-288	152.495086	-24.655397
2020-12-4	2223_AnalyticMS-SR_20201204-265	150.804126	-23.032046
2021-11-19	2276_AnalyticMS-SR_20211119-16	152.610935	-24.547346
2021-11-19	2276_AnalyticMS-SR_20211119-17	152.572667	-24.660986
2021-11-19	2276_AnalyticMS-SR_20211119-19	152.625846	-24.662726
2021-11-19	2276_AnalyticMS-SR_20211119-5	152.824593	-24.419156
2021-11-19	2276_AnalyticMS-SR_20211119-1	152.933789	-24.071491
2021-11-19	2459_AnalyticMS-SR_20211119-75	151.550674	-23.789032
2021-11-19	2459_AnalyticMS-SR_20211119-73	151.320167	-23.491174
2021-11-19	2459_AnalyticMS-SR_20211119-74	151.360228	-23.419173
2021-11-19	241c_AnalyticMS-SR_20211119-53	153.273010	-24.714435
2021-11-19	241c_AnalyticMS-SR_20211119-54	153.287315	-24.741188
2021-11-19	241c_AnalyticMS-SR_20211119-55	153.380067	-24.759795
2021-11-19	241c_AnalyticMS-SR_20211119-51	153.356503	-24.661183
2021-11-19	241c_AnalyticMS-SR_20211119-59	153.399537	-24.915667
2021-11-19	241c_AnalyticMS-SR_20211119-56	153.274204	-24.855071
2021-11-19	241c_AnalyticMS-SR_20211119-58	153.330643	-24.922686
2021-11-19	2459_AnalyticMS-SR_20211119-72	151.525689	-23.178423
2021-11-19	104e_AnalyticMS-SR_20211119-6	152.303169	-24.508935
2021-11-19	104e_AnalyticMS-SR_20211119-7	152.260330	-24.443765
2021-11-19	2276_AnalyticMS-SR_20211119-6	152.901966	-24.476032
2021-11-19	2276_AnalyticMS-SR_20211119-9	152.805451	-24.584179
2021-11-19	2276_AnalyticMS-SR_20211119-10	152.876733	-24.604716
2021-11-19	2276_AnalyticMS-SR_20211119-13	152.798918	-24.757191
2021-11-19	2276_AnalyticMS-SR_20211119-14	152.851416	-24.779978
2021-11-19	2276_AnalyticMS-SR_20211119-4	152.857928	-24.286021
2021-11-19	2276_AnalyticMS-SR_20211119-3	152.809038	-24.188668
2021-11-19	2276_AnalyticMS-SR_20211119-2	153.089199	-23.846271
2021-11-19	2429_AnalyticMS-SR_20211119-60	151.887158	-23.068458
2021-11-19	2429_AnalyticMS-SR_20211119-61	151.944911	-23.176263
2021-11-19	2429_AnalyticMS-SR_20211119-62	151.951677	-23.378129
2021-11-19	2429_AnalyticMS-SR_20211119-63	151.976381	-23.435351
2021-11-19	2429_AnalyticMS-SR_20211119-66	151.577017	-23.809966
2021-11-19	2429_AnalyticMS-SR_20211119-64	151.576591	-23.904059
2021-11-19	2429_AnalyticMS-SR_20211119-65	151.618240	-23.938469
2021-11-19	2434_AnalyticMS-SR_20211119-67	153.017489	-24.783166
2021-11-19	2434_AnalyticMS-SR_20211119-68	152.846093	-24.790498
2021-11-19	2455_AnalyticMS-SR_20211119-274	152.049693	-24.156873
2021-11-19	2455_AnalyticMS-SR_20211119-273	151.898031	-23.976596
2021-11-19	2455_AnalyticMS-SR_20211119-275	151.997794	-24.313330
2021-11-19	2459_AnalyticMS-SR_20211119-76	151.369430	-23.893240
2021-11-19	245d_AnalyticMS-SR_20211119-77	150.794046	-23.016592
2021-11-19	245d_AnalyticMS-SR_20211119-78	150.809624	-23.031841
2021-11-19	245d_AnalyticMS-SR_20211119-79	150.856454	-23.027364
2021-11-19	245d_AnalyticMS-SR_20211119-80	150.881267	-23.114252
2021-11-19	2434_AnalyticMS-SR_20211119-69	152.966910	-24.850695
2021-11-19	2434_AnalyticMS-SR_20211119-70	153.072605	-24.739036
2021-11-19	2434_AnalyticMS-SR_20211119-71	152.885727	-24.606268
2021-11-19	241c_AnalyticMS-SR_20211119-301	152.926020	-24.587905
2021-11-19	241c_AnalyticMS-SR_20211119-52	153.331940	-24.716268
2021-11-19	241c_AnalyticMS-SR_20211119-50	153.355209	-24.624798
2021-11-19	241c_AnalyticMS-SR_20211119-57	153.295956	-24.918134
2021-11-19	2276_AnalyticMS-SR_20211119-7	152.773749	-24.541988
2021-11-19	2276_AnalyticMS-SR_20211119-8	152.748413	-24.590406
2021-11-19	104e_AnalyticMS-SR_20211119-4	152.059197	-23.693039
2021-11-19	104e_AnalyticMS-SR_20211119-3	152.107946	-23.677969
2021-11-19	104e_AnalyticMS-SR_20211119-5	152.064845	-23.751187
2021-11-19	104e_AnalyticMS-SR_20211119-1	152.090568	-23.692839
2021-11-19	104e_AnalyticMS-SR_20211119-2	152.100120	-23.694830
2021-11-22	2420_AnalyticMS-SR_20211122-218	148.486283	-19.879799
2021-11-22	2420_AnalyticMS-SR_20211122-217	148.506662	-19.860172
2021-11-22	2420_AnalyticMS-SR_20211122-220	148.408995	-20.040181
2021-11-22	2420_AnalyticMS-SR_20211122-221	148.403355	-20.054854
2021-11-22	2420_AnalyticMS-SR_20211122-219	148.446567	-19.864244
2021-11-22	2423_AnalyticMS-SR_20211122-222	143.818568	-12.941084
2021-11-22	2449_AnalyticMS-SR_20211122-230	148.687786	-20.175008
2021-11-22	2449_AnalyticMS-SR_20211122-231	148.663291	-20.179102
2021-11-22	2449_AnalyticMS-SR_20211122-232	148.657616	-20.160980
2021-11-22	2449_AnalyticMS-SR_20211122-233	148.611806	-20.165007
2021-11-22	2449_AnalyticMS-SR_20211122-234	148.685765	-20.165009
2021-11-22	2449_AnalyticMS-SR_20211122-226	148.771933	-20.205889
2021-11-22	2449_AnalyticMS-SR_20211122-227	148.798252	-20.198040
2021-11-22	2449_AnalyticMS-SR_20211122-224	148.793588	-20.238211
2021-11-22	2449_AnalyticMS-SR_20211122-225	148.836967	-20.220703
2021-11-22	2449_AnalyticMS-SR_20211122-229	148.719822	-20.211201
2021-11-22	2449_AnalyticMS-SR_20211122-228	148.748884	-20.232443
2021-11-22	2449_AnalyticMS-SR_20211122-223	148.631762	-19.908753
2021-11-22	2458_AnalyticMS-SR_20211122-235	143.752184	-12.384312
2022-11-12	247a_AnalyticMS-SR_20221112-269	150.976255	-22.741935
2022-11-12	247a_AnalyticMS-SR_20221112-268	150.982855	-22.735404
2022-11-12	247a_AnalyticMS-SR_20221112-272	151.005036	-22.733195
2022-11-12	247a_AnalyticMS-SR_20221112-271	150.958128	-22.726739
2022-11-12	247a_AnalyticMS-SR_20221112-270	150.968339	-22.737042
2022-11-12	248b_AnalyticMS-SR_20221112-298	150.472344	-20.968325
2022-11-12	248b_AnalyticMS-SR_20221112-237	150.462885	-20.974808
2022-11-12	248b_AnalyticMS-SR_20221112-239	150.405417	-21.109508
2022-11-12	248b_AnalyticMS-SR_20221112-238	150.395557	-21.164028
2022-11-12	248b_AnalyticMS-SR_20221112-242	150.326327	-21.199865
2022-11-12	248b_AnalyticMS-SR_20221112-243	150.286953	-21.181220
2022-11-12	248b_AnalyticMS-SR_20221112-241	150.511353	-21.180430
2022-11-12	248b_AnalyticMS-SR_20221112-240	150.473474	-21.229723
2022-11-12	248b_AnalyticMS-SR_20221112-244	150.380464	-21.676651
2022-11-12	248b_AnalyticMS-SR_20221112-245	150.429789	-21.653536
2022-11-12	248b_AnalyticMS-SR_20221112-246	150.456589	-21.743701
2022-11-12	248b_AnalyticMS-SR_20221112-247	150.387245	-21.773553
2022-11-12	249c_AnalyticMS-SR_20221112-255	149.843210	-20.246186
2022-11-12	249c_AnalyticMS-SR_20221112-252	149.927134	-20.344609
2022-11-12	249c_AnalyticMS-SR_20221112-253	149.928511	-20.574165
2022-11-12	249c_AnalyticMS-SR_20221112-254	149.842585	-20.657087
2022-11-12	249c_AnalyticMS-SR_20221112-248	149.522754	-21.223677
2022-11-12	249c_AnalyticMS-SR_20221112-251	149.487841	-21.263033
2022-11-12	249c_AnalyticMS-SR_20221112-250	149.538990	-21.682753
2022-11-12	249c_AnalyticMS-SR_20221112-249	149.469871	-21.781525
2022-11-12	2490_AnalyticMS-SR_20221112-256	149.278683	-20.712247
2022-11-12	2490_AnalyticMS-SR_20221112-257	149.209927	-20.817819
2022-11-12	2490_AnalyticMS-SR_20221112-299	149.211504	-20.812684
2022-11-12	2490_AnalyticMS-SR_20221112-258	149.168164	-20.796762
2022-11-12	2490_AnalyticMS-SR_20221112-262	149.116583	-20.942661
2022-11-12	2490_AnalyticMS-SR_20221112-259	149.160879	-20.947884
2022-11-12	2490_AnalyticMS-SR_20221112-260	149.319716	-20.956206
2022-11-12	2490_AnalyticMS-SR_20221112-261	149.330016	-21.136455
2022-11-12	2486_AnalyticMS-SR_20221112-264	148.882316	-20.027943
2022-11-14	2421_AnalyticMS-SR_20221114-236	153.022538	-25.034696
2022-11-14	2473_AnalyticMS-SR_20221114-289	153.400237	-26.158844
2022-11-14	2473_AnalyticMS-SR_20221114-290	153.378258	-26.213396
2022-11-14	2473_AnalyticMS-SR_20221114-291	153.363599	-26.234118
2022-11-14	2473_AnalyticMS-SR_20221114-297	153.477302	-25.828403
2022-11-14	2492_AnalyticMS-SR_20221114-296	152.766137	-25.169286

Appendix 3. Mean reflectance of identified slicks and background water pixels

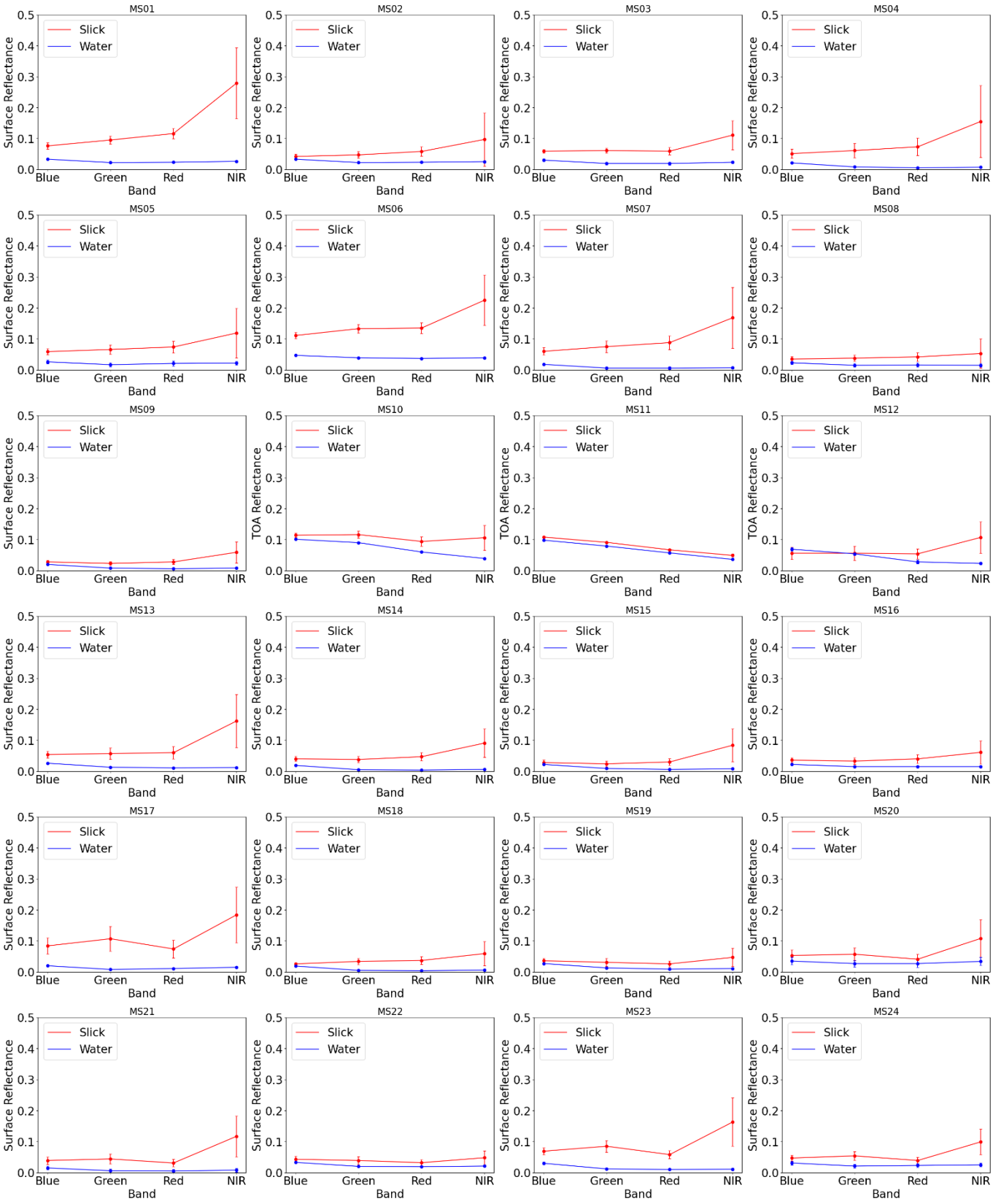

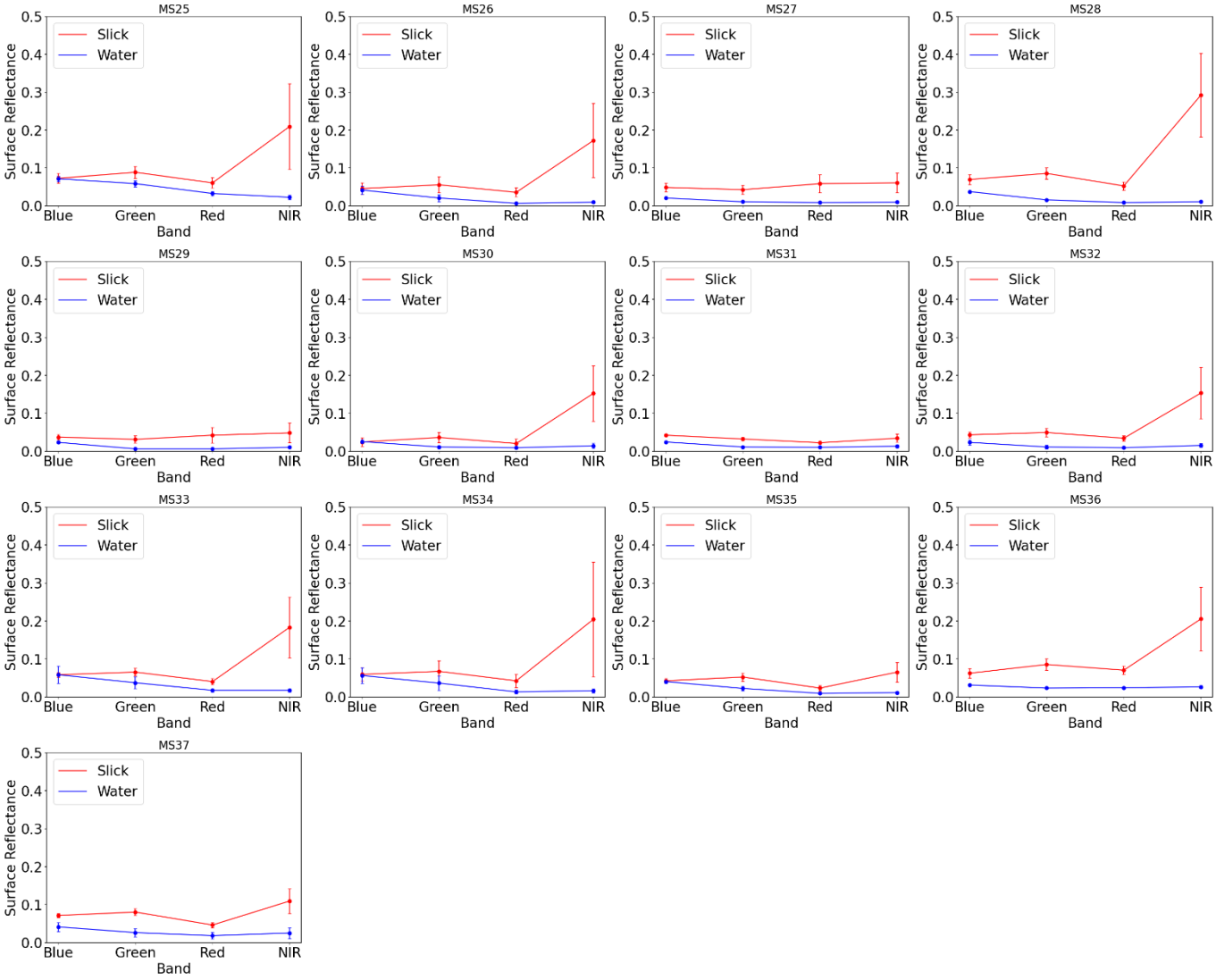
MS25
MS26
MS27
MS28
MS29
MS30
MS31
MS32
MS33
MS34
MS35
MS36
MS37
Slick
Water
Surface Reflectance
Band
Blue
Green
Red
NIR
0.0
0.1
0.2
0.3
0.4
0.5

Appendix 4. Python script developed to create PlanetScope mosaics

```
import os
from osgeo import gdal

def extract_satellite_id(filename):
    parts = filename.split('_')
    if len(parts[2]) < 4:
        return parts[3]
    else:
        return parts[2]

def extract_product_level(filename):
    parts = filename.split('_')
    if len(parts[2]) < 4:
        return parts[4]
    else:
        return parts[3]

def extract_product_type(filename):
    parts = filename.split('_')
    if len(parts[2]) < 4:
        return '-'.join(parts[5:]).replace('.tif', '').replace('-clip', '')
    else:
        return '-'.join(parts[4:]).replace('.tif', '').replace('-clip', '')

def extract_epsg_code(filename):
    dataset = gdal.Open(filename)
    projection = dataset.GetProjection()
    epsg_code = projection.split('"')[-2]
    return epsg_code

def extract_acquisition_date(filename):
    parts = filename.split('_')
    return parts[0]

def create_vrt_files(directory):
    for root, dirs, files in os.walk(directory):
        satellite_product_files = (Frazier & Hemingway, 2021)
        for file in files:
            if file.endswith('.tif') and 'udm2' not in file:
                satellite_id = extract_satellite_id(file)
                product_level = extract_product_level(file)
                product_type = extract_product_type(file)
                epsg_code = extract_epsg_code(os.path.join(root, file))
                acquisition_date = extract_acquisition_date(file)
                key = f"{satellite_id}_{product_level}_{product_type}_{epsg_code}"
                if key not in satellite_product_files:
                    satellite_product_files[key] = []
                satellite_product_files[key].append(os.path.join(root, file))

        for key, tiff_files in satellite_product_files.items():
            output_folder = os.path.dirname(tiff_files[0])
            satellite_id, product_level, product_type, epsg_code = key.split('_')
            vrt_file_name = os.path.join(output_folder,
f"{satellite_id}_{product_level}_{product_type}_{epsg_code}.vrt")

            vrt_ds = gdal.BuildVRT(vrt_file_name, tiff_files, separate=False)
            vrt_ds.FlushCache()
            vrt_ds = None

directory_path = r'\inputpath'

create_vrt_files(directory_path)
```